

Book of Abstract

I FORUM EMR-PL



RZESZÓW 2010

19-21 Maj



I FORUM EMR-PL,
Rzeszów,
19 - 21 May 2010

INSTITUTE OF PHYSICS
UNIVERSITY OF RZESZÓW

INSTITUTE OF PHYSICS
WEST POMERANIAN UNIVERSITY OF TECHNOLOGY
in SZCZECIN

INSTITUTE OF MOLECULAR PHYSICS
POLISH ACADEMY OF SCIENCES
POZNAŃ

POLISH EPR SOCIETY



Scientific Committee

- K. Dziliński - Chairman, Częstochowa University of Technology
Z. Sojka - Secretary, Jagiellonian University, Cracow
Cz. Rudowicz - The President of the Polish EPR Society,
West Pomeranian University of Technology, Szczecin
G. Bartosz – University of Łódź
W. Froncisz - Jagiellonian University, Cracow
N. Guskos - West Pomeranian University of Technology, Szczecin
S. Hoffmann - Institute of Molecular Physics,
Polish Academy of Sciences, Poznań
R. Hrabański - Częstochowa University of Technology
A. Jezierski – University of Wrocław
J. Michalik - Institute of Nuclear Chemistry and Technology, Warsaw
Jerzy Mroziński - University of Wrocław
T. Sarna - Jagiellonian University, Cracow
A. Suchocki - Institute of Physics, Polish Academy of Sciences, Warsaw
H. Szymczak - Institute of Physics, Polish Academy of Sciences, Warsaw
S. Wapłak - Institute of Molecular Physics,
Polish Academy of Sciences, Poznań

Organising Committee

- Ireneusz Stefaniuk - Chairman
Marian Kuźma
Czesław Rudowicz - President, Polish EPR Society
Mirosław Łabuz
Mariusz Bester - Secretary

Welcome Address
at
The First Forum EMR-PL, Rzeszów, 19-21 May 2010

Professor Czesław Rudowicz
The President of the Polish EPR Society

Honoured Guests, Ladies and Gentlemen:

It is a great pleasure for me, on behalf of the Council of the Polish EPR Society [PEPRS] and the Local Organising Committee, ably headed by Dr Irenusz Stefaniuk to welcome you to the First Forum EMR-PL organized under the auspices of the Society.

We all appreciate very much that in spite of a very short period of time for organization and the financial constraints affecting scientific institutions in Poland, the efforts of our colleagues in Rzeszów have brought this Forum to fruition. I am pleased that the University of Rzeszów hosts this Forum. I believe that this Forum may play an important role in enhancing the role of the Rzeszów's EMR research group in Poland.

Continuing with the spirit of the previous RAMIS conferences, this Forum is open to all participants involved in EMR basic research and applications. The main aims are to bring together as many EMR (EPR/ESR & FMR/AFMR) spectroscopists working in Poland as possible and to promote and facilitate collaboration among the Polish EMR community. I am confident that the scientific program of the I Forum EMR-PL will satisfy most of the participants. I am also sure the Forum will help uniting EMR spectroscopists from all over the country and provide a starting point for a new series of conferences. As usual the most important part of any conference is to meet fellow researchers. So hopefully the opportunity for personal discussions provided by this meeting will be fully utilized.

The Forum's opening session is devoted to the memory of the late Professor Jan Stankowski. Two other specialized sessions, namely, (A):

Improvement and development of EMR equipment in Poland and (B) *Perspectives of development of EMR (EPR/ESR) research in Poland*, are planned. I would also like to invite all participants, irrespective of being formally members of the Polish EPR Society in the past or not, to join us at the General Meeting (GM) of the Society, to be held during the Forum. A whole range of topics of interest to the whole EMR community will be discussed, among others, the venue for future Forum and the new organisational structure of the body representing our community. Please note that this GM is going to be a very crucial Meeting for the future of the EMR community. This GM will be also an opportunity to select the best persons, who will coordinate efforts to secure a prosperous future for the EMR community. Hence, your votes and opinions are of great importance as they may shape the future course of events.

My sincere thanks go to all members of the Local Organising Committee, especially Dr I. Stefaniuk, the LOC Chairman, and Prof. M. Kuźma for their dedicated work to make the I Forum EMR-PL a successful meeting. Support from the Scientific Committee in nominating the invited speakers and maintaining the high standard of this Forum is also much appreciated. I wish to express our gratitude to all sponsors for their financial support, especially, the Institute of Physics - University of Rzeszów, the Institute of Molecular Physics – Polish Academy of Science in Poznań, and the Institute of Physics of the West Pomeranian University of Technology in Szczecin. Thanks are due to all speakers and participants, who by attending this meeting have helped to make this Forum a great success.

May I wish you all an enjoyable and stimulating experience at the Forum.

Thank you.



Czesław Rudowicz

I Forum EMR-PL, Rzeszów, 19-21 May 2010

Venue – Hotel President

CONFERENCE PROGRAM

	Wednesday 19.05	Thursday 20.05	Friday 21.05
8.00-9.00	Registration		
9.00 -10.30	Opening Ceremony & Commemorative Session	Session IV	Session VII (Panel A)
10.30 - 11.00	Group Photograph & Coffee Break	Coffee Break	Coffee Break
11.00-13.20	Session I	Session V	Session VIII
13.20 - 14.30	Lunch	Lunch	Lunch
14.30 - 16.00	Session II	Session VI (Poster Session)	Session IX
16.00 - 16.30	Coffee Break	Coffee Break	Coffee Break
16.30 -18.30	Session III	General Meeting & Panel B	Session X & Closing Ceremony
18.30	Dinner	Banquet	Dinner

CONTENTS

<i>In the Memory of Professor Jan Stankowski</i>	11
Snapshots from APES'04 - Prof. Stankowski in Bangalore Czesław Rudowicz	12
The profile of Professor Jan Stankowski - family and scientific remembrances Małgorzata Trybuła, Zbigniew Trybuła	14
My cooperation with prof. J. Stankowski S. Wapłak	17
<i>Lectures</i>	18
Broad-band ferromagnetic resonance in thin magnetic films and nanostructures J. Dubowik and H. Głowiński	19
Electron Paramagnetic Resonance Spectroscopy as a Tool for Controlling the Quality of Food. Radical Processes Induced Thermally in Starches Ewa Bidzińska, Krystyna Dyrek, Elżbieta Wenda	23
EPR of Iron Porphyrins K. Dziliński, T. Kaczmarzyk, T. Jackowski	29
Metoda optycznie detektowanego rezonansu magnetycznego do badań struktur półprzewodników półmagnetycznych Marek Godlewski	35
FMR study of magnetic nanoparticles embedded in non-magnetic matrices N. Guskos, J. Typek , and G. Żołnierkiewicz	36
EPR Study of Phase Transitions in DMAAIS and DMAGaS Crystals R. Hrabański, M. Jackowska, Z. Czapla	41
Spin trapping and radical scavenging methods in studies of bioglycerol Maria Jerzykiewicz	47
Spin number manipulation in the systems of nanoporous carbons with adsorbed molecules M. Kempiański, M. Śliwińska-Bartkowiak, W. Kempiański	52

Localized States in Carbon Nanostructures	
W. Kempinski, M. Kempinski, D. Markowski	54
A New Application of the spin labelin method	
M.Komorowska, M. Dzik, U. Cytlak, K. Gałeczka, E. Głogowska.	56
Application of spectroscopic resonance methods in investigations of metalloptides and the metalloproteins on the example β-amyloid ant the prion protein fragments	
Henryk Kozłowski, Ewa Gralka, Lukasz Szyrwił, Daniela Valensin and Gianni Valensin	58
ESR spectra under slow motion conditions	
Danuta Kruk and Aleksandra Kubica	60
Magnetic resonance in ferromagnetic diluted magnetic semiconductors.	
M. Kuźma, I. Stefaniuk	64
Size manifestation in EPR measurments of small carbon particles	
Szymon Łoś, Laurent Duclaux, Wojciech Kempinski, Maria Połomska	66
Coordinate Systems for Determining the Electron Spin Resonance (ESR) Lineshape	
Lidia Najder-Kozdrowska, Andrzej B. Więckowski.....	67
Structure and magnetic properties of polynuclear iron and vanadium complexes dispersed on oxide surfaces	
Piotr Pietrzyk, Zbigniew Sojka	72
Modeling in EMR spectroscopy - low symmetry aspects	
Czesław Rudowicz and Paweł Gnutek.....	77
Physicochemical nature of the increased phototoxicity of aged and <i>in vitro</i> photoaged retinal pigment epithelial melanosomes: EPR-spin trapping, CIDEP, saturation recovery EPR and W-band EPR study	
Grzegorz Szewczyk, Tadeusz Sarna, Mariusz Zaręba, Andrzej Żądło, Janice Burke, Theodore Camenisch and Aaron Kittell	84
EPR spectroscopy interfaced with DFT calculations	
Zbigniew Sojka*, Piotr Pietrzyk	86
Computer program SPM-MC and its applications in EMR studies of transition ions in crystals	
I. Stefaniuk, C. Rudowicz	91
Ferroic materials studied by EPR	
S. Wapłak.....	97
Electric Current Induced Spin Excitation due to Rashba Field	
Z. Wilamowski, W. Ungier, M. Havlicek, and W. Jantsch	98

Posters	99
Dyson line and modified Dyson line in the EPR measurements	
M. Bester, I Stefaniuk, M. Łabuz, M. Kuźma	100
Magnetic properties of transition metal doped zinc-oxide	
I.Stefaniuk, B.Cieniek, I. Virt	102
Studies on Antioxidants Structure in Glycerol Fractions from Biodiesel Production: Spin Trapping EPR and DFT Investigations	
Irmina Ćwieląg-Piasecka, Maciej Witwicki, Maria Jerzykiewicz	104
EPR spectroscopy of tetraborate glasses, doped with Cu and Mn	
B.V. Padlyak, A. Drzewiecki, O.O. Smyrnov	109
Multiplication of Qubits in a Doubly Resonant Bichromatic Field: A transient nutation EPR study	
R. Fedaruk, A. P. Saiko, S. A. Markevich	110
Superposition model analysis of the zero-field splitting parameters of Fe³⁺: TIBX₂ crystals – insight into local distortions and low symmetry aspects	
Paweł Gnutek, Muhammed Açıkğöz and Czesław Rudowicz	115
The stress influence on the generation of long lived radicals in wheat leaves	
Maria Łabanowska, Maria Filek, Ewa Bidzińska, Katarzyna Obal	120
Spin trapping study of the influence of taxifolin on Fenton reaction in ethanol and methanol	
Katerina Makarova, Katarzyna Łastawska, Katarzyna Zawada, Iwona Wawer ..	121
Effects of genistein on dipalmitoylphosphatidylcholine membranes	
Bożena Pawlikowska-Pawłęga, Lucjan E. Misiak, Wiesław I. Gruszecki, Antoni Gawron.....	127
Effect of chemotherapeutic agents on free radicals in melanin – comparative analysis	
Barbara Pilawa, Ewa Buszman, Magdalena Zdybel, Dorota Wrześniok	132
Spectroscopic properties of Fe²⁺ (S=2) ions at tetragonal sites in K₂FeF₄ and K₂ZnF₄	
Czesław Rudowicz and Danuta Piwowarska	137
The EPR measurements of Al₂O₃ powders and mullites used in aircraft industry for cores and shapes	
I. Stefaniuk, P.Potera, J.Cebulski	142
EPR examinations of free radical formation in thermally sterilized β-lactam antibiotics	

Paweł Ramos, Barbara Pilawa	148
The EPR investigation of defects in BGO:Cr single crystal irradiated by high energy uranium ions	
I.Stefaniuk, P.Potera, I. Rogalska, D.Wróbel.....	154
Carbon Centred Radicals in Zeolites	
Marcin Sterniczuk, Janusz Turek, Jarosław Sadło, Jacek Michalik and Grażyna Strzelczak	159
Radicals Generated Radiolytically in Lithium Formate	
Janusz Turek, Jacek Michalik, Jarosław Sadło, Marcin Sterniczuk, Grażyna Strzelczak, Henk Vrielinck, Freddy Callens	162
EPR studies of influence of storage conditions on free radicals in gamma irradiated aminoglycoside antibiotics	
Sławomir Wilczyński, Barbara Pilawa, Robert Koprowski, Zygmunt Wróbel, Marta Ptaszekiewicz, Janusz Swakoń, Paweł Olko	163
Antioxidant capacity of serum measured using TEMPO scavenging assay in patients with rheumatoid arthritis	
Katarzyna Zawada, Joanna Celińska, Ewa Matyska-Piekarska, Iwona Wawer, Jan K Łącki	169
EPR studies of Cladosporium cladosporioides mycelium with flucytosine	
Magdalena Zdybel, Barbara Pilawa, Ewa Buszman, Teresa Witoszyńska, Honorata Cieśla.....	173
Magnetic frustration in M-Fe-V-O system	
G. Żołnierkiewicz, N. Guskos i J. Typek.....	179

In the Memory of Professor Jan Stankowski

Snapshots from APES'04 - Prof. Stankowski in Bangalore

Czesław Rudowicz

Email: crudowicz@zut.edu.pl

Modeling in Spectroscopy Group, Institute of Physics, West Pomeranian University of Technology, Al. Piastów 17, 70-310 Szczecin, Poland

At the very beginning of my scientific carrier in the early 1970's, there were heated debates among young assistants in Prof. L. Kowalewski's group in the Institute of Physics, A. Mickiewicz University, Poznań, on the foundations of electron paramagnetic resonance (EPR) of transition ions. Especially, we were tackling intriguing questions concerning the effective spin Hamiltonian, fictitious spin, the microscopic spin Hamiltonian theory, and the generalized spin Hamiltonian. Across the town in the Institute of Molecular Physics, Polish Academy of Science, Prof. Jan Stankowski was heading vigorous efforts to study experimentally various materials by the then novel EPR spectroscopy techniques. Prof. Stankowski was a pioneer of research based on EPR spectroscopy and related techniques in Poland. His achievements in this and other areas of science have brought him an international acclaim. Prof. Stankowski was not only an excellent experimenter and manager. He was a true leader and encouraged his younger colleagues to study theoretical aspects involved in their experiments. For this purpose Prof. J. Stankowski has invited a budding theoretician to lecture his EPR group members on the theoretical foundations of EPR. In this way Prof. Stankowski had shaped and reinforced my early interest in EMR (EPR/ESR) spectroscopy of transition ions, which has continued throughout my whole scientific carrier.

Many years have passed before Prof. Stankowski and I have met in a very different setting and personal roles in Bangalore, India. The events described above have prompted me to include in the Welcome Address as the President of the Asia-Pacific EPR/ESR Society given at the Fourth Asia-Pacific EPR/ESR Symposium [APES'04] a 'thank you' note also for Prof. Stankowski. In this presentation, I will share with you some memories of Prof. Stankowski during the Symposium as well as during the official sightseeing trips and, most interestingly, our 'private' sightseeing and shopping escapades around Bangalore. Selected 'snapshots' include some photos taken by Prof. Stankowski himself and kindly sent to me after APES'04.

The history of the Asia-Pacific EPR/ESR Society [APES] and the Asia-Pacific EPR/ESR Symposia are also briefly outlined. This serves a double purpose. First purpose is to provide a background for the nomination by the outgoing President of the Polish EPR Society, Prof. Stankowski, of the new President for the election during the last RAMIS (*XXII International*

Conference on Radio and Microwave Spectroscopy) held in Będlewo in April 2007. Second purpose is to utilize the tested experiences concerning the organization and structure of the APES to work out ways for revival of the Polish EPR Society.

This short presentation will show us Prof. Stankowski not only as a scientist, who always liked to tackle new problems in emerging areas, but also as a human person and a keen traveler, who enjoyed exploring the world. I do also hope that the background information revealed would enable a better understanding of the proposals for continuation of the Polish EPR Society traditions, which will be presented later during the First Forum EMR-PL.

Keywords: Electron magnetic resonance (EMR); Electron paramagnetic resonance (EPR); Electron spin resonance (ESR); Polish EPR Society; Asia-Pacific EPR/ESR Society; Asia-Pacific EPR/ESR Symposium

The profile of Professor Jan Stankowski - family and scientific remembrances

Małgorzata Trybuła, Zbigniew Trybuła

e-mail: mtrybula@ifmpan.poznan.pl

trybula@ifmpan.poznan.pl

Division of Low Temperature Physics in Odolanów

Institute of Molecular Physics Polish Academy of Sciences, Smuluchowskiego 17, 60-179 Poznań, Poland.

“Physics makes my life happy, because I can do what I love”.

These words were written by my father, Jan Stankowski in his memoirs, which he had been writing for several years. Besides being an excellent physicist and teacher, he was also a humanist, who realised that only written thoughts could last. He was a very happy person with a positive outlook on life. When he became ill, he didn't despair, downright opposite; he was saying that he is a fulfilled man and thanked God for everything. He had a wonderful wife Jadwiga, with whom they made a distinctive home. He was surrounded by the loving children, grandchildren and great-grandchildren. However, it was physics that permeated his life. The adventure with physics began when he took part in a final round of Polish Physics Olympiad years ago. He was lucky enough to be a student of Professor Arkadiusz Piekara at Adam Mickiewicz University in Poznań. Professor Piekara was his inspiration till the end of his life.

Professor Jan Stankowski was always fascinated by the great challenges, which realization he used to embark on, although they might have seemed impossible. Just creating in 1975 the standalone Institute of Molecular Physics of the Polish Academy of Sciences in Poznań, where he was the first managing director, shows how important it is to have dreams and realize them consequently. On the night 1st / 2nd of January 1964, together with other members of his team, he put in operation the first ammonia maser in Poland. Before creating the Institute, in the independent Radiospectroscopy Laboratory in Poznan, after the great efforts in 1967 they finally had set up an Electron Paramagnetic Resonance (EPR) spectrometer from JEOL. The spectrometer was working day and night. That was the beginning of intensive academic research in the radiospectroscopy area, including high pressure measurements. To meet the demands for more EPR spectrometers, Professor Stankowski together with his team elaborated and constructed an own EPR spectrometer. Its serial production was carried out by “Radiopan”, a spin-off company created by the Institute of Molecular Physics Polish Academy of Sciences.

Another organizational and scientific challenge was the establishment, within, the Institute of Molecular Physics Polish Academy of Sciences, of the Division of Low Temperatures Physics in Odolanów in 1977.—Professor Stankowski's idea was to use the liquid helium produced in Odolanów for the low temperature research. The low temperature research, initiated by Professor Stankowski, has been conducted for over 30 years reaching temperature down to 0.3 K. These studies comprise, e.g., phase transitions in solids, superconductivity in various materials, attributes of electric transport of carbon materials. The research is being conducted using different equipment, namely, the EPR spectrometer, working in the range of temperatures from 300K to 4.2 K, equipment with the helium 3 cryostat for measuring dielectric permittivity, magnetic susceptibility and transport phenomena, i.e. electric and thermal conduction, in the temperature range from 300 K to 0.3 K, and the scanning tunnel microscope (STM) operating in the range 300 K to 2 K.

During his stay in the USA in 1987, Professor Stankowski had investigated the microwave absorption in the high temperature superconductors $\text{YBa}_2\text{Cu}_3\text{O}_{7-\delta}$ by the use of EPR spectrometer. He then discovered a novel method for studies of superconductors, so-called Magnetic Modulation Microwave Absorption (MMMA). This method is still being used in research of granular superconductors with Josephson junctions [1]. He introduced the concept of the local temperature of Josephson junctions systems, which has enabled thermodynamic description of the effect of the microwave field on the high temperature superconductors.

Another brain-child of Professor Stankowski was the organization of annual academic workshops "*Lato z Helem – Summer with Helium*" by the Division of Low Temperature Physics in Odolanów. For the last 26 years these workshops gave high school students a unique chance to participate in experiments and lectures covering such topics as, e.g. the low temperature studies, cryogenics, and superconductor research, delivered by eminent Polish physicists. Professor Stankowski was an academic guardian of the workshops, for whom the educational aspects and contact with young people were very important. Professor Stankowski's outreach activities were highly recognized by the Polish Physical Society, who awarded him in 2009 the Professor Ernest Medal given for achievements in popularization of science and educational activities.

All what has been said above won't tell everything of what a special man our father was; he taught all of us honesty and respect towards other people. His love towards physics was so strong and contagious that two of his children have chosen to study physics, whereas a great number of his students has become eminent scientists.

During the celebration of his 70th birthday, our Father had said the words that could serve as a hint for all of us on how to live: "*I would like to see*

something what would surprise me. Because, all the publications, quotations and so called career does not bring you happiness, if you are not sure that you didn't waste the time given to you".

In this short presentation we will illustrate various aspects of activity of our father Jan Stankowki by selected photos.

[1] J. Stankowski, P. K. Kahol, N. S. Dalal, and J. S. Moodera, Phys. Rev. **B36**, 7126 (1987) *“Possible Josephson oscillation spectra and electron paramagnetic resonance of Cu^{2+} in Y-Ba-Cu-O”*.

My cooperation with prof. J. Stankowski

S. Waplak

*Institute of Molecular Physics, Polish Academy of Sciences,
Mariana Smoluchowskiego 17, 60-179 Poznań, Poland
Email: stefan.waplak@ifmpan.poznan.pl*

When I started to work at Adam Mickiewicz University (1964) dr Jan Stankowski was very busy man who devote a big effort to construction of first (in my opinion) Polish MASER. I just started to work in his laboratory to be employed as university worker. At that time there were no sharp distinction between University and Polish Academy of Science. Stankowski research group worked with homemade EPR spectrometer.

In 1966 Independent Laboratory of Radiospectroscopy as a part of Polish Academy of Science was organized. His head dr Jan Stankowski equipped this laboratory with JEOL EPR Spectrometer. It was time when we start together studies of doped ferroelectrics like TGS, KDP etc. and discover basic relation between bulk and local parameters in ferroelectric materials. This studies directed mainly for other ferroics were continued at new Institute of Molecular Physics since 1975 year. Ordinary professor Jan Stankowski (1979) was the head of Institute over 10-years.

After 1980-years his attention was turned to cryogenic and study a high temperature superconductor (HTS). He organized “Low Temperature Laboratory of Radiospectroscopy” in Odolanów and arranged the first “Summer with Helium” workshop. In Poznań he was the head of “Superconductivity and Phase Transition” division up to 1999 year. Since 1999 I am a head of this laboratory. Practically our common interest to ferroics and EPR was progressive and exciting for all periods of our common work. I help him, as many others coworkers, in “RAMIS” conference organizing since 1964. We worked with him with pleasure as with charming and charismatic person.

Lectures

Broad-band ferromagnetic resonance in thin magnetic films and nanostructures

J. Dubowik and H. Głowiński

Institute of Molecular Physics, Polish Academy of Sciences, ul. M. Smoluchowskiego 17, 60-179 Poznań, Poland

The present contribution is aimed to give a brief comparison of the broad-band ferromagnetic resonance methods for characterization of thin magnetic films and nanostructures. It is expected that within 2011 a new broad-band ferromagnetic resonance equipment will be installed in the Institute of Molecular Physics, Polish Academy of Sciences (IFM) in the framework of SpinLab Centre financed by the Ministry of Regional Development - Innovative Economy Programme POiG 2.2 [1].

Ferromagnetic resonance (FMR) has been proved to be one of the most useful method for characterizing thin magnetic films and nanostructures [2]. A standard X- or Q- band ESR spectrometers are extensively used for this purpose in IFM [3, 4] in a conventional way, i.e., in so-called field domain. A thin film sample is “swept” through the resonance by means of external magnetic field H (Fig.1a). At the resonance, the microwave losses are increased and the reflected power changes a little. Since, in addition, a small modulated magnetic field H_{mod} is applied with frequency of several kHz, absorption signal is detected with lock-in amplifier and the measured FMR signal is proportional to the field derivative of the imaginary part of rf-susceptibility $d\chi/dH$ (Fig.1b). This conventional FMR with a fixed microwave excitation frequency ω and the magnetic system swept across resonance is also called the field-swept FMR.

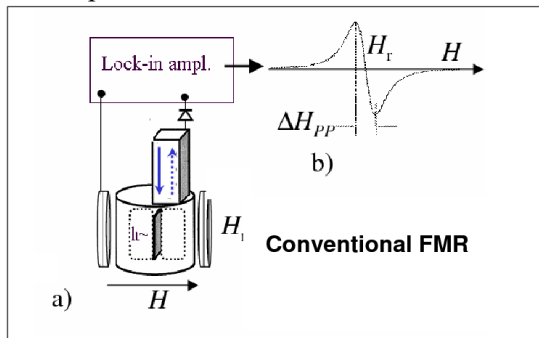


Fig. 1. Sketch of conventional FMR spectrometer (a) with a thin magnetic film placed in the centre of microwave cavity and with field H swept across the resonance. Application of a small modulation field H_{mod} and lock-in amplifier results in FMR signal proportional to the first derivative $d\chi/dH$ (b).

Nowadays, however, with the increasing demand for high-frequency methods for characterization of magnetic nanostructures [5, 6] novel measuring high-frequency techniques have emerged: vector network analyzer ferromagnetic resonance (VNA-FMR) and pulse inductive microwave magnetometry (PIMM). In contrast to conventional FMR measured in the field domain, VNA-FMR is a frequency domain technique since the microwave excitation frequency is swept at the fixed external field. On the other hand, the PIMM method consists in measurements of time evolution of voltage oscillations resulting from a damped precessional motion of the magnetization. Therefore, PIMM is a time domain technique.

We will describe briefly some advantages of the two broad-band FMR methods applied to the magnetic thin films and nanostructures in comparison to conventional FMR. The heart of VNA-FMR (Fig. 2) is Vector Network Analyzer [7]. VNA allows characterization of a transmitted and reflected signals passed to/from a microwave device under investigation over broad frequency range. It consists of a high frequency source, a local oscillator and a mixer arranged in a sophisticated architecture to allow the measurements of all four components of the S-parameters (parameters, which relate incident and reflected electromagnetic waves [7]) which are complex. Hence, in VNA the detection of the transmitted and reflected signals is phase sensitive. What is the most useful for the measurements of the magnetic nanostructures, the measurement of the phase enables the

calculation of both the real and the imaginary part of the susceptibility and, hence, to characterize magnetization dynamics in these nanostructures.

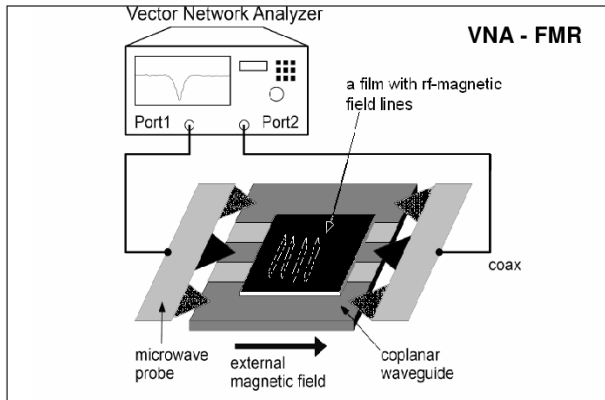


Fig. 2. A sketch of VNA-FMR comprising of VNA, coaxial cables, microwave probes and a coplanar waveguide and a thin magnetic film placed on it. Rf-magnetic field lines are schematically depicted to show that in this arrangement Larmor condition is fulfilled.

The main components of the experimental setup are sketched in Fig. 2. The VNA is connected to a coplanar waveguide (CPW) having a characteristic impedance of 50 using coaxial cables and microwave probes. VNA compares the input and output signals on the coplanar waveguide with respect to their amplitude and phase, allowing measurements of the absorption signal as a function of the frequency. To increase signal to noise ration, the sample is swept in two runs. In the first run the external magnetic field is directed perpendicular to the CPW so that h_{rf} and H are parallel (the Larmor condition is not fulfilled) and the reference spectrum is measured. In the second run the field H is applied along the CPW as it is shown in Fig.2. In such configuration FMR spectrum is expected with less or more complicated FMR absorptions with some noise. After the reference spectrum is subtracted from the noisy FMR spectrum, a pure FMR spectrum without background is obtained at a given external field. Such a procedure enables us to construct a dispersion relation (i.e. the resonance frequency as a function of bias field H) and then, to compare it with the Kittel equations for thin magnetic films with various magnetic anisotropies. Moreover, the magnetic relaxation can be evaluated in the broad range of rf-frequency and/or the magnetic field. Some examples of application of VNA-FMR for investigations of the magnetic properties of thin magnetic films can be found, for example, in Refs. [6, 8]. In VNA-FMR signal-to-noise ratio is higher than in conventional FMR method and this feature enables magnetic nanostructures with a relatively small numbers of spins to be investigated. Moreover, since VNA-FMR can be measured in a small external magnetic field, investigations of the dynamic response of several modes from nanostructures in non-saturated state (i.e., with the domain structure conserved) are possible.

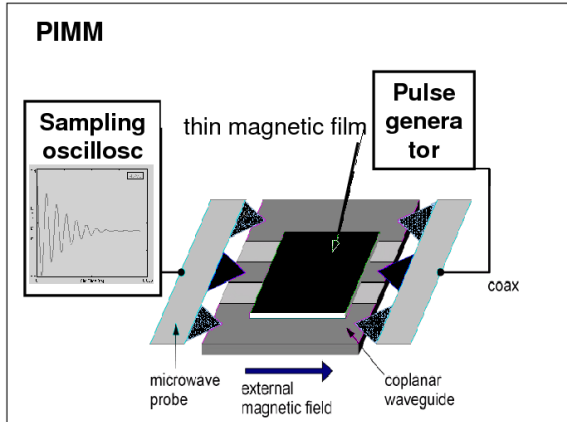


Fig.3. Schematic setup of the pulse inductive microwave magnetometer (PIMM).

In the PIMM measurements a short magnetic field pulse is applied to the coplanar waveguide. The pulse excites in a thin magnetic film placed on the

CPW a damped magnetization precessional motion and this dynamic response of magnetization is monitored as a function of time with a fast sampling oscilloscope as it is shown in Fig. 3.

Having measured a set of such responses in various external fields (or its configuration) we can further construct a dispersion relation to evaluate magnetic parameters of an investigated thin film and characterize its magnetization damping, i.e., we can obtain actually the same results as those from VNA-FMR. A systematic discussion of the PIMM method has been given by Silva et al. [9].

In summary, we presented and compared the high frequency methods for ferromagnetic resonance, which are sensitive and suitable for investigating the magnetization dynamics in submicron-scale magnetic structures. One of them is a broadband VNA-FMR spectrometer, which is preferable for the FMR studies under a constant magnetic field. The VNA-FMR, using a vector network analyzer, provides an insight to a modal spectrum with respect to both frequency and effective damping in the various modes. Besides, a pulse-inductive method (PIMM) which can measure the time domain of dynamical properties in an individual ferromagnetic film and a multilayered spin-valve stack. This method is especially useful for the characterization of intrinsic dynamical properties with a state-of-the-art oscilloscope for high-speed sampling.

Acknowledgments

The authors would like to acknowledge financial support from National Centre of Magnetic Nanostructures for Applications in Spin Electronics – SPINLAB, PO IG 2.2.

References

- [1] <http://www.poig.gov.pl/>
- [2] B. Heinrich. Ferromagnetic resonance in ultrathin film structures. in *Ultrathin Magnetic Structures II*, B. Heinrich and J. A. C. Bland, editors, pages 195-222, Berlin, 1994. Springer.
- [3] J. Dubowik, *Acta Physicae Superficierum*, **VIII**, 173 (2006).
- [4] J. Dubowik et al., *Acta Physica Polon. A*. **115**, 315 (2009).
- [5] A. Yamaguchi et al., *Phys. Rev. B*, **78**, 104401 (2008).
- [6] J. F. Sierra et al., *Appl. Phys. Lett.* **94**, 012506 (2009).
- [7] Agilent Technologies. Application Note 1287-1: *Understanding the Fundamental Principles of Vector Network Analysis*. Agilent, U.S.A., 2000.
- [8] I. Neudecker et al., *J. Magn. Magn. Mater.* **307**, 148 (2006).
- [9] T.J. Silva et al., *J. Appl. Phys.* **85**, 7849 (1999).

Electron Paramagnetic Resonance Spectroscopy as a Tool for Controlling the Quality of Food. Radical Processes Induced Thermally in Starches

Ewa Bidzińska, Krystyna Dyrek¹, Elżbieta Wenda

*Faculty of Chemistry, Jagiellonian University,
30-060 Krakow, Ingardena 3, Poland*

Abstract

Quantitative EPR measurements were performed for determination the number of radicals generated thermally in native and modified starches in the temperature range commonly used for preparing food. Influence of oxidation, phosphorylation, pretreatment of the starch with high hydrostatic pressure and additives of sweeteners on the radical processes in modified starches were studied. Paramagnetic Cu²⁺ ions were used as a probe informing about the mechanism of radical formation.

Key words: native starch, thermal treatment, radicals; oxidation, phosphorylation, high pressure treatment

1. Introduction

Starch is an important raw material of the food industry. It is a biodegradable polymer with formula (C₆H₁₀O₅)_n composed of amylopectin (75-80 weight %), a semi-crystalline highly branched polysaccharide, and amorphous amylose (about 25 weight %) exhibiting linear chains of glucose units. Amylopectin and amylose are packed in the starch granule forming concentric amorphous and crystalline layers, resulting in ring structure of dimensions up to 100 μm in size.

In order to meet steadily increasing demands for improved specific starch functionalities, required by food industry, modification of native starches are performed by chemical, physical and biological methods [1]. Chemical modifications lead to substitution of OH groups in the starch matrix by other functional groups, e.g. -COOH, -CHO, ≡ PO₄, which results in changing the chemical reactivity and rheological properties of the starch [2]. Physical modifications consisting on irradiation with UV, γ or microwaves, treatment with high hydrostatic pressure or high temperature cause partial depolymerization of the starch and free radical formation. Biological modifications consist on suppression or over expression of appropriate enzymes of starch biosynthesis changing the size of the granules, chain length, content of incorporated trace elements etc. These modifications influence advantageously

¹ E-mail address: dyrek@chemia.uj.edu.pl

certain properties of the starch, important for food industry, e.g. stability during freeze-thaw cycles, gelatinization and pasting behavior, etc., but simultaneously some of them enhance degradation of the starch through free radical formation [3].

Several evidences are given in literature that free radicals are not indifferent for human health, because they may cause serious diseases [4,5] and accelerate cellular changes associated with aging [6]. Determination of the factors significant for free radical formation is therefore an important aspect of the food quality control. Electron paramagnetic resonance (EPR) spectroscopy is an useful method for investigation of these processes. The present work summarizes several applications of EPR spectroscopy resulting in recognition of the most important factors controlling the number of radicals generated thermally in native and modified starches and in determination of the properties of these radical species.

2. Experimental

2.1. Materials

Origin of native starches investigated in this work and procedures used for their modifications are described in papers listed in References.

2.2. Methods

2.2.1. Thermal treatment

Starch samples of about 30 mg were placed in EPR quartz tubes (inner diameter = 3 mm), heated in an oven for 30 min at 150°C and afterwards for 30 min at 210°C or 230°C. During heating the tubes were open, i.e. the samples were in contact with air. After treatment the tubes were closed with a paraffin membrane.

2.2.2. EPR technique

EPR measurements were performed at room temperature with a Bruker ELEXSYS 500 spectrometer (Karlsruhe, Germany) operating in X-band (9.2 GHz) at modulation frequency 100 kHz, modulation amplitude 0.3 mT and microwave power 3 mW. The EPR spectra were recorded at room temperature. The number of spins was determined by comparison of the integral signal intensity of the investigated samples with that of the standard with the known amount of paramagnetic centers. $\text{VOSO}_4 \cdot 5\text{H}_2\text{O}$ diluted with diamagnetic K_2SO_4 , containing 5×10^{19} spins/g, was used as a primary standard. All necessary precautions, discussed in papers [7,8] were followed in order to assure good precision of the quantitative EPR measurements. Generation of radicals was investigated on native and modified samples before and after pressurization and heat treatment. EPR parameters of the radicals were determined by a simulation procedure using the program EPR SIM 32 [9]. The accuracy of determination of g values was ± 0.001 and that of A values was ± 0.05 mT.

3. Results and discussion

3.1 Radicals generated in starches by conventional heating or by irradiation with microwaves

Heating of the potato or corn starch in the temperature range 200 – 250°C, commonly used for preparing food, generates radicals with two-component anisotropic EPR signals (signal I and II) and g_{av} value equal to 2.006–2.007 (Fig.1) [10]. One of the components (signal I) exhibits hyperfine structure with $A_{av} = 1.2$ mT. The presence of two components was evidenced by measuring the EPR spectra at two microwave frequencies, i.e. in X and Q band, and at different power levels. Signals I and II exhibit different saturation ability and at higher values of microwave power signal II became saturated whereas signal I, with HFS, is more distinctly visible.

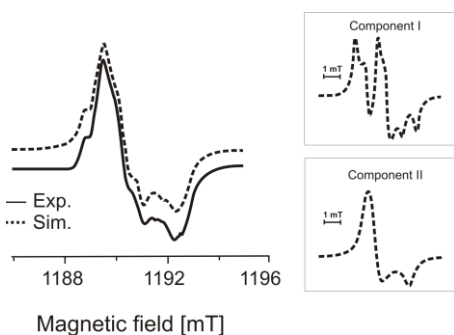


Fig.1. EPR signal of radicals generated thermally in starch (after [10])

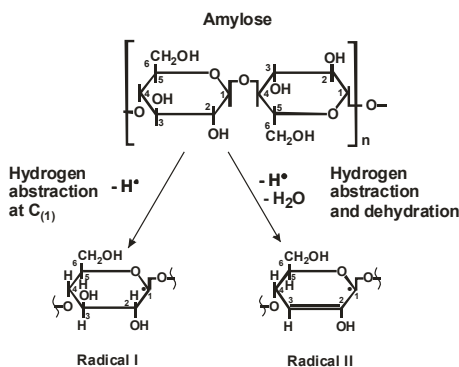


Fig.2. Scheme of the formation of thermally generated radicals (after [10])

The radical with signal I is generated thermally by abstraction of hydrogen ($H\cdot$) from C_1 atom of the glucose unit (Fig. 2). Signal I exhibits hyperfine structure due to the interaction of unpaired electron with nuclear spin of hydrogen ($I = 1/2$) localized at neighboring carbon C_2 . Signal II, without HFS, represents carbon radical not interacting with vicinal hydrogen. The formation of this radical requires simultaneous abstraction of hydrogen at C_1 and dehydration, i.e. removal of H_2O molecule formed by hydrogen atom at C_2 and OH group at C_3 (Fig.2). This process eliminates from the structure hydrogen atom responsible for appearance of HFS.

Similar radicals are generated by heating in the same temperature range the oxidized corn starch [11] and by irradiation with microwaves the native potato and corn starches [10,12]. The content of radical I and radical II in the overall EPR spectrum of native starches depends on botanical origin of the starch and on temperature of heat treatment. After heating at 210°C the amount of radical I in amaranth starch amounts about 10 % whereas in potato starch

over 40 %. With increasing temperature of thermal treatment the content of radical II in all starches increases at the expense of radical I. This effect is caused by the more intensive dehydration of the starch occurring at higher temperatures.

3.2. Cu^{2+} ions as a paramagnetic probe to study the mechanism of radical formation

Interaction of paramagnetic Cu^{2+} ions with the starch matrix leads to the formation of copper complexes coordinating OH groups of the glucose units and water molecules [13]. The EPR parameters of these complexes give information about the changes occurring in the starch structure upon thermal treatment generating the radicals. The mechanism of this process consists on breaking of R-CO-Cu^{2+} bonds and formation of transient $\text{RCO}\cdot$ species active in abstraction of hydrogen from the neighboring C atom of the glucose unit, at which the unpaired electron became localized.

The Cu^{2+} probe was also used for investigation of the distribution of water molecules in the starch granules which underwent freezing and dehydration [14] and to study availability of phosphate groups in the granules of phosphorylated starches [15].

3.3. Effect of pretreatment with high hydrostatic pressure of the starches containing various amounts of amylopectin/amylose

Free radicals were generated thermally in native and high pressure treated waxy maize starch containing almost exclusively amylopectin and Hylon VII containing mostly amylose [16]. Various stable radicals and short living radical species, stabilized by N-tert-butyl- α -phenylnitrone (PBN spin trap), were formed. It was found, that at given experimental conditions waxy maize, i.e. amylopectin, reveals a higher tendency to generate radicals than Hylon VII, containing mostly amylose (Fig. 3). Pretreatment with high pressure resulted in diminishing of the amount of thermally generated stable and short living radicals in comparison to the non pressurized starches (Fig. 3), the effect being more pronounced in waxy maize than in Hylon VII.

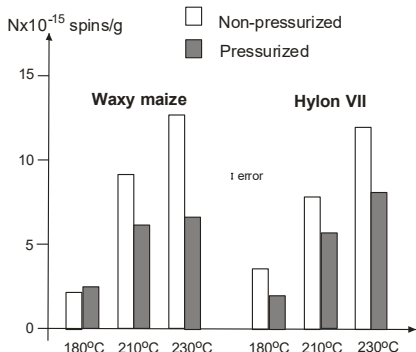


Fig.3. Effect of pretreatment of the starch with high pressure on the number of thermally generated radicals (after [16].radicals)

3.4. Radical processes in chemically modified starches

The number of radicals generated thermally in oxidized potato and corn starch is always higher than in similarly treated native starches [11]. Evidently, transformation of OH groups of the glucose units into carbonyl or carboxyl groups destabilizes the starch structure.

Artificial sweeteners, recommended for diet instead of sucrose in the case of diabetes change in a different way the behaviour of starch during thermal degradation: additives of acesulfam K lead to an increase whereas that of sorbitol to a decrease in the number of thermally generated radicals [17]. The reasons of the opposite behaviour of these two sweeteners are different shape of their molecules and presence (in sorbitol) or absence (in acesulfam K) of the OH groups. Small molecule of sorbitol can easily penetrate the starch structure stabilizing it by using its own OH groups to form hydrogen bonds with glucose units. Acesulfam K does not exhibit any OH group and its heterocyclic ring with sticking out CH₃ group and three double bonded oxygen atoms may damage the elements of the starch structure during penetration. Such defects certainly facilitate formation of radicals.

Modification of the starch by phosphorus with formation of monostarch or distarch phosphates improves some functional properties (gelatinization and pasting behaviour, stability during freeze-thaw cycles, etc.) but simultaneously changes the inclination of the starch to be thermally degraded. Deterioration of the starch structure upon incorporation of phosphorus is more significant for monostarch than for distarch phosphates. In distarch derivatives some crosslinking occurs which stabilizes the structure [18].

4. Conclusions

EPR spectroscopy with Cu²⁺ ions used as a paramagnetic probe is an effective method of detection and characterization of radicals generated thermally in native and modified starches. An insight may be gained into the changes of the starch structure and the mechanism of radical processes induced by various treatments.

Simulation of the spectra allows to identify particular component signals. The factors influencing accessibility and stability of these radical species may be determined. In favorable cases the number and properties of generated centers may be controlled by establishing suitable experimental conditions.

Acknowledgements

This work was partially financed by the Polish Ministry of Education from the grant Nr N N312 103438

References

- [1] O. B. Wurzburg, *Modified starches – properties and uses*. CRS Press Inc., Boca Raton, Florida, 1986.
- [2] P. Tomasik, C. H. Schilling, *Adv. Carbohydr. Chem. Biochem.* 59 (2004) 176-322.
- [3] P. Tomasik, M. Pałasiński, S. Wiejak, *Adv. Carbohydr. Chem. Biochem.* 47 (1989) 203-344.
- [4] C. F. Babbs, *Free Radicals in Biology and Medicine* 8 (1990) 191-200.
- [5] D. Steinberg, *Lancet* 346 (1995) 36-38.
- [6] B.T. Ashok, R. Ali, *Experimental Gerontology* 34 (1999) 293-303.
- [7] K., Dyrek, A. Madej, E. Mazur, A. Rokosz, *Colloids and Surfaces* 45 (1990) 135-144.
- [8] K. Dyrek, A. Rokosz, A. Madej. *Applied Magnetic Resonance* 6 (1994) 309–332.
- [9] T. Spalek, P. Pietrzyk, Z. Sojka, *Journal of Chemical Information and Modelling* 45 (2005)18-29.
- [10] K. Dyrek, E. Bidzińska, M. Łabanowska, T. Fortuna, I. Przetaczek, S. Pietrzyk, *Starch/Stärke* 59 (2007) 318-325.
- [11] E. Bidzińska, K. Dyrek, T. Fortuna, M. Łabanowska, S. Pietrzyk, *Starch/Stärke* 56 (2004) 461-468.
- [12] T. Fortuna, I. Przetaczek, K. Dyrek, E. Bidzińska, M. Łabanowska, *Electronic Journal of Polish Agricultural Universities* 11 (2008) 1-8.
- [13] M. Łabanowska, E. Bidzińska, K. Dyrek, T. Fortuna, S. Pietrzyk, J. Rożnowski, R. P. Socha, *Starch/Stärke* 60 (2008) 134-145.
- [14] M. Łabanowska, E. Bidzińska, K. Dyrek, J. Szymońska, *Biopolymers* 82 (2006) 549 –557.
- [15] A. Blennow, K. Houborg, R. Andersson, E. Bidzińska, K. Dyrek, M. Łabanowska, *Biomacromolecules* 7 (2006) 965-974. [16] W. Błaszczak, E. Bidzińska, K. Dyrek, J. Fornal, E. Wenda, *Carbohydrate Polymers* 74 (2008) 914-921.
- [17] M. Łabanowska, K. Dyrek, E. Bidzińska, T. Fortuna, S. Pietrzyk, I. Przetaczek, J. Rożnowski, R. C. Socha, *Food Sci. Tech. Int.* 15 (4) (2008) 357-365.
- [18] W. Błaszczak, E. Bidzińska, K. Dyrek, J. Fornal, E. Wenda, *Carbohydrate Polymers* (submitted).

EPR of Iron Porphyrins

K. Dziliński*, *T. Kaczmarzyk*, *T. Jackowski*

*Corresponding author: dzil@wip.pcz.pl

Institute of Physics, Częstochowa University of Technology, al. Armii Krajowej 19, 42-200 Częstochowa, Poland

Abstract

EPR study of electronic structure of iron porphyrin complexes containing Fe(III) and Fe(I) ions are reviewed in this paper. It was found that the increase of a number of nitrogen atoms at *meso* positions of Fe(III)-azaporphyrins changes the character of the quantum-mechanically mixed spin state of Fe(III) ions ($S = 5/2, 3/2$) by the increase of the intermediate-spin ($S=3/2$) contribution. Electron configuration of Fe(I)-porphyrins corresponds to the low-spin state and remains unchanged during the *aza*-substitution and interaction with THF solvent. EPR data have been correlated with results of Mössbauer spectroscopy.

Keywords: EPR spectroscopy; iron porphyrins; electronic structure; reduction process

1. Introduction

Metalloporphyrins, in particular iron complexes, perform important functions in many biological processes. Iron porphyrins participate in the biological cycles as the heme prosthetic groups such hemoproteins as hemoglobin and myoglobin as well as some cytochromes, peroxidases and catalases [1]. Iron ions, placed at the centre of the prosthetic groups, play a key role in biological processes which involve hemoproteins. Sufficient background information on the relationship between porphyrin ligand structure and an electronic configuration of the iron ions is provided to form a basis for discussion on the complex bioprocesses. Apart from the biological aspects, the molecular structure and physical properties of iron porphyrins promote these complexes for application in such contemporary technologies as non-linear optics, molecular semiconductors, liquid crystals and so on [2].

It is well known that electron configuration of Fe ion, which is the main reaction center of the iron porphyrins, is sensitive to molecular structure of the surrounding porphyrin and axial ligands. In this paper we report results obtained from EPR spectroscopy for Fe(III)-porphyrins and their *aza*-substituted analogues such as Fe(III)Cl-monoazaetioporphyrin {Fe(III)(Cl)(MAEP)} (Fig. 1a), Fe(III)(Cl)-diazaoctaethylporphyrin {Fe(III)(Cl)(DAOEP)} and Fe(III)(Cl)-teraazaoctaethylporphyrin {Fe(III)(Cl)(TAOEP)} complexes. It also considered results of the reduced forms of the above complexes containing Fe(I) (Fig. 1b) instead of Fe(III) ions. The *aza*-substitution is one of the modifications of the porphyrin macrocycle in which *CH* methine bridges are replaced with nitrogen

atoms (Fig. 1a,b). The nearest surrounding of the Fe(III) as well as Fe(I) ions is the same in the complexes studied and the effect of *meso*-nitrogen atoms on their electron configuration is achieved through the delocalized π -electrons interaction with *d*-orbitals of the iron. Interaction between iron porphyrins and structurally smaller molecules of tetrahydrofuran (THF), which is one of the solvents commonly used in spectroscopic study of porphyrins and metalloporphyrins is also discussed. It has been observed that THF is not an inert solvent in the case of Fe(I) porphyrins.

2. Experimental details

Fe(III)-octaethylporphyrin {Fe(III)(OEP)Cl} complex was synthesized in the same way as it was described in paper [3]. Fe(MAEP)Cl and Fe(DAOEP)Cl were synthesized according to the procedures [4,5]. Reduced complexes were prepared chemically by contact of THF solution with a sodium mirror. THF solvent was carefully degassed by freeze-thaw cycles. Stop wise reduction was controlled by means of electronic absorption spectra. The reduction products are air sensitive and the reaction was carried out on a vacuum line. A special cuvette which contained a vessel where reduction reaction was carried out, a cell for absorption and a quartz tube for EPR spectra, allowed to carry out the reaction in anaerobic conditions. EPR measurements were performed at liquid-nitrogen temperature using a conventional X-band spectrometer, equipped with an IBM PC data acquisition system. EPR parameters were found by fitting the experimental spectra to the theoretical ones using least-squares procedures.

3. Results and discussion

Azaporphyrins may be considered to be structural intermediates between relatively well-studied porphyrins and their structural analogues - phthalocyanines. The azaporphyrins provide excellent examples to explore the subtle effects of ligand structure on the electron configuration of coordinated iron ions in porphyrin complexes. Much can be learned from a comparison of the azaporphyrin spectroscopic characteristics with the ones of related porphyrin structures.

Let's consider F(III)-complexes at first. The electron configuration of Fe(III) ion in chloroiron porphyrins with unsubstituted methine bridges corresponds to the pure high spin state ($S=5/2$) [6,7] while in the case of chloroiron tetraazaporphyrin (four methine bridges substituted by nitrogen atoms) the pure intermediate spin state ($S=3/2$) of the Fe(III) ion has been found [8]. It is interesting to know how electron configuration of Fe-ions changes during successive substitution of the methine bridges by nitrogen atoms.

The typical feature of the EPR spectrum of Fe(III) ions in axial symmetry is an intensive low-field component close to $g_{\perp}=6$ and a less prominent absorption derivative near $g_{\parallel}=2$ (Fig. 1c).

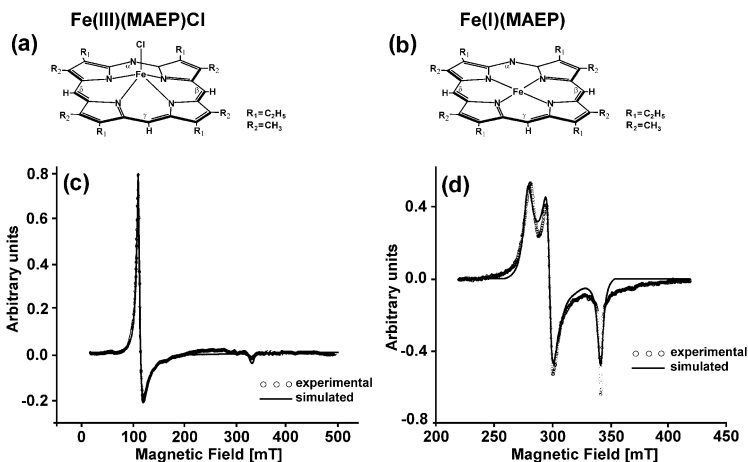


Fig. 1. Molecular structures (a,b) and EPR spectra (c,d) of Fe-monoazaetioporphyrin complexes.

The difference in the intensity of the g_{\perp} and g_{\parallel} components is due to a larger number of molecules with symmetry axes nearly perpendicular to the applied magnetic-field direction (g_{\perp}), that is, molecules with axes approximately in the equatorial plane about the field direction, in comparison with very few molecules with the symmetry axis aligned close to the single field direction (g_{\parallel}). An EPR spectrum of the Fe(MAEP)Cl complex (Fig. 1c) is similar in shape to the spectrum characteristic for high-spin state of the Fe(OEP)Cl one. Numerical analysis of Fe(MAEP)Cl spectrum has shown some splitting of the intensive component with g -factors deviated from the value equal to 6.00. The splitting of the g_{\perp} component indicates slight distortion of axial symmetry in the nearest surrounding of iron(III) ions caused by substitution of the CH methine bridge by nitrogen atom at α position in the case of Fe(III)(MAEP)Cl complex and at α, γ positions in the Fe(III)(DAOEP)Cl one. The distortion of axial symmetry estimated by the E/D ratio on the basis of the simple expression $g_x - g_y = 48E/D$ [6] was found to be marginal and equal to 0.0015 for the Fe(III)(MAEP)Cl complex and 0.0035 for the Fe(III)(DAOEP)Cl (maximum E/D value equal to 0.33 corresponds to ‘pure’ rhombic symmetry).

It was found [9,10] that the increase of a number of nitrogen atoms at *meso*-positions leads to the increase of the intermediate ($S=3/2$) contribution to the quantum-mechanically mixed spin states ($S=5/2, 3/2$) of Fe(III) ions. This feature is reflected in EPR spectra by the shift of the g_{\perp} values from $g_{\perp} = 6.0$, characteristic for the pure high-spin state ($S=5/2$), towards the value $g_{\perp} \cong 4$, characteristic for the pure intermediate ($S=3/2$) spin state. A contribution of the intermediate spin component ($S = 3/2$) to the quantum mechanically mixed spin

state ($S = 5/2, 3/2$), estimated on the basis of the Maltempo model [11] is equal to about 5% for Fe(III)(MAEP)Cl and 8% for Fe(III)(DAOEP)Cl. Comparing g_{\perp} values for Fe(III)(OEP)Cl and Fe(III)(TAOEP)Cl with the corresponding g_{\perp} factors for the partly substituted iron(III) complexes of the azaporphyrins one can conclude that there is no simple relationship between mixed spin-state character estimated on the basis of the g_{\perp} values and a number of methine CH groups replaced by nitrogen atoms.

It should be noted that an additional hyperfine structure in the form of three intensive lines and a complex hyperfine structure in the form of many low-intensity lines were observed in EPR spectrum of Fe(III)(Cl)(DAOEP) instead of the single weak-intensity line observed near $g_{//} = 2$ in EPR spectrum of Fe(III)(Cl)(MAEP). The elemental analysis of the Fe(III)(Cl)(DAOEP) complex suggests that a dimethylamine radical $(CH_3)_2N^{\cdot}$ was bonded to the porphyrin ligand during the synthesis of this complex. The three intensive lines belong to the nitrogen atom. These lines are detectable at room temperature in contrary to the hyperfine lines of the relatively low intensity which appear in the EPR spectrum at about 220 K. The low-intensity hyperfine structure can be detected to the moment when the sample is frozen. When the sample was thaw and next again frozen the relative intensity of the lines was significantly changed while the intensity of the three former intensive lines remains the same. It suggests that the hyperfine structure with the three intensive lines can be assigned to one paramagnetic centre while the low-intensity lines have to be attributed to many centres. The changeable form of this part of the EPR spectrum indicates that the hyperfine-interaction lines correspond to some statistically average orientation of CH_3 groups with respect to the Fe(III) ion. We suppose that the observed hyperfine structure is a result of the overlapping of a great number of spectra with somewhat different hyperfine splittings from local orientations of CH_3 groups in relation to d_{xz} and d_{yz} orbitals of the Fe(III) ion containing unpaired electrons. In such a case numerical simulation of this hyperfine structure is rather impossible.

Let's consider now the Fe(I)-porphyrins. At the first stage of the reduction process divalent Fe(II)-porphyrins are generated which can be diamagnetic or paramagnetic with integer spins. Because of large magnitude of the resulting zero-field splitting in the integer-spin Fe(II) ions, there are no allowed EPR transitions in the field range and microwave frequency available to conventional spectrometers and Fe(II) complexes will not be considered in this paper. The next step of the reduction process leads to Fe(I)-porphyrins. Characteristic feature of Fe(I)-porphyrin EPR spectra is relatively intensive $g_{//}$ component (Fig. 1d). EPR spectra of the Fe(I)-azaporphyrins are similar in shape and parameters to the spectrum of the unsubstituted Fe(I)(OEP). It means that the electron configuration of Fe(I) ions coordinated to the mono- and diazaporphyrins correspond to the low-spin state ($S=1/2$) as it was established

for unsubstituted Fe(I)-porphyrins. In the low-spin Fe(I) systems the deviation of g_{\perp} factor from 2.0 is dependent on the inverse of separation between 2A ground state and the nearest 2E excited state [12]. Comparing the g_{\perp} values for unsubstituted Fe(I)(OEP) with the average value of g_x and g_y for the Fe(I)-azaporphyrins one can notice that this separation slightly decreases with an increasing number of nitrogens at *meso* positions. EPR spectra of the Fe(I)-porphyrins in THF solution show a low-intensity hyperfine structure similar to that observed in the case of the Fe(III)(Cl)(DAOEP) complex but there is not observed hyperfine structure from a nitrogen ion. We suggest that hyperfine structure in Fe(I)-porphyrin spectra can be connected with interaction of unpaired electron with protons of THF molecules. Such an explanation indicates that one or two THF molecules can be bonded to Fe(I) ion. Pure form of the Fe(I) EPR spectrum (without this hyperfine structure) recorded for Fe(I)(MAEP) in DME solution (Fig. 1d) confirms the above suggestion. It should be noted that THF bonded to the Fe(I)-porphyrins does not change the electron configuration of the Fe(I) ion, in contrary to Fe(II) ions. The EPR signal exhibits noticeable rhombicity caused by distortion of axial symmetry in the *aza*-porphyrins.

The EPR results correlate with Mössbauer data for the complexes studied.

4. Conclusions

In conclusion, it should be underlined that the quantum-mechanically mixed spin state of Fe(III) ions in the azaporphyrins changes with the increase of a number of nitrogen atoms at *meso* positions of the porphyrin ring. It suggests interaction between π -electrons of the porphyrin ligand and *d*-orbital electrons of the iron ion. The electron configuration of Fe(I) ions in the unsubstituted porphyrins and the *aza*-substituted ones corresponds to the low-spin state which is not sensitive to the interaction with THF molecules.

Acknowledgements

The authors would like to thank A.M. Shulga from the Institute of Molecular and Atomic Physics Belarus Academy of Sciences for synthesis of the Fe(III)-azaporphyrin complexes.

References

- [1] K.M. Kadish, K.M. Smith, G. Guilard (Eds.), The porphyrin handbook, vol 11: Bioinorganic and bioorganic chemistry, 1st ed. Academic Press, Amsterdam, 2003.
- [2] K.M. Kadish, K.M. Smith, G. Guilard (Eds), The porphyrin handbook, vol 6: Applications: Past, present and future, 1st ed. Academic Press, San Diego, 2000.
- [3] D. Dolphin, J.R. Sams, T.B. Tsin and K.L. Wong, J. Am. Chem. Soc. 98 (1976) 6970.
- [4] A.D. Adler, F.L. Longo, F. Kampas, J. Kim, Inorg. Nucl. Chem. 32 (1970) 2443.
- [5] J. Engel, A. Gossauer, A.W. Johnson, J. Chem. Soc., Perkin Trans. I, (1978) 871.

- [6] G.Pamler. in: *Iron Porphyrins, Part I*, A.B.P. Lever Gray, (Eds.), London- Tokyo: Addison-Wesley Publishing Company, Inc. 1983, p. 64.
- [7] D. Lexa, M. Momenteau, J.Mispelter, *Biochim. Biophys. Acta*, 338 (1974) 151.
- [8] J.P. Fitzgerald, B.S. Hagerty, A.R. Rheingold, L. May, G.A. Brewer, *Inorg. Chem.*, 31 (1992) 2006.
- [9] K. Dziliński, T. Kaczmarzyk, G.N. Sinyakov, G.D. Egorova, *Mol. Phys. Reports* 34/2 (2001) 65.
- [10] K. Dziliński, T. Kaczmarzyk, T. Jackowski, G.N.Sinyakov and G.D. Egorova”, *Mol. Phys. Reports*, 37 (2003) 35.
- [11] M.M. Maltempo and T.H. Moss, *Quart.Rev.Biophys.*, 9 (1976) 181.
- [12] K. Yamaguchi and I. Morishima, *Inorg. Chem.*, 31 (1992) 3216.

Metoda optycznie detektowanego rezonansu magnetycznego do badań struktur półprzewodników półmagnetycznych

Marek Godlewski

*Instytut Fizyki Polskiej Akademii Nauk, 02-668 Warszawa, Al. Lotników 32/46,
Wydz. Matematyczno Przyrodniczy Szkoła Nauk Ścisłych, UKSW, Warszawa*

W referacie omówię podstawy dwóch technik optycznie detektowanego rezonansu magnetycznego (ODMR) i cyklotronowego (ODCR). Obie te techniki pomiarowe są rozwijane przez nas w Instytucie Fizyki PAN od wielu lat. Następnie opiszę zastosowanie obu tych technik do badania procesów rekombinacji promienistej, niepromienistej i dynamiki oddziaływań spinowych w materiałach do zastosowań spintronicznych tzw. półprzewodnikach półmagnetycznych (DMS). Omówię wyniki badań dla dwóch z tych materiałów – ZnMnS i CdMnTe, dla kryształów, studni kwantowych i nanocząstek.

W oparciu o wyniki badań dla tych dwóch materiałów omówię mechanizmy optycznej detekcji rezonansu ESR jonów manganu. W szczególności wyjaśnię jaką informację możemy otrzymać z tych badań o oddziaływaniach Mn-nośnik. Te badania pozwoliły nam wyjaśnić obecność ultra-szybkich składowych zaniku luminescencji jonów manganu w nanocząstkach ZnMnS.

Na końcu referatu wprowadzę opracowaną przez nas technikę rozdzielczo-czasowego ODMR. Tego typu pomiary umożliwiają nam bezpośrednio wyznaczenie czasów rekombinacji spinowej w badanych materiałach DMS.

FMR study of magnetic nanoparticles embedded in non-magnetic matrices

N. Guskos^{1,2}, J. Typek², and G. Żołnierkiewicz²

¹Solid State Section, Department of Physics, University of Athens, Panepistimiopolis, 15 784 Zografos, Greece

²Institute of Physics, West Pomeranian University of Technology, Al. Piastów 48, 70-311 Szczecin, Poland

Abstract

Samples containing small amounts of fine magnetic particles (α -Fe/C, Fe₃C/C, γ -Fe₂O₃, Fe₃O₄ and Ni/C) embedded in various non-magnetic matrices, such as polymer, concrete or wax, have been studied by using the ferromagnetic resonance (FMR) method in the 4–300 K temperature range. Generally, an intense magnetic resonance line was recorded at all temperatures. All FMR parameters strongly depends on temperature, reflecting reliance on dynamic processes influenced by concentration of magnetic nanoparticles, agglomeration state, type of matrix characterized by its physical properties (critical points) and the kind of used fine particles. The temperature gradient of the resonance field, ($\Delta H_r/\Delta T$), was introduced that is connected with the reorientation processes of a correlated spin system. The value of this parameter usually increases over one order of magnitude in low temperatures range and straightforwardly shows matrix's phase transitions, e.g. to a spin glass state or other freezing processes present in the matrix. It is believed that after large statistics of experimental data is collected it could be a useful and simple method of characterization of different type of materials.

1. Introduction

The oxides containing 3d transition metals with their strongly correlated spin system are the subject of intense studies for many years. Electronic and magnetic properties of fine magnetic particles embedded at low concentration in different non-magnetic matrices could be used for manufacturing of new generations of functional materials [1-10]. Small amount of iron or iron oxide magnetic nanoparticles embedded in a non-magnetic matrix could be a very sensitive indicator of the dipole-dipole interaction [2,6,10,11]. It was shown that a small amount of nanoparticles could change essentially the melting and polymer-glass transition temperatures [10,12,13]. The resonance field (H_r) vs. temperature dependence ($\Delta H_r/\Delta T$ gradient) has shown a very intense change which could be associated with the spin reorientation processes inside the matrix. Interestingly, for similar matrices a drastically different behavior was observed for different kind of magnetic nanoparticles [14]. Theoretically it could be described well by using magnetization dynamics in Landau-Lifshitz-Gilbert formulation [15].

The aim of this report is to review works of our group devoted to the study of small concentration of magnetic nanoparticles used as a filler in different non-

magnetic matrices. We are interested in magnetic properties of the resulting nanocomposites by registering ferromagnetic resonance (FMR) spectra and static magnetization at various temperatures. The concentration dependence of magnetic properties at different temperatures could be very useful for better understanding of the reorientation processes and matrix influences *via* magnetic dipole-dipole interaction at the nanosize scale. These experimental data could also be very valuable for those working in application of the functional materials.

2. Results and discussion

Figures 1 and 2 present FMR spectra of small amounts of magnetic nanoparticles in different agglomerated states in non-magnetic matrices (in this case polymers). Strong magnetic correlated spin system in agglomerated state (α -Fe, Fe₃C) produces a broad, intense and strongly shifted FMR line (Fig. 2c). The ferromagnetic coupled system γ -Fe₂O₃ in a different agglomerated state displays a very intense resonance FMR line (Fig. 1a and b) with about two times smaller linewidth that shifts with decreasing temperature what is especially evident at low temperatures (Fig. 1c). The temperature dependence of the FMR spectrum is essentially different for small and large in size agglomerates. The very small concentration of magnetic nanoparticles Ni/C (Ni is covered by carbon) has shown a very intense line with about two times smaller value of the linewidth than sample with γ -Fe₂O₃. A strongly shifted resonance line is seen at low temperatures (Fig. 1c and Fig. 2b).

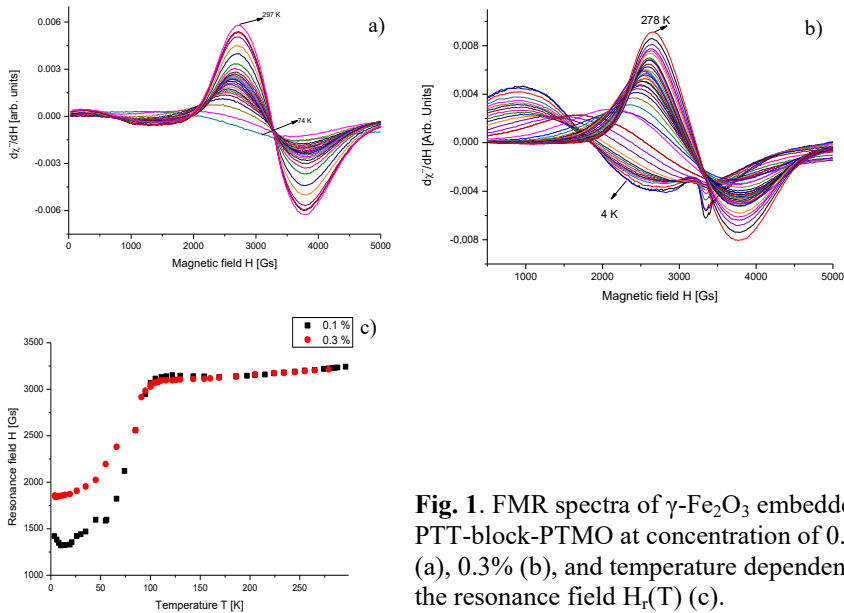


Fig. 1. FMR spectra of γ -Fe₂O₃ embedded in PTT-block-PTMO at concentration of 0.1% (a), 0.3% (b), and temperature dependence of the resonance field $H_r(T)$ (c).

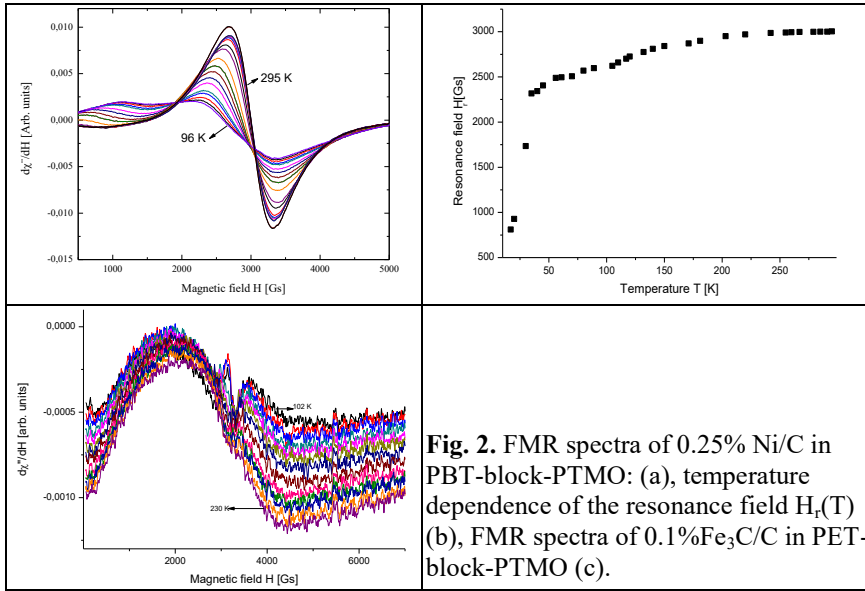


Fig. 2. FMR spectra of 0.25% Ni/C in PBT-block-PTMO: (a), temperature dependence of the resonance field $H_r(T)$ (b), FMR spectra of 0.1%Fe₃C/C in PET-block-PTMO (c).

The blocking temperature is higher for samples with smaller sizes of agglomerates of magnetic nanoparticles. It could be deduced from the temperature dependence of the dc magnetic susceptibility observed for small values of applied magnetic field [6].

In this report we concentrate on newly introduced FMR parameter, $\Delta H_r/\Delta T$, which plays a very important role in the reorientation processes of a correlated spin system. The resonance condition strongly depends on internal magnetic field formed by a coupled spin system. The resonance condition is the following: $h\nu = g\mu_B(H_0 - H')$, where $H' = H_{dem} + H_{dip}(\text{inter-agglomerate}) + H_{dip}(\text{intra-agglomerate})$. Macroscopic size of an agglomerate produces the gradient $\Delta H_r/\Delta T \sim 0.08$ mT/K [16] which is similar to the value measured for an assemble of many smaller agglomerates in the high temperature range (see Table 1). On the other hand, very small agglomerates of Ni has produced greater value and the dipole interaction that could influence the value of an internal magnetic field. The same character is observed for low temperatures (Table 1). These processes could be very important in changing the physical properties of a matrix, especially could shifts the critical point in the polymer, e.g. melting, and α -, β -, γ -relaxations [10,12]. Magnetic nanoparticles at small concentration could form an additional bonding term which might shift the melting point to higher temperatures. They could also change significantly the mechanical properties of concrete [17].

Table 1. The values of the $\Delta H_r/\Delta T$ for Ni/C in PBT-block-PTMO(I) and Fe₂O₃ in PET-block-PTMO (II) and PTT-block-PTMO (III) (for solution and solid magnetic nanoparticles with greater sizes of agglomerates - Fe₂O₃).

Sample designation	$\Delta H_r/\Delta T_{(<160\text{ K})}$ [mT/K]	$\Delta H_r/\Delta T_{(160-95\text{ K})}$ [mT/K]	$\Delta H_r/\Delta T_{(70-50\text{ K})}$ [mT/K]	$\Delta H_r/\Delta T_{(>41\text{ K})}$ [mT/K]	Reference
0.1% Ni/C-I	0.13(1)	0.95(1)	0	6.56(2)	[11]
0.25% Ni/C-I	0.12(1)	0.14(1)	0.34(1)	6.15(2)	[13]
0.1% Fe ₂ O ₃ -II	0.002(1)	0.002(1)	0.08(1)	0.08(1)	[6]
0.3% Fe ₂ O ₃ -II	0.13(1)	0.13(1)	0.65(1)	0.65(1)	[6]
0.1% -Fe ₂ O ₃ -II	0.007(3)	0.007(3)	0.09(1)	0.09(1)	[6]
0.3% -Fe ₂ O ₃ -II	0.07(1)	0.07(1)	0.79(1)	0.79(1)	[6]
0.1%- Fe ₂ O ₃ -III	0.058(5)	0.058(5)	3.5(1)	0.98(7)	[6]
0.3%- Fe ₂ O ₃ -III	0.078(5)	0.078(5)	1.9(2)	0.57(3)	[6]

In summary, the FMR method could be a very important tool for characterization of different materials. Addition of small amount of magnetic nanoparticles could change the physical properties of a doped matrix. This method could be more useful if large sets of experimental data are collected.

References

- [1]. J. L. Dorman, D. Fiorani, and E. Troc, *Adv. Chem. Phys.* **98**, 1770 (1997).
- [2]. Y. A. Koksharov, S. P. Gubin, I. D. Kosobudsky, G. Y. Yurkov, D. A. Pankratov, L. A. Ponomarenko, M. G. Mikheev, M. Beltran, Y. Khodorkovsky, and A. M. Tishin, *Phys. Rev. B* **63**, 012407 (2000).
- [3]. V. Skumryev, S. Stoyanov, Y. Yong Zhang, G. Hadjipanayis, D. Givord, and J. Noguez, *Nature* **423**, 850 (2003).
- [4]. C. C. Berry and A. S. G. Curtis, *J. Phys. D* **36**, R198 (2003).
- [5]. P. Dutta, A. Manivannan, M. S. Seehra, N. Shah, and G. P. Huffman, *Phys. Rev. B* **70**, 174428 (2004).
- [6]. N. Guskos, S. Glenis, V. Likodimos, J. Typek, M. Maryniak, Z. Roslaniec, M. Kwiatkowska, M. Baran, R. Szymczak, and D. Petridis, *J. Appl. Phys.* **99**, 084307 (2006); N. Guskos, V. Likodimos, S. Glenis, M. Maryniak, M. Baran, R. Szymczak, Z. Roslaniec, M. Kwiatkowska, and D. Petridis, *J. Nanosci. Nanotech.* **8**, 2127 (2008); N. Guskos, M. Maryniak, J. Typek, A. Guskos, R. Szymczak, E. Senderek, Z. Roslaniec, D. Petridis, and K. Aidinis, *J. Non Cryst. Solids.* **354**, 4401 (2008); N. Guskos, M. Maryniak, G. Zolnierkiewicz, J. Typek, A. Guskos, E. Senderek, Z. Roslaniec, and D. Petridis, *Appl. Mag. Res.* **34**, 175 (2008).
- [7]. A.A. Zezin, V.I. Feldman, N.A. Shmakova, S.P. Valueva, V.K. Ivanchenko, N.I. Nikanorova, *Nuclear Instruments and Methods in Physics Research B* **265**, 334 (2007).
- [8]. V. Castel, J. B. Youssef, and C Brosseau, *Journal of Nanomaterials* 27437 (2007).
- [9]. Y. Tang, D. Zhao, D. Shen, J. Zhang, B. Li, Y. Lu, and X. Fan, *Thin Solid Films* **516**, 2094 (2008).
- [10]. M. Maryniak, N. Guskos, J. Typek, A. Guskos, K. Goracy, Z. Roslaniec, M. Kwiatkowska, *Polimery (Poland)* **54**, 546 (2009).
- [11]. N. Guskos, M. Maryniak, J. Typek, P. Podsiadly, U. Narkiewicz, E. Senderek, and Z. Roslaniec, *J. Non-Cryst. Solids* **355**, 1400 (2009).

- [12]. J. Majszczyk, N. Guskos, J. Typek, M. Maryniak, Z. Roslaniec, M. Kwiatkowska, and D. Petridis, *J. Non-Cryst. Solid* **352**, 4279 (2006).
- [13]. N. Guskos, J. Typek, B.V. Padlyak, Yu.K. Gorelenko, I. Pelech, U. Narkiewicz, E. Senderek, A. Guskos, and Z. Roslaniec, submitted for publication in *J. Non-Cryst. Solids*.
- [14]. U. Narkiewicz, N. Guskos, W. Arabczyk, J. Typek, T. Bodziony, W. Konicki, G. Gąsiorek, I. Kucharewicz and E. Anagnostakis, *Carbon* **42**, 1127 (2004); N. Guskos, E. A. Anagnostakis, V. Likodimos, J. Typek, M. Maryniak, U. Narkiewicz, *J. Appl. Phys.* **97**, 0204304 (2005); N. Guskos, J. Typek, M. Maryniak, U. Narkiewicz, W. Arabczyk, and I. Kucharewicz, *J. Phys.: Conference Series* **10**, 151 (2005); N. Guskos, J. Typek, T. Bodziony, Z. Roslaniec, U. Narkiewicz, M. Kwiatkowska, and M. Maryniak, *Rev. Adv. Mat. Sci.* **12**, 133 (2006).
- [15]. M. R. Dudek, N. Guskos, B. Grabies, and M. Maryniak, *J. Non-Cryst. Solids* **354**, 4146 (2008).
- [16]. N. Guskos, G. Zolnierkiewicz, J. Typek, A. Guskos, Z. Czech, and A. Mickiewicz, *Rev. Adv. Mat. Sci.* **23** (2010).
- [17]. J. Blyszko, W. Kiernozycki, N. Guskos, G. Zolnierkiewicz, J. Typek, U. Narkiewicz, and M. Podsiadly, *J. Non-Cryst. Solids*. **354**, 4515 (2008).

EPR Study of Phase Transitions in DMAAIS and DMAGaS Crystals

R. Hrabanski*¹⁾, M. Jackowska¹⁾, Z. Czaplak²⁾

*Corresponding author: hrab@wip.pcz.pl

¹⁾ Institute of Physics, Czestochowa University of Technology, Czestochowa, Poland

²⁾ Institute of Experimental Physics, University of Wroclaw, Wroclaw, Poland

Abstract

X-band electron paramagnetic resonance (EPR) investigations of single crystals of Cr³⁺-doped dimethylammonium aluminium sulphate hexahydrate (DMAAIS) and dimethylammonium gallium sulphate hexahydrate (DMAGaS) are presented in paraelectric and ferroelectric phases. Both crystal undergoes an order-disorder phase transition to ferroelectric phase at T_{C1}=152 K and T_{C1}=134 K, respectively. Additionally, DMAGaS shows at T_{C2} = 116 K a further first-order transition into an intermediate non-ferroelectric phase before it becomes antiferroelectric at T_{C3}= 60 K. The rotation pattern of the spectra show in the ferroelectric phase two chemically and magnetically equivalent Al and Ga sites in unit cell, which can be substituted by Cr³⁺ ions. The spin Hamiltonian parameters and the positions of the principal axes of the zero field splitting tensors have been determined and compare their values for the both crystals.

Keywords: EPR, order-disorder, ferroelectrics, antiferroelectric, phase transition

2. Introduction

The crystal structure of dimethylammonium aluminium sulfate hexahydrate (DMAAIS) (CH₃)₂NH₂Al(SO₄)₂·6H₂O and the isomorphic gallium dimethylammonium sulfate hexahydrate (DMAGaS) is built up of Al or Ga cations coordinating six water molecules, regular SO₄ tetrahedra and [(CH₃)₂NH₂]⁺ (DMA) cations, all hydrogen bonded to a three dimensional framework [1-4]. Both crystals are ferroelastic in the paraelectric phase and showing the monoclinic space group P2₁/n. Both of them exhibit an order-disorder type transition into a ferroelectric phase at T_{C1} = 152 K and T_{C1} = 134 K, respectively. Additionally, only DMAGaS shows at T_{C2} = 116 K a further first-order transition into an intermediate non-ferroelectric phase before it becomes antiferroelectric at T_{C3}= 60 K. The reason for this different behaviour of DMAAIS and DMAGaS is not yet fully understood. The ferroelectric transition is associated with the polar DMA cations, which execute hindered rotations in the ferroelastic phase and order partly in the ferroelectric phase. The intermediate phase seems to be modulated with tremendous disorder in a DMA cation system.

Crystals of DMAAIS and DMAGaS have been widely studied with different experimental methods [1-20]. In particular, magnetic resonance

methods have already been employed in studies of the phase transitions in both systems [10-20]. In the present paper we report on the EPR measurements of chromium doped DMAAIS and DMAGaS performed in the X-band (~ 9.5 GHz) in the temperature range from room temperature (RT) down to liquid helium temperature. The rotation pattern of the spectra both in paraelectric, ferroelectric and antiferroelectric phases of both crystals are studied in detail and compared. The influence of the arrangements of the polar DMA units on the line shape of EPR spectra in high temperature polar and low temperature non-polar phases is shortly discussed.

3. Experimental details

Chromium-doped DMAAIS and DMAGaS single crystals were grown from aqueous solution containing 1 mol % $\text{Cr}_2(\text{SO}_4)_3 \cdot 18\text{H}_2\text{O}$. The trivalent chromium ions with the electron configuration $3d^3$ substitute statistically at aluminium and gallium sites. The paramagnetic chromium ions are very sensitive probes on the slight changes of their environment.

EPR measurements were performed in the X-band (9.5 GHz) with standard spectrometers, equipped with a sample cavity of TE_{102} mode and 100 kHz modulations. Most of the spectra were recorded with the spectrometer, which was interfaced with a microcomputer via USB port for controlling the instrument, acquisition and display of the acquired spectra.

A goniometer sample holder provided the rotation of the sample ($\pm 0.5^\circ$) about the given vertical axis. The rectangular laboratory xyz axes frame chosen for the angle-dependent measurements was related to the **a**, **b**, **c** crystallographic monoclinic axes [3] as follows: $x \parallel \mathbf{a}^*$, $y \parallel \mathbf{b}$, $z \parallel \mathbf{c}$, where $\mathbf{a}^* = \mathbf{b} \times \mathbf{c}$. The spectra were recorded by varying the orientation of the external magnetic field in a given plane at 5° angle intervals. The temperature of the sample was established by regulation the temperature of the cooling gas streaming around the sample and was controlled by usage of Wildmad and Oxford Instrument cryostats with an accuracy of relative and absolute temperature values of 0.1 and 1 K, respectively.

4. Results and discussion

Angular dependences of the EPR spectra were studied at paraelectric and ferroelectric phases in three planes perpendicular to the \mathbf{a}^* -, **b**- and **c**-axes, respectively. The rotation patterns taken in the $\mathbf{a}^*\mathbf{b}$, \mathbf{cb} and \mathbf{ca} planes for paraelectric and ferroelectric phases in DMAAIS are shown in Figs. 1. The rotation pattern of the spectra show in both phases of both crystals two magnetically equivalent sets of lines in accordance with two chemically equivalent Al sites in a unit cell, which can be substituted by Cr^{3+} ions. For the each set, three allowed ($\Delta M_s = \pm 1$) and three quasi-forbidden transitions ($\Delta M_s =$

± 2 and ± 3) between the four spin states $3/2$, $1/2$, $-1/2$ and $-3/2$, due to the effective spin quantum number $S = 3/2$, were clearly identified in the each plane. The quasi-forbidden transitions are not shown in the figures. The spectra can be described by means of the spin Hamiltonian (SH):

$$\hat{H} = \beta \mathbf{B} \cdot \mathbf{g} \cdot \mathbf{S} + \frac{1}{3} (b_2^0 O_2^0 + b_2^2 O_2^2) \quad (1)$$

where S is the electron spin operator of the Cr^{3+} ion, β is the Bohr magneton, B is the external magnetic field, g is the spectroscopic splitting tensor and the $b_n^m O_n^m$ terms represent crystal field contributions. The SH parameters were calculated with exact diagonalization of the energy matrices using a computer program provided by V.G. Grachev [21]. In the literature the zero-field splitting parameters D and E are often used and are related to b_n^m as $D = b_2^0$ and $E = b_2^2/3$. A procedure used for determination SH parameters was as follows. First, a least-squares fitting performed for the three planes studied leads to all b_n^m parameters ($b_2^1, b_2^{-1}, b_2^{-2}$ have to be added for general orientation). The symmetric crystal field splitting tensor (usually $S \cdot D \cdot S$ term in SH) can readily be identified with the b_n^m parameters through the following relations: $D_{xx} = (-1/3)(b_2^0 - b_2^2)$, $D_{yy} = (-1/3)(b_2^0 + b_2^2)$, $D_{zz} = (2/3)b_2^0$, $D_{xy} = (1/3)b_2^{-2}$, $D_{xz} = (1/6)b_2^1$, $D_{yz} = (1/6)b_2^{-1}$. The matrix D was then diagonalized and the principal values of fine-structure tensor D_{xx} , D_{yy} , D_{zz} and eigenvectors (the direction cosines) corresponding to the tensor principal axes X, Y, Z with respect to the laboratory the system x, y, z were obtained. The principal values of the fine structure tensor give the values of b_2^0 and b_2^2 parameters of SH (1). The procedure described above was used for analyses of the X-band experimental results obtained in paraelectric and ferroelectric phases. The SH parameters determined for both phases are listed in table 1. There is a very good agreement between the experimental line positions and the theoretical ones calculated by the use of optimized SH parameters.

Table 1. Spin-Hamiltonian parameters for Cr^{3+} in paraelectric (RT) and ferroelectric phases of DMAAIS and DMAGaS. Zero field splitting parameters are in 10^{-4} cm^{-1} .

Crystal	Temperature	g	b_2^0	b_2^2	Reference
DMAAIS	RT	1.980±0.003	950±15	198±10	[17]
	108 K	1.980±0.005	1133±15	214±10	[17]
DMAGaS	RT	1.982±0.002	890±15	386±15	[20]
	125 K	1.982±0.002	1088±15	39±15	[20]
	40 K	1.976	1425	1120	[20]

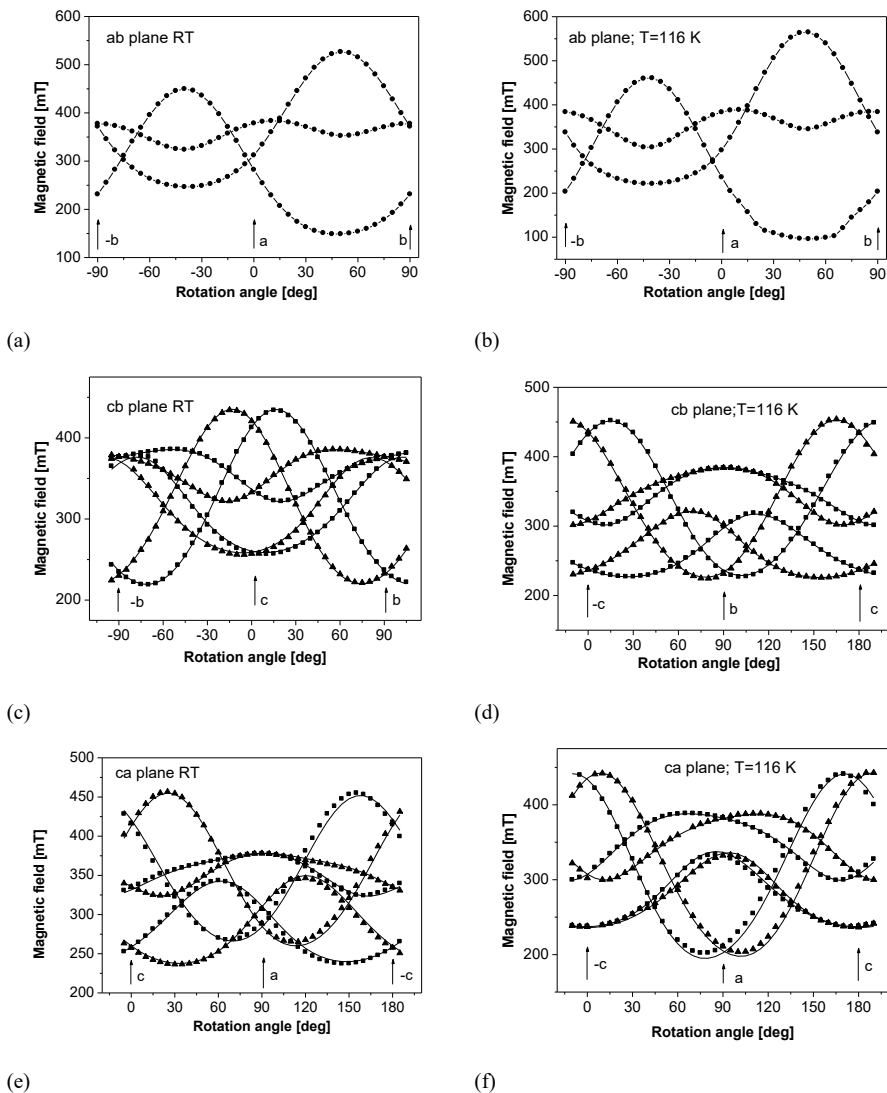


Figure 1. The angular dependence of the Cr^{3+} EPR spectra in the paraelectric phase in DMAAIS at X-band: (a) in ferroelastic phase at RT and (b) in ferroelectric phase at 116 K. Closed circles and triangles represent the experimental data of two different sets of the fine structure lines. The solid lines show the fit result with the parameters given in table 1.

Our experiments showed that no difference occurred between the fine structure parameters of two sites within the experimental errors for both system studied. The structural data indicates that six water molecules arranged in

slightly disordered octahedral array surround each Cr^{3+} ions. The changes are seen both in the SH parameters themselves and also in the positions of the principal axes of the zero field splitting tensor if we compare their values in the both phases. The direction cosines of this tensor for DMAAIS crystal are given in table 2.

Table 2. Direction cosines of I and II site of Cr^{3+} ions in DMAAIS at RT.

Site	Principal axes of the complex	Direction cosines		
		x	y	z
I, II	X_I, X_{II}	± 0.385	± 0.555	0.738
	Y_I, Y_{II}	0.673	± 0.378	± 0.635
	Z_I, Z_{II}	0.631	0.740	± 0.228

The temperature dependence of EPR spectra was studied from RT down to liquid helium temperature. Both in DMAAIS and in DMAGaS, a strong broadening and then a line tripling is observed already in the ferroelastic phase far above phase transition. The satellites of these triplets disappear in the ferroelectric phase and lines narrow drastically on lowering the temperature. The appearance of triplets in the vicinity of ferroelectric phase transition was explained taking into account the influence of four possible configuration of two neighbouring DMA groups on the water octahedron with the chromium probes substitution at the aluminium and gallium sites [11]. At the temperature $T_{C2} = 116$ K crystal DMAGaS undergoes phase transition into the non-ferroelectric low-temperature phase, the spectrum abruptly changes associated with large shifts of line positions, striking line broadening and multiplication of the number of lines. Völkel et. al. [16] have studied DMAGaS at Q-band below $T_{C2} = 116$ K and explained the temperature behaviour of the spectra assuming the existence of a modulated phase in the crystal with commensurate regions and discommensurations before it becomes antiferroelectric at $T_{C3} = 60$ K. A modulation of the DMA order parameter has been postulated along the DMA–Ga(H₂O)₆–DMA direction.

References

- [1] L.F. Kirpichnikova, A. Pietraszko, K. Lukaszewicz., L.A. Shuvalov, V.V. Dolbinina L.M. Yakovleva. *Crystallogr. Rep.* 39 (1994) 990.
- [2] L.F. Kirpichnikova, L.A. Shuvalov. N.R Ivanov., B.N. Prasolov, E. F Andreyev, *Ferroelectrics* 96 (1989) 313.
- [3] A. Pietraszko, K. Lukaszewicz and L.F. Kirpichnikova, *Polish J. Chem.* 67 (1993) 1877.
- [4] A. Pietraszko, K. Lukaszewicz and L.F. Kirpichnikova, *Polish J. Chem.* 69 (1995) 922.

- [5] V. Kapustianik, M. Bublyk, I. Polovinko, S. Sveleba, Z. Trybula and E. Andreyev, *Phase Transitions*, 49 (1994) 231.
- [6] V. Kapustianik, M. Fally, H. Kabelka and H. Warhanek, *J. Phys. Condens. Matter* 9 (1997) 723.
- [7] S. Dacko and Z. Czapla, *Ferroelectrics* 189 (1996) 143.
- [8] V.Yu. Kazimirov, V.A. Sarin, M.B. Smirnov, L.A. Shuvalov, *Ferroelectrics* 299 (2004) 59.
- [9] V. Stasyuk and O.V. Velychko, *Phase Transitions* 73 (2001) 483.
- [10] N. Alsabbagh, D. Michel, Z. Czapla and J. Furtak, *Phys. Stat. Sol. A* 167 (1998) 77.
- [11] G.Völkel, N. Alsabbagh, R. Böttcher, D. Michel, B. Milsch, Z. Czapla and J. Furtak, *J. Phys. Condens. Matter* 12 (2000) 4553.
- [12] G.Völkel, R. Böttcher, Z. Czapla D. Michel, *Ferroelectrics* 268 (2002) 181.
- [13] W. Bednarski, S. Waplak and L.F. Kirpichnikova, *J. Phys. Condens. Matter* 11 (1999) 1567.
- [14] J. Dolinšek, M. Klanjšek, D. Arčon, Hae Jin Kim, J. Seliger, V. Žagar, *Phys. Rev. B* 59 (1999) 3640
- [15] G. Völkel, R. Böttcher, D. Michel, Z. Czapla, *Phys. Rev. B* 67 (2003) 24111.
- [16] G. Völkel, R. Böttcher, D. Michel, Z. Czapla and J. Banys, *J. Phys. Condens. Matter* 17 (2005) 4511
- [17] R. Hrabanski, M. Janiec, M. Jackowska and V. Kapustianik, *Ferroelectrics*, 291, (2003) 241.
- [18] R. Hrabanski, M. Janiec, V. Kapustianik, *Appl. Magn. Reson.* 27 (2004) 19.
- [19] R. Hrabanski, M. Janiec-Mateja, Z. Czapla, *Acta Phys. Pol.* 108 (2005) 283
- [20] R. Hrabanski, M. Janiec-Mateja and Z. Czapla, *Phase Transitions*, 80 (2007) 163.
- [21] V.G. Grachev, *Visual EPR program v. 2.08*, Osnabrück: Fachbereich Physik, Universität Osnabrück 1998.

Spin trapping and radical scavenging methods in studies of bioglycerol

Maria Jerzykiewicz

mariaj@wchuwr.pl

Faculty of Chemistry, Wroclaw University

Abstract

Bioglycerol - 1,2,3-propanetriol consisting fractions from biodiesel production- was examined towards its antioxidant activity. All investigated glycerol fractions (GF) exhibited high, in comparison with biodiesel and oil (origin material), free radical scavenging properties. Free radical scavenging activity measured by EPR spectroscopy paralleled standard antioxidant/anticorrosive investigations (Herbert Test, Folin-Ciocalteu method).

Spin trapping electron paramagnetic resonance spectroscopy and density functional theory (DFT) were used to study the structure of antioxidant species present in GF. The reaction with H₂O₂ was examined *via* EPR measurements of formed PBN spin adducts. Additionally, pure glycerol, α - and δ -tocopherol along with oil were used as reference chemical systems, since they are potential constituents of GF. The hyperfine parameters calculated from simulated glycerol fraction-PBN adduct EPR spectra indicate the α – tocopherol origin of PBN trapped radicals. The parameters ($a_{\text{iso}}(^{14}\text{N}) = 15.3$ G and $a_{\text{iso}}(^1\text{H}) = 3.8$ G) of PBN adducts derived from α – tocopherol and glycerol fractions are indistinguishable. Results obtained from DFT calculations of EPR parameters stay in good accordance with experimental ones especially when the solvent effects are included in the calculations - PCM formalism and two explicit ethanol molecules interacting with the radical center. Surprisingly, DFT results exclude trapping of oxygen centered radical and suggest carbon centered type.

Keywords: spin trapping, radical scavenging, bioglycerol, biodiesel

5. Introduction

Glycerol fraction (GF) called also bioglycerol is a product of transesterification reaction of edible oils or/and animal fats. During last decades the main interest of transesterification products was pointed only at biodiesel. Glycerol fraction was treated as unwanted waste material. The problem of bioglycerol overproduction indicated exploration of its new properties [1] which will be helpful in finding of the new utilization. One of such feature is antioxidants content in the fraction. Polyphenolic antioxidants in vegetable oils were already studied [2-4], but their possibly changed structure and concentration when transferred to glycerol fraction during biodiesel production was not investigated yet. Glycerol fractions from various biodiesel technologies were found to be a very interesting subject of antioxidant studies by electron paramagnetic resonance (EPR). The issue of finding the antioxidant routes in the transesterification process from oil to the products is of great importance.

6. Experimental details

Glycerol fractions from different technologies

Glycerol fractions, oil and biodiesel from 7 different biodiesel producers were investigated. Samples were obtained from biodiesel producers applied with different, patented technologies. Fractions originated in various technological scale, from industrial (100 000 tonnes of biodiesel a year) to laboratory scale. Also different oils, catalysts and alcohols were used [5]. Raw samples are meant as crude glycerol fractions before removal of soap and neutralisation. All glycerol fractions were pre-treated by distilling off water and alcohol.

Electron Paramagnetic Resonance investigations

Primary EPR investigations were performed for row samples without any solution, scans were accumulated 5 times due to low concentration of radicals.

Advanced EPR analysis was conducted using free radical scavenging and spin trapping method. The measurements of the oils and esters samples were performed for hexane whilst glycerol samples for ethyl alcohol [5]. Galvinoxyl free radical (Sigma-Aldrich) solution (1.1mmol/dm^3) in ethyl alcohol/hexane accordingly was used for scavenging investigations. The blank sample was located in one cavity, and the analyzed sample in the second one. For quantitative calculation of antioxidants gallic and caffeic acid were used.

Spin trapping investigations were performed using 0.5ml of (0.067M) PBN (Sigma-Aldrich) solution or every 0.2500g of bioglycerol or oil. As a reference material pure glycerol, α - and δ -tocopherol and oil were used.

All Electron Paramagnetic Resonance (EPR) spectra were recorded using Bruker ESP300E spectrometer with a 100 kHz magnetic field modulation equipped with a Bruker NMR gaussmeter ER 035M and a Hewlett-Packard microwave frequency counter HP 5350B operating at X-band frequencies at room temperature. Microwave power, 20 mW, modulation amplitude 1 G and double resonance cavities were used. Measurements were performed for both cavities over the same period of time with at least five replications.

For calculations of the EPR spectra the WINEPR and SimFonia of Bruker program was used.

All computations were performed with GAUSSIAN 09 suite of programs. The PBN spin trap adducts geometries were optimized using Becke's three-parameter hybrid functional (UB3LYP) and the double- ζ Pople-type basis set plus polarization quality (6-31(d,p)).

7. Results and discussion / Methods and results

Methyl esters, oils, and glycerols show different effectiveness of galvinoxyl radical scavenging (Fig. 1). Glycerol fractions were found to have the strongest free radical scavenging activity and most of investigated glycerol samples quenched the galvinoxyl radical in the first few minutes of measurements. Oil

samples have medium scavenging properties and esters shows the smallest effect.

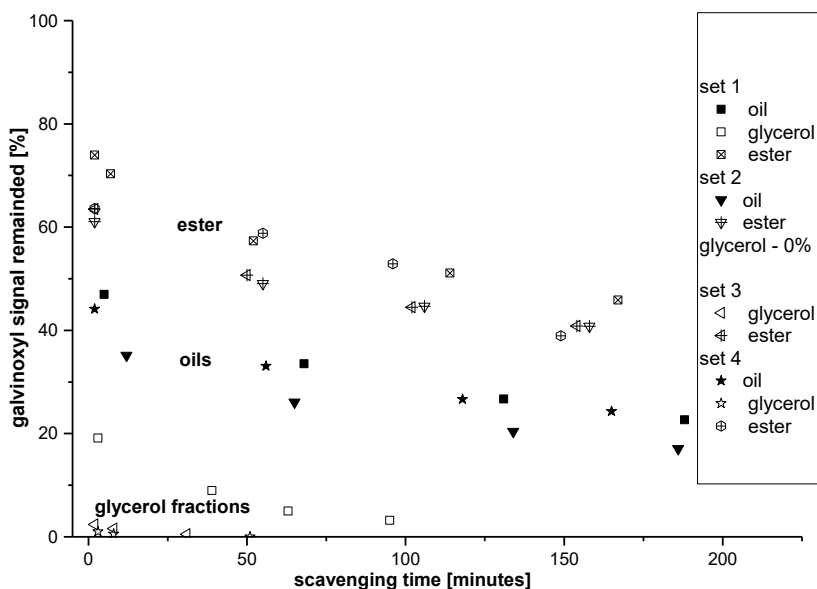


Figure 1. Dependence of galvinoxyl radical scavenging in oils and its product vs. time

Important is also the fact of different antioxidant properties for different glycerol fractions (two examples given in table 1). Galvinoxyl radical scavenging activity vary for different producers and is independent from the scale of technology, type of used catalyst or alcohol. Diversity of radical quenching ability divide glycerol fractions among three groups of low, medium and high antioxidant properties. Bioglycerol with the highest galvinoxyl radical scavenging properties are the same samples which for crude fractions exhibit EPR signal ($g=2.0046$) attributed to oxygen centered radical from polyphenolic antioxidants.

Table 1. Antioxidant concentration (gallic acid as standard) and hyperfine parameters of PBN-bioglycerol and α -tocopherol adducts

	Antioxidant concentration [mmol/l]	First day		1 week		3 weeks	
		$a_{iso}(^{14}N)$	$a_{iso}(^1H)$	$a_{iso}(^{14}N)$	$a_{iso}(^1H)$	$a_{iso}(^{14}N)$	$a_{iso}(^1H)$
Bioglycerol 1	5.75	15.3	3.8	15.3	3.8	15.3	3.8
Bioglycerol 2	0.20	15.3	3.8	15.3	3.2	15.5	1.8
α -tocopherol	-	-	-	15.3	3.9	15.3	3.8

Parameters obtained from simulation of PBN-adduct EPR spectra (fig. 2, tab. 1) define unequivocally that antioxidants present in glycerol fraction from biodiesel production have structure of α – tocopherol. Hyperfine splitting constants of bioglycerol samples having the highest antioxidant content remained unchanged during the whole experiment and were the same as for α – tocopherol ($a_{\text{iso}}(^1\text{H}) = 3.8\text{G}$ $a_{\text{iso}}(^{14}\text{N}) = 15.3\text{G}$). These parameters for samples with medium and low antioxidant content differ in time. At the beginning of the experiment parameters are the same as for α – tocopherol, but in time when antioxidant is consumed and the parameters change to those similar to oil (lipid-PBN adduct).

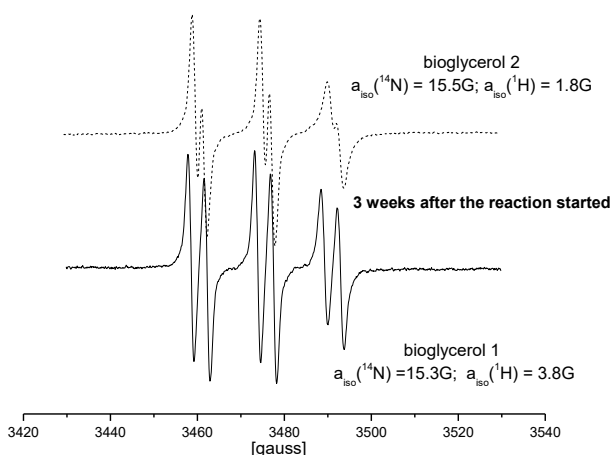


Figure 2. EPR spectra of PBN bioglycerol adducts

The comparison of experimental and DFT predicted $a_{\text{iso}}(^1\text{H})$ values reveals that the carbon centered α – tocopherol radical is trapped by PBN. However, this fact cannot be unambiguously associated with the antioxidant activity. Though it was shown that antioxidant activity of α -tocopherol against hydroxyl radicals is not selective and can take place at several positions. Moreover one should keep in mind that in experiments reported herein α -tocopherol was exposed to hydroxyl radicals constantly, even after exhaustion of its antioxidant capability, therefore the probability of formation and trapping of carbon centered radical was additionally increased.

The DFT calculations showed that accurate inclusion of solvent effects (combination of PCM method and explicit ethanol molecules) is mandatory for correct prediction of $a_{\text{iso}}(^1\text{H})$, $a_{\text{iso}}(^{14}\text{N})$ and g-tensor in radical systems under studies.

8. Conclusions

The presented results show that most well-known phenolic antioxidants occurring naturally in oils during esterification reaction are transferred to the glycerol fraction. Additionally, hyperfine parameters obtained from simulated spectra and calculated by DFT method suggest that the carbon centered α – tocopherol radical is trapped by PBN

The proven high content of phenolic antioxidants in the glycerol fraction indicates new possibilities of using the fraction without very expensive purification processes.

References

- [1] M. Pagliaro, M. Rossi, Future of Glycerol, 2008
- [2] A Koski, E. Psomiadou, M. Tsimidou, A. Hopia, P. Kefalas, K. Wähälä, M. Heinonen, *Eur Food Res Technol*, 214:294-298 (2002)
- [3] T.A. Isbell, T.P. Abbott, K.D. Carlson, *Industrial Crops and Products*., 9:115-123 (1999)
- [4] O. Okogeri and M. Tasioula-Margari, *J. Agric. Food Chem.* 50:1077-1080 (2002)
- [5] M. Jerzykiewicz; I. Cwielag; W. Jerzykiewicz, *J. Chem. Technol. Biotechnol.* 2009; 84: 1196–1201

Spin number manipulation in the systems of nanoporous carbons with adsorbed molecules

M. Kempniński^{*1)}, M. Śliwińska-Bartkowiak¹⁾, W. Kempniński²⁾

** Corresponding author: matt@amu.edu.pl*

¹⁾ Faculty of Physics AMU, Poznań, Poland

²⁾ Institute of Molecular Physics PAS, Poznań, Poland

Carbon structures made of quasi-graphitic nanoparticles exhibit specific properties of electrical transport. Quantum effects result from the size and type of connections between the nanoparticles, treated as the individual conducting objects with strong localization of charge carriers.

We present the electron paramagnetic resonance (EPR) and electrical transport measurements of activated carbon fibers (ACF) and Carbon Mesostructure by KAIST (CMK).

Coulomb-gap variable-range hopping model (CGVRH) [1] is used to describe the electrical transport in ACF. It is characteristic of granular metal systems near the dielectric regime, where small conducting granules are suspended in the dielectric matrix [2].

With the adsorption of various molecules in ACF's porous system we can change the dielectric surroundings of the conducting carbon nanoparticles, significantly influencing the electronic and structural properties of the particles. Strong changes in spin localization, observed with EPR, result mostly from changing the potential barriers for hopping of charge carriers [3]. When H₂O molecules are adsorbed in the pores more spins are localized than in case of CCl₄ adsorption.

The structure of ACF's nanoparticles is also affected in effect of interaction with guest molecules, as they cause the high internal pressure within the pores. Host-guest interactions seem to give the possibility of spin manipulation in nanoscale. Systems of carbon nanoparticles can even be treated as a quantum-dots matrices. Different modifications are expected to occur while using different molecules as well as after adding the external electric or magnetic fields to modify the host-guest interactions. Carbon nanomaterials with controlled localized spin population can be very important from the point of view of possible future molecular electronics applications, as there are many successful attempts of creating controlled structures of carbon nanoparticles, e.g. CMK-type carbons.

Keywords: carbon nanostructures, granular metals, electron paramagnetic resonance

References

- [1] A. W. P. Fung, Z. H. Wang, M. S. Dresselhaus, G. Dresselhaus, R. W. Pekala, M. Endo, *Phys. Rev. B* 49 (1994) 17325.
- [2] Abeles, P. Sheng, M. D. Coutts, and Y. Arie, *Adv. Phys.* 24 (1975) 407.
- [3] Kempieński, J. Kaszyński, M. Śliwińska-Bartkowiak, *Appl. Phys. Lett.* 88 (2006) 143103.
- [4] M. Kempieński, M. Śliwińska-Bartkowiak, W. Kempieński *Rev. Adv. Mater. Sci.* 14 (2007) 14.

Localized States in Carbon Nanostructures

W. Kempniński^{*1)}, M. Kempniński²⁾, D. Markowski¹⁾

** Corresponding author: wojkem@ifmpan.poznan.pl*

*¹⁾ Institute of Molecular Physics, Polish Academy of Sciences,
Smoluchowskiego 17,
60-179 Poznań, Poland*

*²⁾ Faculty of Physics, Adam Mickiewicz University, Umultowska 85, 61-614
Poznań, Poland*

Three kinds of carbon nanostructures will be presented to show how localization effect can generate special behavior of studied nanocarbon materials.

In C_{60} fullerites doped by alkali metals electrons are transferred from alkali atoms to the C_{60} surface and are localized within the C_{60} molecules. Such an electron transfer leads to the formation of superconducting behavior of A_3C_{60} fullerides, where A stands for potassium or rubidium atoms. EPR technique has been applied to show the appearance and evolution of spins while superconductivity was demonstrated by Magnetically Modulated Microwave Absorption (MMA) method. Redistribution of alkali ions from octahedral to tetrahedral sites of the C_{60} lattice has been observed in terms of C_{60}^{-1} reduction to C_{60}^{-3} radical-EPR-lines in the process of intercalation of C_{60} by alkali metals. Based on the redistribution process, evolution of superconducting phases is discussed as well [1].

Strong localization of spins at low temperature region within nanographitic units (NGU) of activated carbon fibers (ACF) was described by the model which is a fusion of two approaches: Curie law behavior studied by EPR and granular metal model. NGU are linked structurally to constitute porous system. In such systems conducting properties strongly depend on potential barriers between NGU. If to modify these barriers for hopping of carriers by guest molecules, strong changes in spin localization is possible to observe. Host-guest interactions is the unique method of spin manipulation in nanoscale. This interaction studied by EPR and electric conductivity method enable to treat ACF nanographitic system as a quantum dots matrix – very attractive system from the application (spintronics) point of view [2].

The problem of inner or outer connections of NGU system as a quantum dot matrix in ACF push us to modify the polyacrylonitrile-based fibers by a perfect nanowires: multi-walled-carbon-nanotubes. Changes in transport properties of such carbon system define new conditions for quantum dots matrix with carbon nanotubes as a contact-nanowires. Results are discussed in the frame of the model of electric transport in granular metals [3]. System of carbon nanotubes has also been studied as a system sensitive for the external magnetic field.

Ordering effect appear at low temperature region where localization of spins within the single carbon nanotube is observed.

Keywords: nanostructures, nanocarbon, localization, quantum dots, spintronics

References:

- [1] W. Kempański, P.Scharff, J.Stankowski, L.Piekara-Sady, Z.Trybuła Physica C 274 (1997) 232-236
- [2] M. Kempański, W. Kempański, J. Kaszyński, M. Śliwińska-Bartkowiak, Appl. Phys. Lett. 88 (2006) 143103,
- [3] W. Kempański, M. Kempański, M. Śliwińska-Bartkowiak, A. Frączek, S. Błażewicz, 3rd International Conference on Opoelectronics and Spectroscopy of Nano-structured Thin Films and Materials, October 15-19, Beijing China ed. Yan Fang, CNU (2007) pp. 82-84

A New Application of the spin labelin method

M.Komorowska, M. Dzik, U. Cytlak, K. Galecka, E. Głogowska.

Wrocław University of Technology

Institute of Biomedical Engineering and Instrumentation

Wybrzeże Wyspiańskiego 27, 50-370 Wrocław

e-mail: malgorzata.komorowska@pwr.wroc.pl

Nitroxide spin labels have been used extensively in EPR studies of the structure and function of biological membranes. Despite the proven usefulness of the technique, key studies are sometimes precluded by the unavailability of site specific labels having suitable spectral, physical or chemical properties. Also, there is a constant concern that the spin labeled biological system does not accurately reflect the behavior of its naturally occurring analogue owing to the steric bulk of the nitroxide moiety. We proposed a new application nitroxide spin probes.

1. The kinetics of the hemoglobin aggregation studied by means EPR spectroscopy

4-isothiocyanate 2,2,6,6 tetramethylpiperidine-1-oxyl binds to the terminal amino and SH groups. For each molecule of hemoglobin, there are four N-terminal ends and two reactive sulfhydryl groups. The data taken from literature suggest that isothiocyanate nitroxide spin label attaches to hemoglobin at two sites. One site, α -amino site, is sensitive to pH and the state of ligation, while the other, SH site, is insensitive to both. Nitroxides located on the (SH) β -93 are less mobile than those on the α -amino site. $2a_{||}$ for the immobile site is around 6.4 mT but for mobile $2a_{||}$ equals 3.8 mT. The effects of oxygen binding and pH on the motion clearly showed as the pH increased the mobile component increases indicating a greater freedom of rotation at the α -amino site but only for oxyhemoglobin. For deoxyhemoglobin, there is a little change in the motion of the mentioned groups with pH. Restricted motion of α -amino bonded spin-label in acidic pH discovered in oxyhemoglobin probably arises from the intra-subunit interaction. These features make isothiocyanate a convenient probe for analysis of the local environment of the spin labeled hemoglobin and its changes during aggregation due to reaction with glutaraldehyde or physical factors like radiation. The intend of presented study was to monitor the kinetics of the aggregation or polymerization reaction of hemoglobin.

2. The usefulness of spin labels technique for evaluation the response of different structures of RBC subjected to shear

The red cell (RBC) is of biconcave shape in the normal state. Thanks this cell easily deforms, elongates under flow due to facilitate oxygen transfer

and to reduce flow resistance. When RBC flows *in vivo* it experiences stress from shear and extensional flows. The flow in the blood vessels do not deform strongly the cells with exception the flow in capillaries. However, when RBC flows *in vitro* as in the bypass to the extra corporeal cardiovascular devices it experiences significant deformation, what could lead to mechanical haemolysis. Biomedical devices are widely used to repair or replace a number of cardiovascular system elements. The successful functioning of these devices strongly depends on the way they disturb blood. Studies of the material elastic properties are of great potential importance because they imply specific information concerning the cell membrane structure. Hyperelastic properties suggest elastomerlike organization the cell membrane. The mechanical aspects of mechanisms determine erythrocyte survival or early destruction in the microcirculation.

We propose a method which could estimate the deformability and contribution of deformability of the different structures building the RBC's cell as well as the changes in environment of the cell. Controlled shear would be imposed in two ways: the osmotic pressure and centrifugation in microcapillaries. The mobility changes, of a spin probes introduced into different parts of RBC and plasma is a measure of the deformability. We also estimated the relaxation processes when stress was removed.

3. Application of the imidazoline nitroxides: hydrogen ions concentration in the RBC interface.

The measurement of pH is one of the most important problem of biology. The traditional pH measurement method is an electrometric method. The main drawback of the mentioned procedure is that it cannot be introduced inside closed structures for example inside RBC interface .The most promising for application as pH probes are imidazoline radicals due to considerable differences in paramagnetic resonance parameters in R and RH^+ forms. We presented the first time results of application pH sensitive spin probe for determination of concentration H^+ ions in the RBC interface. What we estimated, about one pH unit above and below the pK_a value of the probe (6,5), it is possible to use the ratio of the signal intensities of the protonated and nonprotonated moiety as a very sensitive indicator.

Application of spectroscopic resonance methods in investigations of metallopeptides and the metalloproteins on the example β -amyloid and the prion protein fragments

Henryk Kozłowski^{*1)}, Ewa Gralka¹⁾, Lukasz Szyrwiel¹⁾, Daniela Valensin²⁾ and Gianni Valensin²⁾

1) Faculty of Chemistry, University of Wrocław, F. Joliot-Curie 14, 50-383 Wrocław, Poland,
henrykoz@wchuwyr.pl

2) Department of Chemistry, University of Siena, Via Aldo Moro 53100 Siena, Italy

Keyword: copper(II), zinc(II), neurodegeneration, prion protein, β -amyloid, NMR, EPR.

The interaction of copper(II) with histidine containing peptides has recently acquired renewed interest following the established link between the abnormal protein behavior in neurodegenerative processes accompanying by the disorder in the metals homeostasis.

The prion proteins seem to play a critical role in copper homeostasis. Biological function of this protein is still not well understood. In mammals prion protein, PrP, may be found in two different conformations. The regular cellular form PrP^C and the second one so called scrape form PrP^{Sc}. The change of conformation from PrP^C to PrP^{Sc} lead to neurodegenerative diseases [1] like Kuru or Creudfold-Jacob in humans or bovine encephalopathies in cattle [2]. PrP^C contains C-terminal domain with well defined structure and the N-terminal comprising about 100 amino which is unstructured. The latter domain contains the effective metal ion binding sites [3,4]. Cu(II) ions interact with PrPC within the N-terminal octa-repeat region containing octapeptide (PHGGGWGQ) repeats. Besides the octarepeat region the other metal binding sites is located within the neurotoxic region comprising two histidine residues [5,6]. The mysterious biology of prion proteins and their relation to metal homeostasis has focused much of research on these proteins derived from mammals down to fishes [7].

Alzheimer's disease is the most common fatal neurodegenerative disorder involving the abnormal accumulation and deposition of β -amyloid-peptide derived from the amyloid precursor protein (APP). The APP is the metal binding protein, including copper ion [8].

β -amyloid-peptide is also very effective ligand for Cu(II) ions and the interactions of this peptide with copper and iron seem to have strong effect on the oxidative processes in the brain area.

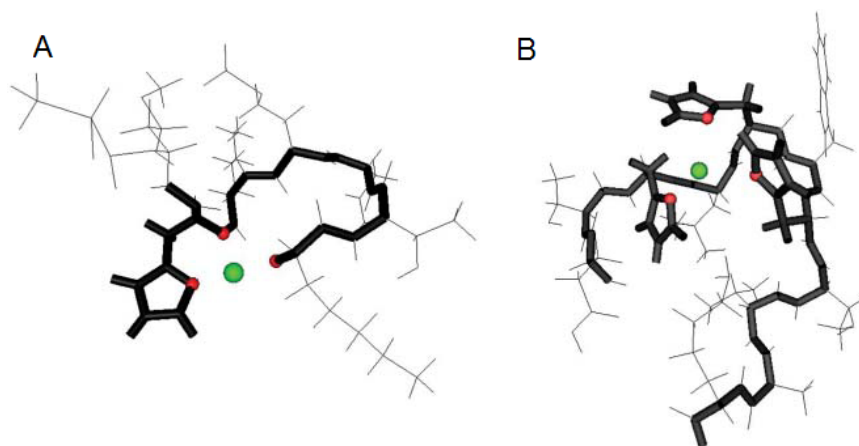


Figure 1. The structure of Cu(II)–PrP106–113 (A), Cu(II)–APP(145–155) (B).

References

- [1] S. B. Prusiner, Proc. Natl. Acad. Sci. U.S.A. 1998, 95, 13363-83.
- [2] C. M. Dobson, Philos Trans R Soc Lond B Biol Sci, 2001, 356, 133–145.
- [3] Sigel, A. ; Sigel, H.; Sigel, R.K.O.; Wiley, J.; Metal Ions in Life Sciences Volume 1.
- [4] Kozłowski, H. ; Brown, D.R.; Valensin, G.; Metallochemistry of Neurodegeneration, RSC Publishing, Cambridge, 2006.
- [5] H. Kozłowski, D.R. Brown, G. Valensin, Metallochemistry of Neurodegeneration, The Royal Society of Chemistry, Cambridge, 2006.
- [6] D.R. Brown, B.S. Wong, F. Hafiz, C. Clive, S.J. Haswell, I.M. Jones, *Biochem. J.* 1999, 344, 1-5.
- [7] H. Kozłowski, A. Janicka-Klos, P. Stańczak, D. Valesnin, G. Valensin. K. Kulon, *Chord. Chem. Rev.*, 2008, 252, 1069-1078.
- [8] E. Gaggelli, H. Kozłowski, D. Valensin, G. Valensin, *Chem Rev.*, 2006, 106, 1995.

ESR spectra under slow motion conditions

Danuta Kruk* and ***Aleksandra Kubica***

Institute of Physics, Jagiellonian University, Reymonta 4, PL-30-059 Krakow, Poland

** Corresponding author: danuta.kruk@uj.edu.pl*

1. Introduction

Perturbation approaches give a valuable insight into electron spin relaxation, but many systems violate the assumptions of the perturbation theory [1-3]. Very often amplitudes of the zero field splitting and g-tensor anisotropy interactions combined with motional conditions bring the electron spin beyond validity regimes of the Redfield theory [1,2] and the electron spin relaxation times cannot explicitly be defined. This fact has led to developing general (slow motion) treatments based on the stochastic Liouville equation (SLE). The name “slow motion” originates from the situation when the mean interaction strength is larger than, or comparable to, the inverse of the correlation time that corresponds to the motion modulating the interaction. The methods based on the stochastic Liouville equation were introduced by Freed and co-workers [4,5] to describe ESR lineshapes for systems with the electron spin quantum number $S = 1/2$, including interactions with neighbouring nuclear spins under very general anisotropic motional conditions. In this work we propose an extension of this treatment to an arbitrary electron spin quantum number.

2. Theoretical background

An ESR lineshape function $L(\omega_S - \omega)$ is determined by the spectral density

$$s_{-1,-1}(\omega) = \int_0^{\infty} \langle S_{-1}^+(\tau) S_{-1}(0) \rangle \exp(-i\omega\tau) d\tau \quad (L(\omega_S - \omega) \propto s_{-1,-1}(\omega)) \quad (1)$$

corresponding to the single-quantum transitions of the electron spin [3]. More explicitly the lineshape function is given as [3]:

$$L(\omega_S - \omega) = \int_0^{\infty} Tr_S \left\{ S_{-1}^{1+} \left[\exp(-i\hat{L}_L \tau) S_{-1}^1 \right] \rho_S^{eq} \right\} \exp(-i\omega\tau) d\tau \propto [S_{-1}^1]^\dagger \left[\hat{M}_{ESR} \right]^{-1} [S_{-1}^1] \quad (2)$$

The lattice Liouville operator, \hat{L}_L , contains all degrees of freedom which are relevant for the ESR spectrum: $\hat{L}_L = \hat{L}_Z(S) + \hat{L}_{ZFS}^S + \hat{L}_{ZFS}^T + \hat{L}_D + \hat{L}_R$. The contributing operators represent the Zeeman interaction for the electron spin (S), the static and transient zero field splitting, distortional and rotational motions of the complex. The Zeeman Hamiltonian, $H_Z(S)$ associated with the Liouville operator, $\hat{L}_Z(S)$, has the obvious form: $H_Z(S) = \omega_S S_z$ (ω_S is the electron frequency). The forms of the static and transient ZFS (in the laboratory frame) depend on the models of motion incorporated into the theory [3,6]. The static (permanent) zero field splitting (ZFS) is a part of the entire ZFS interaction, $H_{ZFS}(t) = H_{ZFS}^S(t) + H_{ZFS}^T(t)$, obtained as a result of averaging over molecular distortions (vibrations). The reorientational motion is modeled as isotropic rotational diffusion. A pseudorotational diffusion modulating the orientation of the principal axis system of the transient ZFS with respect to a molecule fixed frame is supposed to reflect any distortional motion of the molecule leading to stochastic fluctuations of the transient ZFS tensor. The superoperator \hat{M}_{ESR} originating from the Liouvilian is defined as [3,6]:

$$\hat{M}_{ESR} = -i \left[\hat{L}_Z(S) + \hat{L}_{ZFS}^S + \hat{L}_{ZFS}^T + \hat{L}_R + \hat{L}_D + \hat{1}\omega \right] \quad (3)$$

The matrix form of the \hat{M}_{ESR} operator is set up in a basis $\{|O_i\rangle\}$ given as an outer product of vectors associated with the degrees of freedom of the system: $|O_i\rangle = |ABC\rangle \otimes |LKM\rangle \otimes |\Sigma\sigma\rangle$ [3,6] with the distortional, rotational and spin components $|ABC\rangle$, $|LKM\rangle$ and $|\Sigma\sigma\rangle$, respectively.

The vector $[S_{-1}^1]$ contains expansion coefficients of the tensor operator S_{-1}^1 in the basis $\{|O_i\rangle\}$. In fact, there is just one non-zero coefficient, namely the one associated with the basis vector $|ABC\rangle |LKM\rangle |\Sigma\sigma\rangle = |000\rangle |000\rangle |1-1\rangle$. Thus the

ESR lineshape is determined by one element of the inverted matrix $\left[\hat{M}_{ESR} \right]^{-1}$.



Fig. 1. Schematic representation of the \hat{M}_{ESR} matrix.

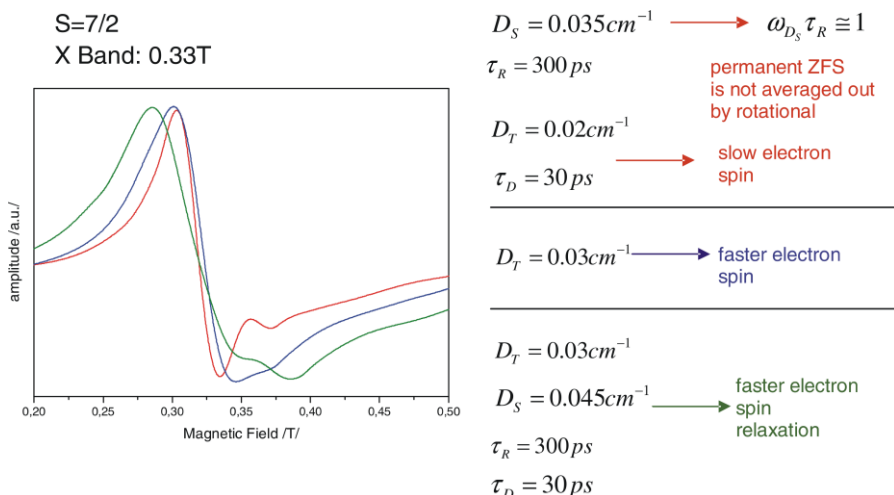


Fig.2. Examples of ESR spectra, D_S, D_T - axial parts of the static and transient zero field splitting, respectively, τ_R - rotational correlation time, τ_D - distortional correlation time.

Conclusions

The presented theory of ESR lineshape obviously is also valid for arbitrary interaction strengths and rates of isotropic reorientation. Even though one cannot explicitly define the electron spin relaxation operator (and, in consequence, electron spin relaxation times), the spectral density function $s_{-1,-1}(\omega)$ describing the lineshape has a well defined meaning. The discussed

treatment has a broad application range, especially for biological systems. Several illustrative examples will be shown.

Acknowledgements

This work was financed by Polish Ministry of Science and Education, grant No N N202 105936.

References

- [1] C.P. Slichter, Principles of Magnetic Resonance, Springer - Verlag, Berlin, 1990.
- [2] C.P. A.G. Redfield, in Encyclopedia of Nuclear Magnetic Resonance, 4085 Eds. D.M. Grant and R.K. Harris, Wiley, Chichester, 1996). Slichter, Principles of Magnetic Resonance, Springer - Verlag, Berlin, 1990.
- [3] D. Kruk, Theory of Evolution and Relaxation of Multi-Spin Systems, Arima, Bury St Edmunds, 2007.
- [4] J. H. Freed, in Spin Labeling Theory and Applications, 53, Ed. L.J. Berliner, Academic Press, N.Y. 1976.
- [5] D.J. Schneider and J.H. Freed, Adv. Chem. Phys. 73, (1989) 387.
- [6] T. Nilsson, J. Kowalewski, J. Magn. Reson. 146, (2000) 345.

Magnetic resonance in ferromagnetic diluted magnetic semiconductors.

M. Kuźma, I. Stefaniuk

Institute of Physics, University of Rzeszow, Rejtana 16A, 35-959 Rzeszow, Poland

The most investigated diluted magnetic semiconductors (DMS) base on a classical semiconductors of the types: $A^{II}B^{VI}$ ($A=Cd, Zn, B=S, Se, Te,$), $A^{III}B^{VI}$ ($A=Ga, In, Al, B=As, P, N$). In DMS a fraction of cations is replaced by magnetic ions (Mn, Fe, Co). Magnetic properties of such systems originate from a strong exchange interaction between delocalized s and p electrons (forming conduction and valence bands), and d localized electrons of the magnetic impurity. The s-d exchange is positive (ferromagnetic) for all DMS and its value is near $N\alpha \approx 0.2$ eV. Contrary, the exchange interaction between valence band p electrons (formed by p electrons of anions) and d electrons is antiferromagnetic one ($-N\beta \approx 1,2-1,9$ eV) almost in all DMS's containing Mn ions. In this case the p-d exchange is indirect. Due to much greater value of this interaction, the resulting magnetism is of the antiferromagnetic ordering (in the materials containing Mn, Fe as well as Co).

Exceptional group of diluted magnetic semiconductors is that predicted theoretically by Blinowski et al [1], in which the ions with a less than half filled shell (e.g. V, Ti, Cr) are incorporated into a semiconductor matrix. Ferromagnetic properties of such DMS should result mainly from location of the unoccupied t_x and t_d orbitals above the top of the valence band.

The concentration x and temperature dependence of the EPR spectra in $Cd_{1-x}Mn_xTe$, $Cd_{1-x}Mn_xSe$ and $Cd_{1-x}Mn_xS$ were presented in many papers (see e.g.[2-4] and References therein). The general features of the spectra are: For small Mn concentrations ($x < 0.005$) the fine structure of the spectra is visible. As the concentration increases ($x > 0.005$) the spectrum becomes structureless single line. For $x > 0.03$ the line approximates Lorentz function very well and the line width increases significantly with temperature decreasing or concentration increase. The broadening of the linewidth describes Huber's law very well [5].

IV-VI chromium based DMS were investigated widely by Story, Wilamowski and Dobrowolski [6, 7].

Vallin [8] studied Cr doped ZnS, ZnSe, ZnTe, CdTe, CdTe for small Cr concentration. A significant static tetragonal Jahn-Teller distortion was observed in changes of the fine structure of the spectra due to the axial pressure applied to the sample. The Jahn-Teller effect is not essential in the DMS with manganese. Therefore it is a new feature, which contributes to the ferromagnetic properties of AIIIBVI semiconductors with chromium.

We investigate CdTe samples with high concentration of chromium. The EPR results were addressed in FMR formalism. The anisotropy effects and temperature dependence of the resonance line points on ferromagnetic properties at room temperature.

References

- [1] Blinowski J and Kacman P 1992 *Phys. Rev. B* **46** 12298
- [2] Sayad H A and Bhagat S M 1985 *Phys. Rev. B* **31** 591
- [3] Kremer R E and Furdyna J K 1985 *Phys. Rev. B* **31** 1
- [4] Furdyna J K and Kossut J 1988 *Semiconductors and Semimetals*, vol. 25 ed Boston – Toronto: Academic Press INC
- [5] Huber D L 1972 *Phys. Rev. B* **6** 3180
- [6] Story T, Wilamowski Z, Grodzicka E and Dobrowolski W 1995 *Acta Phys. Pol.* **87** 229
- [7] Dobrowolski W, Arciszewska M and Brodowska M 2006 *Sci. of Sintering* **38** 109
- [8] Vallin J T and Watkins D G 1974 *Phys. Rev.* **B9** 2051

Size manifestation in EPR measurements of small carbon particles

Szymon Łoś^{1*}, Laurent Duclaux², Wojciech Kempniński¹, Maria Połomska¹

** Corresponding author: szymon@ifmpan.poznan.pl*

Institute of Molecular Physics, Polish Academy of Science, ul.

Smoluchowskiego 17, 61179 Poznań, Poland

Université de Savoie, 73376 Le Bourget du Lac Cedex, France

Two kinds of microporous activated nanostructured carbons were studied by electron paramagnetic resonance (EPR) spectroscopy. They have different specific surface areas: 1500 m²/g (AC I) and 2500 m²/g (AC II). It was observed that the EPR spectra shapes and their temperature evolution between 300 K and 4 K were depending on the types of carbon sample. Roomtemperature spectra show dissimilar line-widths $\Delta B = 0.5$ mT and 1.6 mT for AC I and AC II, respectively. The AC I carbon EPR spectra show: (a) a broadening at the beginning of the cooling process, similar to the EPR behavior of graphite and, subsequently and (b) a quick narrowing below 130 K. For the super-activated carbon (AC II), a monotonic narrowing process is observed on decreasing the temperature. These different behaviors were attributed to the size manifestation of graphenes in both activated carbons. From additional investigation done upon X-ray diffraction pattern and Raman spectra was possible to deduce an average values of the nanodomain sizes. These two methods together with an electrical conductivity measurement consistently confirmed the gradation of the crystallite sizes. And finally, it was determined that the size of the AC I and AC II carbon particles are 1.7 nm and 1.5 nm, respectively.

Keywords: Nanostructure, Size-characterization, Electron paramagnetic resonance, Raman, X-ray diffraction

Coordinate Systems for Determining the Electron Spin Resonance (ESR) Lineshape

Lidia Najder-Kozdrowska**, *Andrzej B. Więckowski

** Corresponding author: <lkozdrowska@wp.pl>*

Institute of Physics, Faculty of Physics and Astronomy, University of Zielona Góra, Szafrana 4a, 65-516 Zielona Góra, Poland

The investigation of interactions between paramagnetic centres can be carried out by analysis of the shape and the width of the resonance curve, normally having the form of the first derivative of absorption. In the case of solids, when dipolar and exchange interactions are present, the ESR profile is known to consist of a Lorentzian central part with wings of Gaussian form. We developed a method of linear anamorphosis, in which the integral or the derivative of the resonance curve will be utilized. In special coordinate systems we have presented the ESR lineshape of ultramarine blue. This presentation proves that the central part of resonance curve of ultramarine blue is Lorentzian in shape and the outer wings are Gaussian.

Keywords: electron spin resonance ESR ; exchange narrowing ; lineshape; linear anamorphosis

1. Introduction

The method of linear anamorphosis of single symmetric ESR lines proposed by Tikhomirova and Voevodskii [1] can be used for analysis of the shape of an ESR line narrowed by exchange interaction. This method gives better results than the method of moments [2] or the cut-off method [3-4]. Using this method it was found by Więckowski [5] that the paramagnetic polysulphide radical-anions S_3^- , responsible for the blue colour and paramagnetism of ultramarine blue, form a face-centred cubic lattice.

2. Experimental details

The ESR measurements of ultramarine blue sample were performed using an X-band spectrometer BRUKER EMX-10 with microwave frequency 9.35 GHz. The amplitude of second magnetic field modulation with frequency 100 kHz was 0.05 mT. Time constant was 82 ms. The ESR spectra were recorded at the temperature of liquid nitrogen (77 K) for sample placed in a quartz tube.

The resolution of magnetic field axis was 1024 points. The ESR spectrum obtained in the form of the first derivative of absorption was integrated next with the BRUKER WIN-EPR Simphonia program, version 3.03. On figure 1 the ESR spectra of ultramarine blue is shown.

The investigated sample of ultramarine blue (with the approximate formula $[Si_3Al_3O_{12}]Na_4S_2$) was manufactured by the factory Polifarb, Kalisz, Poland.

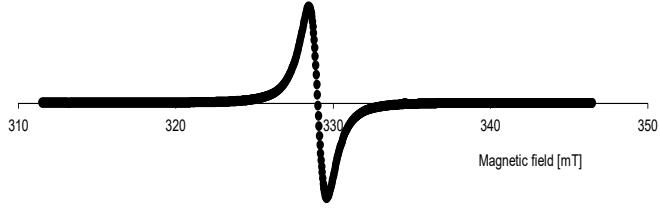


Fig. 1. The ESR spectrum of ultramarine blue.

3. Results and discussion

3.1. Line shape functions

According to the theories of Anderson and Weiss [6] and Kubo and Tomita [7-8], the function of the line shape function $f(x)$ of a single ESR line is the Fourier transform of the characteristic function $\varphi(t)$. In simplified form the line shape function $f(x)$ can be given by the following formula [9]:

$$f(x) = (2\pi)^{-1} \int \varphi(t) \exp(-itx) dt, \quad (1)$$

$$\varphi(t) = \exp[-(\sigma^2/\omega_e^2)[(\pi/2)^{1/2} \omega_e t \Phi(\omega_e t) + \exp(-\omega_e^2 t^2/2) - 1]], \quad (2)$$

$$\Phi(\omega_e t) = (2/\pi)^{1/2} \int_0^{\omega_e t} \exp(-t^2/2) dt \quad (\text{Gauss probability integral}), \quad (3)$$

where: x – frequency (or magnetic field) measured from the centre of the line, σ – linewidth of the Gaussian curve caused by dipole interactions, ω_e – exchange frequency (or exchange field).

The most often used approximations of the single EPR lines are limited to the Lorentzian function, the Gaussian function, and the Voigt function which is a convolution of the Lorentzian and the Gaussian function. Also rational fractions (Padé approximations) [10-11] and Tsallis functions [12] were used for approximation of the resonance curve.

3.2 Linear anamorphosis of the ESR line

To apply numerical methods for fixed-frequency EPR lineshape analysis, we will use shape functions in the following simplified forms:

$$y = a_G \exp[-x^2/(2b_G^2)], \quad \text{Gaussian function} \quad (4)$$

$$y = a_L/(1 + x^2/b_L^2), \quad \text{Lorentzian function} \quad (5)$$

where: y – absorption ordinate, x – magnetic field abscissa measured as the distance from the centre of the line (resonance field), a_G , a_L – amplitude of

absorption, b_G – slope-width (half-width between points of maximum slope of absorption line), b_L – half-width (half-width at half height of the amplitude a_L). Differentiation of these lineshape functions yields:

$$y' = -(a_G/b_G^2)x \exp[-x^2/(2b_G^2)] = -(1/b_G^2)xy, \quad \text{Gaussian function} \quad (6)$$

$$y' = -2(a_L/b_L^2)x/(1 + x^2/b_L^2)^2 = -2/(a_L b_L^2)xy^2, \quad \text{Lorentzian function} \quad (7)$$

where: y' – first derivative of absorption ordinate.

It follows immediately that with the variables:

$$Y = y'/y^2, \quad X = x/y, \quad (8)$$

$$Y = y'/y, \quad X = x, \quad (9)$$

$$Y = y', \quad X = xy, \quad (10)$$

the Gaussian function gives a straight line described by the equation

$$Y = -(1/b_G^2)X, \quad (11)$$

and the Lorentzian function gives a curve.

Similarly, with the variables:

$$Y = y'/y^2, \quad X = x, \quad (12)$$

$$Y = y'/y, \quad X = xy, \quad (13)$$

$$Y = y', \quad X = xy^2, \quad (14)$$

the Lorentzian function gives a straight line described by the equation

$$Y = -2/(a_L b_L^2)X, \quad (15)$$

and the Gaussian function gives a curve.

In these special coordinate systems we have analysed the EPR lineshape of ultramarine blue. On Figure 2 we present two examples of the analysis. For better observation of our results, on Figure 2 b) we show only one quadrant of coordinate system.

This presentation proves that the central part of the resonance curve of ultramarine blue is Lorentzian in shape and the outer wings are Gaussian. These methods visualize the differences in lineshape of the central part of a single ESR spectrum and their wings.

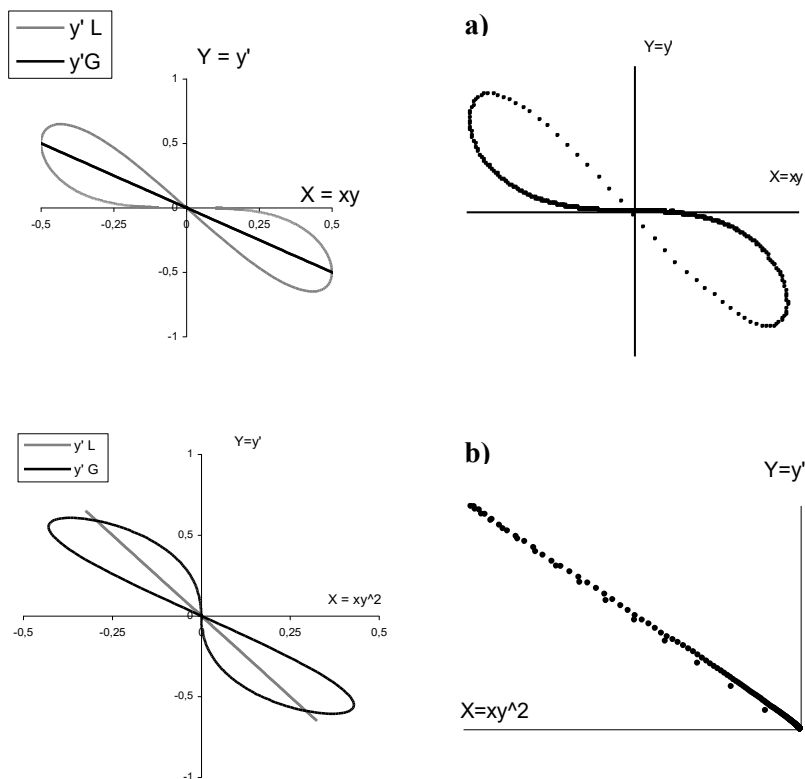


Fig. 2. The ESR lineshape of ultramarine blue in following coordinate system: a) $Y = y'$ and $X = xy$. Theoretical diagram (on left) and experimental data (on right). b) $Y = y'$ and $X = xy^2$. Theoretical diagram (on left) and experimental data (on right).

Acknowledgements

The authors are highly indebted to Prof. Dr. hab. Ryszard Krzyminiewski and Dr. Bernadeta Dobosz (Division of Medical Physics, Institute of Physics, Adam Mickiewicz University, Poznań, Poland) for their assistance during performing the ESR measurements.

References

- [1] N.N. Tikhomirova NN, V.V. Voevodskii, Opt. Spektrosk. 7(6) (1959) 829-832.
- [2] J.H. Van Vleck, Phys. Rev. 74(9) (1948) 1168-1183.
- [3] P.W. Anderson, Phys. Rev. 82(2) (1951) 342.
- [4] C. Kittel, E. Abrahams, Phys. Rev. 90(2) (1953) 238-239.
- [5] A. Więckowski, Phys. Status Solidi 42(1) (1970) 125-130.
- [6] P.W. Anderson, P.R. Weiss, Rev. Mod. Phys. 25(1) (1953) 269-276.
- [7] R. Kubo, K.J. Tomita, J. Phys. Soc. Japan 9(6) (1954) 888-919.
- [8] R. Kubo, J. Phys. Soc. Japan 9(6) (1954) 935-944.

- [9] A.B. Więckowski, *Nukleonika*, 42(2) (1997) 589-594.
- [10] M.M. Maltempo, *J. Magn. Reson.* 68(1) (1986) 102-111.
- [11] J.C. Sartorelli, J.A. Ochi, W. Sano, *J. Magn. Reson.* 70(2) (1986) 299-302.
- [12] D. Howarth, J. Weil, Z. Zimpel, *J. Magn. Reson.* 161(2) (2003) 215-221.

Structure and magnetic properties of polynuclear iron and vanadium complexes dispersed on oxide surfaces

Piotr Pietrzyk*, ***Zbigniew Sojka***

** Corresponding author: pietrzyk@chemia.uj.edu.pl*

Faculty of Chemistry, Jagiellonian University, ul. Ingardena 3, 30-060 Kraków

Abstract

Oxo-clusters of vanadium and iron cut off from ZSM-5 zeolite or amorphous silica were optimized with DFT techniques, their ground spin states were established, and magnetic parameters such as g , hyperfine, and zero-field splitting tensors were calculated. Structures of dimer iron and dimer vanadium cores connected with oxo or hydroxo bridges were optimized in high-spin states. Based on broken-symmetry calculations antiferromagnetic coupling between spin magnetic moments of the individual metal centers was unraveled and characterized with J value.

Keywords: spin-orbit interaction; zero-field splitting; J coupling; iron; vanadium; zeolite;

1. Introduction

Mono- and polynuclear surface complexes of iron(II/III) and vanadium(IV/V) are known from its catalytic activity in homogeneous and heterogeneous systems. A vast group of such catalytically active systems is constituted by inorganic materials such as zeolites functionalized with iron or vanadium cores. The active sites comprise both mononuclear and polynuclear complexes in form of the isolated cations, hydroxocations, oxocations or mixed-ligand complexes. Owing to their particular electron configuration, Fe(II) and Fe(III) monocations can exhibit various spin multiplicities, depending on the nature of their chemical environments. In the polynuclear oxide systems, iron centers exhibit preferably high-spin configurations with $S = 2$ ($3d^6$) and $S = 5/2$ ($3d^5$). In case of vanadium, common diamagnetic-paramagnetic redox cycle V(V)/V(IV) can occur. Because of the inherent paramagnetism, those systems are primarily examined with electron paramagnetic resonance (EPR) technique and their spectra are characterized by structure sensitive fine structure and/or hyperfine couplings. However, in polynuclear species, magnetic exchange interactions between neighboring cores can lead to ferromagnetic or antiferromagnetic alignment of the individual magnetic moments.

The aim of this work was to examine the electronic and magnetic structures of the intrazeolitic and surface silica mononuclear and polynuclear oxo-iron and oxo-vanadium cores. Population analysis of the ground-state spin structures was used for unraveling the radical character of the bound oxo-ligands. DFT

calculations aimed at prediction of spin-Hamiltonian parameters, i.e. g , ZFS and J coupling characteristic of the investigated groups of complexes.

2. Theoretical background

Constrained geometry optimization of the cluster models cut-off from the ZSM-5 structure (stoichiometry of the clusters $\text{Si}_6\text{AlO}_8(\text{OH})_{12}^-$ and $\text{Si}_8\text{Al}_2\text{O}_{12}(\text{OH})_{16}^{2-}$) and cluster mimicking surface sites of amorphous silica $\text{Si}_5\text{O}_5\text{H}_7(\text{OH})_3$ were carried out with Gaussian03 software [1]. B3LYP [2] hybrid exchange-correlation potential along with TZV and LanL2DZ basis set [3] were utilized. The positions of terminating hydrogen atoms were kept frozen during this step in order to mimic rigid chemical environments of the investigated entities. Because of the open-shell nature of the investigated system, in order to establish the ground state structures optimization procedures were carried out in various multiplicities. The final wave functions were tested for stability and reoptimized when needed. Based on the obtained geometries, computational spectroscopic study with the relativistic DFT calculations of the characteristic g and D tensors was carried out with one-component spin-orbit mean-field (SOMF) method as implemented in ORCA program [4]. Alternatively, g tensors were calculated according to self-consistent two-component zero-order regular approximation (ZORA) [5] and scalar relativistic Pauli [6] Hamiltonians with ADF program [7]. In case of ZFS, two contributions, calculated according to Neese [8], were taken into account: the direct spin-spin coupling (SS) and the spin-orbit coupling (SOC). The estimation of the spin-orbit coupling (for all g , A , and ZFS) coupled-perturbed approach (SOC-CP), valid for hybrid functionals, was carried out. The SS contributions were included on the basis of the spin-density formula. In the case of the complexes with spatially separated magnetic moments, such as diiron, divanadium(IV) centers and some oxo-iron cores, broken-symmetry calculations [9] were carried out in order to establish the mechanism of magnetic couplings and the values of J constants.

3. Results and discussion

Two step DFT calculations were carried out to obtain molecular models of polynuclear iron and vanadium complexes. At the beginning monomeric cores such as FeO^+ , FeO^{2+} , and VO^{2+} were calculated and characterized. The second step involved formation of dimeric complexes: $\text{Fe}^{\text{III}}\text{O}-\text{O}(\text{OH})-\text{Fe}^{\text{III}}\text{O}$, $\text{Fe}^{\text{III}}\text{O}-\text{O})_2-\text{Fe}^{\text{III}}\text{O}$, $\text{V}^{\text{IV}}\text{O}-\text{O}-\text{V}^{\text{IV}}\text{O}$, $\text{V}^{\text{IV}}\text{O}-\text{OH}-\text{V}^{\text{IV}}\text{O}$. Geometry optimization was carried out for high-spin case and then broken-symmetry calculations were set to obtain correct magnetic state.

It is commonly accepted that for the multiple-state (spin states) reactivity systems, the active sites comprise a radical ligand coordinated to a transition-metal ion. Such systems, e.g., are proposed as active sites responsible for N_2O decomposition [10] or C–H bond activation [11]. In order to elucidate the

electronic and magnetic structure of such systems we have investigated bare iron(III), iron-oxo, and iron hydroxo mono- and polynuclear complexes entrapped in ZSM-5 zeolite. In all cases the ground state was found to be consistent with the high-spin sextet. However, for $\text{FeO}^+/\text{FeO}^{2+}$ cores we observed a characteristic spin transfer from the metal to oxo ligand that acquires a distinct radical character. In such a case, isotropic exchange coupling constant J can be calculated after Yamaguchi et al. [12]: $J = - (E_{\text{HS}} - E_{\text{BS}}) / (\langle S^2 \rangle_{\text{HS}} - \langle S^2 \rangle_{\text{BS}})$, where HS stands for high-spin state, and BS for broken-symmetry state. This interpretation nicely interpolates between strong and weak coupling limit and allows for covering many different chemical situations. For the FeO^+ species, the spatial redistribution of spin density ($\rho_{\text{Fe}} = 3.87$, $\rho_{\text{O}} = 0.98$) gave rise to strong ferromagnetic coupling $J = + 1014 \text{ cm}^{-1}$ (superexchange) between iron and oxygen moieties. In the case of FeO^{2+} this effect is much weaker owing to the pronounced spin polarization of the $\text{Fe}=\text{O}$ bond. The unusual spin density redistribution within the FeO^+ core with the distinct radical character of the terminal oxygen account for its unique reactivity in catalytic reactions requiring spin barrier crossing.

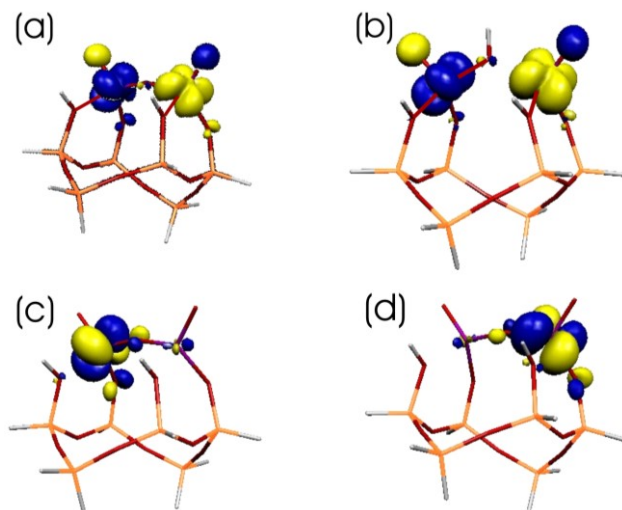


Fig. 1. Broken-symmetry spin density contours of the (a) VO–O–VO and (b) VO–OH–VO ground state structures of silica-supported complexes along with corresponding spin-orbitals contours of the broken-symmetry solution (c) spin α , (d) spin β showing antiferromagnetic coupling of the odd electrons of the vicinal VO^{2+} cores.

Geometry optimization showed that two vicinal FeO^+ or VO^{2+} centers tend to agglomerate and form binuclear $(\text{FeO})^+-(\text{O})-(\text{FeO})^+$ or $(\text{VO})^{2+}-(\text{O})-(\text{VO})^{2+}$ (Fig. 1a) cores with μ -oxo bridge. Another investigated binuclear complex

$\text{Fe}^{3+}(\text{O},\text{O})\text{Fe}^{3+}$ contains double bis- μ -oxo bridge. The most characteristic feature for the binuclear cores was a broken-symmetry ground state, giving rise to small antiferromagnetic coupling equal to $J_{\text{Fe}(\text{O},\text{O})\text{Fe}} = -0.44 \text{ cm}^{-1}$ and $J_{\text{VO}(\text{O})\text{VO}} = -5.4 \text{ cm}^{-1}$. The analysis of the mechanism of this coupling based on the calculation of the corresponding magnetic orbitals (Fig. 1c,d) revealed involvement of the lone pairs of oxo bridges in the coupling mechanism.

In case of the $(\text{VO})^{2+}-(\text{O})-(\text{VO})^{2+}$ core, according to the Noodleman equation [9] $E(S) = -JS(S+1)$ that gives the energies of a spin states ladder, the ground spin state is tantamount to the broken-symmetry (BS) state ($S = 0$). However, because the true antiferromagnetic (AF) state is multideterminant in nature, the BS state provides only approximation to AF state that is situated $2J$ in energy scale below. The high-spin (HS) state ($S = 1$) is situated approximately 11 cm^{-1} above the ground BS state. However, the separation of the states strongly depends on the bridging ligands. Substitution of $(\text{VO})^{2+}-(\text{O})-(\text{VO})^{2+}$ with $(\text{VO})^{2+}-(\text{OH})-(\text{VO})^{2+}$ core results in substantially enhanced exchange coupling value equal to $J_{\text{VO}(\text{OH})\text{VO}} = -40.0 \text{ cm}^{-1}$.

4. Conclusions

DFT calculations showed that for the iron(III)-oxo complexes both Fe and O atoms bear unpaired electron density. Population analysis indicated that the electronic structure of such species is tantamount with a strongly ferromagnetically coupled $(\text{Fe}^{2+}-\text{O}^-)^+$ unit with radical oxygen, being spin sextet in total. On the contrary, biiron(III) with mono or bis-oxo bridges as well as bivanadyl(IV) cores with oxo or hydroxo bridges exhibit broken-symmetry states with J values ranging from -0.4 to -40 cm^{-1} . The oxygen bridges were found to facilitate antiferromagnetic coupling of the iron and vanadium spin magnetic moments and the extent of this interaction is strongly related to the nature of the bridging ligand.

Acknowledgements

This work was supported by the Ministry of Science and Higher Education (MNiSW) of Poland, grant no. N N204 239334.

References

- [1] Gaussian03, Gaussian, Inc., Wallingford CT, 2004.
- [2] P. J. Stephens, F. J. Devlin, C. F. Chabalowski, M. J. Frisch, *J. Phys. Chem.* 98 (1994) 11623.
- [3] A. Schäfer, C. Huber, R. Ahlrichs, *J. Chem. Phys.* 100 (1994) 5829.
- [4] F. Neese, ORCA Program, Lehrstuhl für Theoretische Chemie, Bonn, 2007.
- [5] E. van Lenthe, E. J. Baerends, J. G. Snijders, *J. Chem. Phys.* 99 (1993) 4597.
- [6] G. Schreckenbach, T. Ziegler, *J. Phys. Chem. A* 101 (1997) 3388.
- [7] ADF2006, SCM, Theoretical Chemistry, Vrije Universiteit, Amsterdam.
- [8] F. Neese, *J. Chem. Phys.* 127 (2007) 164112.

- [9] L. Noodleman, *J. Chem. Phys.* 74 (1981) 5737.
- [10] M. V. Parfenov, E.V. Starokon, S. V. Semikolenov, G. I. Panov, *J. Catal.* 263 (2009) 173.
- [11] R. T. Jonas, T. D. P. Stack, *J. Am. Chem. Soc.* 119 (1997) 8566.
- [12] K. Yamaguchi, Y. Takahara, T. Fueno in: V.H. Smith (Ed.) *Applied Quantum Chemistry*. Reidel, Dordrecht, 1986, pp. 155.

Modeling in EMR spectroscopy - low symmetry aspects

Czesław Rudowicz* and Paweł Gnutek

* Corresponding author: crudowicz@zut.edu.pl

Modeling in Spectroscopy Group, Institute of Physics, West Pomeranian University of Technology, Al. Piastów 17, 70–310 Szczecin, Poland

Abstract

Paramagnetic centers with orthorhombic, monoclinic, and triclinic site symmetry occur often in various technologically important materials. For such centers intricate low symmetry aspects arise, which bear on meaningful interpretation of electron magnetic resonance (EMR) data and their correlation with structural data. The focus of this presentation is on providing an overview of the modeling techniques for analysis and interpretation of EMR data, including the zero-field splitting parameters (ZFSPs) and g -factors, for transition ions at low symmetry sites in crystals worked out by us. Illustrative examples taken from our recent studies of low symmetry ion-host systems are discussed. This presentation serves as a primer for experimentalists

Keywords: Electron magnetic resonance (EMR); Spin Hamiltonian (SH); Zero-field splitting (ZFS); Crystal-field (CF); Low symmetry aspects; Transition ions in crystals; Computer modeling packages

1. Introduction

Electron magnetic resonance (EMR) studies of paramagnetic centres exhibiting orthorhombic (C_{2v} , D_2 , D_{2h}), monoclinic (C_2 , C_s , C_{2h}) and triclinic (C_1 and C_i) site symmetry have gained renewed importance, since such centres occur often in various technologically or biologically important systems. The low symmetry aspects arising for such centres bear on meaningful interpretation of EMR data and their correlation with structural data. A review of the modeling techniques for analysis and interpretation of EMR data for transition ions at low symmetry sites in crystals has recently been published [1]. This presentation provides a succinct description of the modeling techniques and capabilities of the computer packages worked out by us over the years as well as a listing of most recent applications. For theoretical background underlying EMR and optical spectroscopy of transition ions, including, crystal (ligand) field (CF) theory, effective and microscopic spin Hamiltonian (SH), zero-field splitting parameters (ZFSPs) and g -factors, and low symmetry aspects, we refer the readers to [1] and references therein. This presentation provides a primer for experimentalists who wish to utilize these modeling techniques for their analysis and interpretation of low symmetry EMR data.

2. Modeling techniques and computer programs dealing with low symmetry ZFS parameters

Modeling in EMR and optical spectroscopy is defined as [1]: *theoretical interpretation of experimental parameters {EPs}, measured by various techniques, in terms of more fundamental microscopic parameters {MPs}, obtainable from other independent experiments as well as comparative analysis of EP datasets from various sources.* This comprises, e.g. derivations of analytical expressions or numerical relationships: $\{EPs\} \propto \{MPs\}$. As a reference notation for SH [1] we utilize the extended Stevens (ES) operators O_k^q [2]:

$$\begin{aligned} H = H_{Ze} + H_{ZFS} &= \mu_B \mathbf{B} \cdot \mathbf{g} \cdot \mathbf{S} + \sum B_k^q O_k^q(S_x, S_y, S_z) = \\ &= \mu_B \mathbf{B} \cdot \mathbf{g} \cdot \mathbf{S} + \sum f_k b_k^q O_k^q(S_x, S_y, S_z), \end{aligned} \quad (1)$$

$f_k = 1/3, 1/60, 1/1260$ for $k = 2, 4,$ and $6,$ respectively. For analysis and interpretation of EMR data, several modeling techniques and related computer packages described below were developed [1].

2.1 Conversions, standardization, and transformations of ZFS parameters - CST package

For orthorhombic site symmetry a natural symmetry-adapted axis system is formed by three mutually perpendicular symmetry axes or directions, labeling of which as either $x,$ or $y,$ or z may be arbitrary. Different choices are interrelated and correspond to specific axes transformations. The intrinsic properties of orthorhombic ZFSPs are described by the rhombicity ratio: $\lambda = E/D$ (conventional) and $\lambda' = B_2^2/B_2^0$ (ES notation). The standardization idea enables to limit the ratio: λ and λ' to the range $(0, 1/3)$ and $(0, 1),$ respectively. To this end, the six choices of labeling of the orthorhombic symmetry axes and respective transformations Si that depend on the initial value of the ratio λ (λ') were defined w.r.t. an original axis system $SI(x, y, z).$ These transformations yield different yet correlated ZFSP values, which are physically equivalent and yield identical energy levels.

Implications of orthorhombic and lower symmetry standardization for analysis and modeling of ZFSPs may be summarized as follows: (1) fitted rhombicity ratio may be obtained in various ranges; (2) large non-standard values of λ or λ' do not indicate large orthorhombic distortions in crystals, misunderstanding of this aspect may lead to wrong physical conclusions, (3) fitted and/or theoretical ZFSPs or CF parameters (CFPs) may be meaningfully compared only if expressed in the same region of the parameter space – the most convenient choice is to adopt the standard range of the ratio λ (λ'); (4) the

alternative ZFSP sets (standard and non-standard) generated by orthorhombic standardization transformations may be utilized in the multiple correlated fitting technique; this technique utilizes independent fittings starting from various regions of parameter space to improve the reliability of final fitted ZFSPs (CFPs). Pertinent calculations are facilitated by the package CST, which includes modules for conversions, standardization, and transformations of ZFS and CF parameters.

2.2 Superposition model of ZFS (CF) parameters – SPM package

The superposition model (SPM) enables separation of the geometrical and physical information contained in ZFS parameters for transition ions at arbitrary symmetry sites in crystals. Hence, the H_{ZFS} (as well as H_{CF}) can be expressed as the sum of separate axially symmetric contributions from all nearest neighbour ligands of the transition metal ion. Thus for a given ML_n complex of the central metal (M) ion surrounded by n ligands (L), the ZFSPs may be parameterized, in the ES notation, as:

$$B_k^q = \sum_{i=1}^n \bar{B}_k(R_i) \cdot K_k^q(\theta_i, \varphi_i), \quad (2)$$

where $(R_i, \theta_i, \varphi_i)$ are the polar coordinates of the i^{th} ligand. The intrinsic parameters \bar{B}_k represent the strength of the k^{th} -rank ZFS contributions from ligands of a given type located at the distance R_i , whereas the coordination factors K_k^q describe the geometrical information. The distance dependence of \bar{B}_k 's is assumed as the adjustable power-law dependence: $\bar{B}_k(R_i) = \bar{B}_k(R_0) (R_0/R_i)^{t_k}$, where R_0 is the reference distance, which in practice is fixed arbitrarily as the standard average M-L distance for a particular cation, whereas t_k is the power-law exponent. Assumption that the value of R_0 should be applicable for SPM calculations for a particular cation enables meaningful comparisons of the results and prediction of ZFSPs for other structurally similar ion-host systems.

SPM enables to simplify, especially for low symmetry cases, the set of adjustable parameters to a smaller set than that formed by the original ZFSPs (CFPs) for a given site symmetry. SPM is useful for modeling of ZFSPs for transition ions in undistorted hosts as well as structural distortions of ML_n complex. SPM has predictive powers - the model parameters obtained semi-empirically for one ion-host system may be used to calculate ZFSPs for the same ion in structurally similar crystals where the model parameters were not yet determined. The package SPM is suitable for arbitrary symmetry and facilitates modeling. It includes the transformations module adopted from the package CST. SPM modeling may be combined with the crystal field analysis

(CFA) package to provide input CF parameters for the CFA/MSH modeling [3] as well as with the techniques 3DD and PAM (see below).

2.3 Diagonalization of 2^{nd} -rank ZFS and other terms - 3DD package

The method 3DD is based on diagonalization of a 3x3 matrix:

$$R_z(\gamma)^T \cdot R_y(\beta)^T \cdot R_x(\alpha)^T \cdot \begin{pmatrix} D_{xx} & D_{xy} & D_{xz} \\ D_{yx} & D_{yy} & D_{yz} \\ D_{zx} & D_{zy} & D_{zz} \end{pmatrix} \cdot R_x(\alpha) \cdot R_y(\beta) \cdot R_z(\gamma) = \begin{pmatrix} D_{xx} & 0 & 0 \\ 0 & D_{yy} & 0 \\ 0 & 0 & D_{zz} \end{pmatrix} \quad (3)$$

$R_x(\alpha), R_y(\beta), R_z(\gamma)$ are the rotation matrices; Euler angles are defined in the R.H.S. axis system as: ($\alpha/z, \beta/\text{new } y', \gamma / \text{final } z''$). Utilizing the relations between the ZFSPs expressed in the conventional and ES notation, the package 3DD has enabled applications, for the first time, to monoclinic and triclinic CFPs. The package 3DD finds: (1) Euler angles (α, β, γ) of the principal axis system, (2) the principal values of any 2^{nd} -rank terms, and (3) the transformed 4^{th} - and 6^{th} - rank parameters.

Major applications of the 3DD module concern monoclinic and triclinic symmetry cases and consist in: (i) determination of the orientation of the principal axis system of 2^{nd} -rank ZFS ‘tensors’ and respective principal values, (ii) standardization of ZFSPs for triclinic symmetry, (iii) reduction of the number of parameters for fittings, (iv) generation of alternative ZFSP sets for the multiple correlated fitting technique to increase reliability of final parameter sets. The implication of triclinic standardization of ZFSPs is the correct interpretation of the 4^{th} - and 6^{th} -rank ZFSPs in the principal axis system of the 2^{nd} -rank parameters. Note that the rhombicity ratio $\lambda' = B_2^2 / B_2^0 \in (0,1)$ is not meaningful for triclinic ZFSP sets. Only after reduction of low symmetry ZFSPs to zero: $B_2^1, B_2^{-1}, B_2^{-2} = 0 \Rightarrow \alpha, \beta, \gamma \neq 0$ and bringing the 2^{nd} -rank ZFS terms to the orthorhombic-like form, this ratio is meaningful.

2.4 Pseudo-symmetry axes method – PAM package

The pseudo-symmetry axes method (PAM) searches for the minimum of the factor ε_{sym} defined as:

$$\varepsilon_{sym} = \sum_{q \neq q(sym)} (B_k^q(\alpha, \beta, \gamma) / c_q^k)^2 / N_k, \quad N_k = \sum_q (B_k^q / c_q^k)^2. \quad (4)$$

The minimal value of ε_{sym} yields the Euler angles (α, β, γ), defined w.r.t. the original axis system, which determine a new pseudo-symmetry axis system of the 4^{th} - and 6^{th} -rank ZFSPs corresponding to a given higher symmetry approximation. An important feature of the ZFSPs expressed in these approximated pseudo-symmetry axes is that the higher symmetry ZFS

parameters adopt maximal values, while the lower symmetry ones are reduced to nearly zero.

Applications of PAM enable to extract physical information concerning the nearest surrounding of transition ion in crystals, i.e. the local site symmetry and the nature and strength of structural distortion. For triclinic local site symmetry all ZFSPs exist in any axis system, whereas the PAM orthorhombic approximation yields the best approximated pseudo four-fold axes. Importantly, all ZFSP sets transformed by the Euler angles (α, β, γ) arising from PAM are physically equivalent, i.e. they yield the same energy levels and thus EMR spectra. Higher symmetry approximations adopted within PAM enable relating ZFSP sets with the local site symmetry of transition ion and determining the orientation of the local site symmetry axes w.r.t. the crystallographic axis system. The 4-, 3-, 2-fold axes determined in this way may be compared with the ion-ligands bonds in crystals. The quantities $S_k = \sqrt{N_k/(2k+1)}$ are rotational invariants w.r.t. any rotation of the axis system. Hence, a useful quantity is the difference between the rotational ZFSP invariants: $(S_k - S_k^*)$, where S_k contains the full ZFSP set, whereas S_k^* contains only components with $q = q_{sym}$ (including $q = 0$) for the rank $k = 4$ and 6 representing the chosen higher symmetry PAM approximation. The quantity $(S_k - S_k^*)$ provides a ‘measure’ of the strength of low symmetry effects.

2.5 Comparison of datasets in n -D space - CF/NR package

The closeness factors C_k for a given rank k and the global ones C_{gl} reflect the ‘angles’ between ‘vectors’ in multidimensional space for the 2nd-, 4th-, and 6th-rank ZFSPs (CFPs), whereas the norms ratios R_k (R_{gl}) compare the ‘magnitudes’ of ‘vectors’. The usefulness of the quantities C_k and R_k stems from their limiting values: $C \in \{-1, 1\}$ and R or $1/R \in \{0, 1\}$, which indicate how any two ‘vectors’, e.g. $\{B_k^q\}$ and $\{B_k^q\}$, are close (or otherwise) to each other. If these quantities tend to 1, the two sets are numerically very close, whereas if they differ significantly from 1, the two sets are disparate. The closeness factors and norms ratios facilitate quantitative comparison of compatible data sets from various sources, as well as identification of similar data sets of compatible type. These quantities are applicable also for other types of data, e.g. sets of energy levels.

3. Applications

Recent applications of the packages outlined above in the area of optical spectroscopy concern reanalysis of crystal field (CF) parameter sets for several ion-host systems: Pr^{4+} in BaPrO_3 [4], Ho^{3+} in $\text{HoCl}_3 \cdot 6\text{H}_2\text{O}$ [4], Nd^{3+} in $\text{Nd}_2\text{BaCuO}_5$ and $\text{Nd}_2\text{BaZnO}_5$ [6], Tm^{3+} in $\text{TmBa}_2\text{Cu}_4\text{O}_8$ and $\text{TmBa}_2\text{Cu}_3\text{O}_{7-8}$ [7], Cr^{4+} in $\text{Li}_2\text{MgSiO}_4$ and Nd^{3+} in $\beta\text{-BaB}_2\text{O}_4$ [8], Nd^{3+} in

[Nd(hfa)₄(H₂O)](N(C₂H₅)₄) [9], Eu³⁺ and Er³⁺ in RE₂BaXO₅ (RE = rare-earth, X = Co, Cu, Ni, Zn) [10], Er³⁺ and Nd³⁺ in YAlO₃ [11], Tb³⁺ in TbAlO₃ [12], Er³⁺ and Tm³⁺ ions at C₂ symmetry sites in hexahydrated trichloride crystals [13], Tm³⁺ ions in Tm₂BaXO₅ (X = Co, Cu, Ni) [14], and Tm³⁺ in KGd(WO₄)₂ and KLu(WO₄)₂, and Ho³⁺ and Er³⁺ ions in KGd(WO₄)₂ [15].

Applications for analysis and modeling of low symmetry aspects inherent in EMR data considered so far comprise: PAM analysis for Fe³⁺ and Gd³⁺ in monoclinic zirconia [16], EMR studies of orthorhombic to monoclinic structural phase transition in hexagonal BaTiO₃ doped by Fe³⁺ ions [17], standardization of ZFSP sets for Mn²⁺ ions in various hosts exhibiting orthorhombic symmetry [18], SPM/CFP and CFA/MSH modeling of the local structure using CF and SH parameters for the tetragonal Fe_K³⁺-O_I²⁻ defect centre in KTaO₃ [3], and SPM analysis of low symmetry aspects inherent in the structural and ZFS parameters for Fe³⁺: TlInS₂ [19] and TlGaS₂ [20]. Currently in progress is analysis and modeling of ZFS parameters for: Cr³⁺ and Fe³⁺ ions in pure and Co²⁺-doped YAlO₃, Gd³⁺ ions at triclinic sites in CsSrCl₃, and Fe³⁺ ions in LiNbO₃.

4. Conclusions

The modeling techniques for analysis and interpretation of EMR data for transition ions, which are especially useful for low symmetry cases, are reviewed. These modeling techniques enable deeper analysis and interpretation of the low symmetry aspects involved in the fitted and theoretical ZFSPs. The computer packages, which facilitate extracting useful structural information inherent in orthorhombic, monoclinic, and triclinic ZFSP sets, are available from the authors upon request.

Acknowledgments

This work was partially supported by the research grant from the Polish Ministry of Science and Tertiary Education for the years 2009-10 to complete PhD studies by PG under the CZR supervision.

References

- [1] C. Rudowicz, P. Gnutek, *Physica B* 404 (2009) 3582.
- [2] C. Rudowicz, *Magn. Reson. Rev.* 13 (1987) 1; Erratum, *ibidem* 13 (1988) 335.
- [3] P. Gnutek, Z.-Y. Yang, C. Rudowicz, *J. Phys.: Condens. Matter* 21 455402 (2009).
- [4] C. Rudowicz, P. Gnutek, *J. Alloys Compd.* 456 (2008) 16.
- [5] M. Karbowski, C. Rudowicz, P. Gnutek, A. Mech, *J. Alloys Compd.* 451 (2008) 111.
- [6] C. Rudowicz, P. Gnutek, M. Karbowski, *Phys. Rev. B* 76 (2007) 125116.
- [7] C. Rudowicz, P. Gnutek, M. Lewandowska, M. Orłowski, *J. Alloys Compd.* 467 (2009) 98.

- [8] P. Gnutek, C. Rudowicz, *Opt. Mater.* 31 (2008) 391.
- [9] A. Mech, Z. Gajek, M. Karbowski, C. Rudowicz, *J. Phys.: Condensed Matter* 20 (2008) 385205.
- [10] C. Rudowicz, P. Gnutek, M. Lewandowska, *J. Alloys Compd.* 467 (2009) 106.
- [11] P. Gnutek, C. Rudowicz, *J. Rare Earth* 27 (2009) 619.
- [12] C. Rudowicz, P. Gnutek, M.G. Brik, *J. Rare Earth* 27 (2009) 627.
- [13] M. Karbowski, P. Gnutek, C. Rudowicz, *Physica B*, 405 (2010) 1927.
- [14] C. Rudowicz, M. Lewandowska, P. Gnutek, *J. Alloys Compd.* 497 (2010) 32.
- [15] C. Rudowicz, P. Gnutek, *J. Phys.: Condens. Matter* 22 (2010) 045501.
- [16] C. Rudowicz, P. Gnutek, *Physica B* 403 (2008) 2349.
- [17] C. Rudowicz, P. Gnutek, P. Budzyński, *J. Phys.: Condensed Matter* 20 (2008) 295219.
- [18] R. Kripal, D. Yadav, P. Gnutek, C. Rudowicz, *J. Phys. Chem. Solids* 70 (2009) 827.
- [19] P. Gnutek, M. Açıkgöz, C. Rudowicz, *Optical Materials* – in press (2010).
- [20] M. Açıkgöz, P. Gnutek, C. Rudowicz, *Solid State Commun.* 150 (2010) 1077.

Physicochemical nature of the increased phototoxicity of aged and *in vitro* photoaged retinal pigment epithelial melanosomes: EPR-spin trapping, CIDEP, saturation recovery EPR and W-band EPR study
**Grzegorz Szewczyk^a, Tadeusz Sarna^a, Mariusz Zaręba^a Andrzej Żądło^a,
Janice Burke^b Theodore Camenisch^c and Aaron Kittell^c**

^aDepartment of Biophysics, Jagiellonian University, Gronostajowa 7,
30-387 Krakow, Poland,

^bDepartment of Ophthalmology and ^cDepartment of Biophysics, Medical
College of Wisconsin, Milwaukee, 925 North 87th Street and 8701 Watertown
Plank Road, Milwaukee, WI 53226 USA

Natural melanins are biological pigments with unique physicochemical properties. They contain persistent free radical centers, exhibit distinct electron-exchange and ion-exchange capability and show remarkable optical properties. Although the exact molecular structure of melanins has not been determined, it is believed that the pigment granules – the melanosomes – are heterogeneous supermolecular systems, in which melanin is present in the form of oligomeric nanoaggregates. These oligomers are products of a series of non-enzymatic and enzyme-catalyzed oxidation-reduction and tautomeric reactions of tyrosine or dopa. Melanin is commonly viewed as an efficient photoprotective pigment and physiological antioxidant. Indeed in several model systems of different complexity it has been demonstrated that melanin can protect cells and biomolecules, such as DNA, proteins and lipids, against oxidative damage induced by singlet oxygen and free radicals. Unlike in the skin, where melanin undergoes relatively quick metabolic turnover, in the retinal pigment epithelium (RPE), melanin is formed early during fetal development and must perform its biological functions with little or no metabolic turnover. Therefore RPE melanin, being *in situ* chronically subjected to intense visible light from focal irradiation and high oxygen tension in the presence of endogenous photosensitizers, may undergo significant oxidative modifications that could affect its normal biological functions. These oxidative modifications of RPE melanin are expected to escalate with aging. We found that human RPE melanosomes from old donors and porcine RPE melanosomes subjected to experimental photobleaching – our *in vitro* model of melanosome aging, exhibit higher phototoxicity in ARPE-19 cells *in vitro* and increased aerobic photoreactivity.

In this study, we analyzed the ability of human RPE melanosomes from donors of different age and experimentally photobleached bovine RPE melanin granules, to photogenerate superoxide anion by using EPR-spin trapping and DMPO as a spin trap. To determine the nature of excited state precursors in RPE melanin, time resolved CW EPR was used to detect spin polarization after

excitation of melanin with visible or near- ultraviolet nanosecond laser pulses. To determine how experimental photoaging of bovine RPE melanosomes modifies the topography of bound to melanin metal ions and the susceptibility of melanin free radicals to interact with exogenous reactants, we employed saturation recovery EPR using dysprosium (III) as a unique molecular probe with outstanding spin-lattice relaxation properties. Changes in the structure of melanin, induced by experimental photobleaching of bovine RPE melanosomes, were monitored by W-band EPR spectroscopy. Our data show that photoaged bovine RPE melanosomes, compared with non-treated pigment granules, have a greater potential to photogenerate superoxide anion. Enhanced photoreactivity and photosensitizing ability of photoaged melanosomes probably result from their reduced efficiency to scavenge superoxide anion and hydrogen peroxide, and to sequester redox-active metal ions such as iron. Although the observed CIDEP in synthetic and bovine RPE melanin can be explained by a triplet excited state precursor, it is unlikely that triplet state photochemistry determines the aerobic photoreactivity of eumelanins. Photobleached RPE melanosomes exhibit substantially modified supermolecular structure, which facilitates the interaction of chemical reactants with melanin free radicals and the release from the photobleached pigment granule of reactive oxygen species such as superoxide anion and hydrogen peroxide. We have demonstrated that W-band EPR spectroscopy is a convenient tool for monitoring age-related changes in RPE melanosomes, which cannot be detected at X-band EPR spectroscopy

Supported in part by Ministry of Science in Higher Education and by NIH.

EPR spectroscopy interfaced with DFT calculations

Zbigniew Sojka*, **Piotr Pietrzyk**

* *Corresponding author: sojka@chemia.uj.edu.pl*

Faculty of Chemistry, Jagiellonian University, ul. Ingardena 3, 30-060 Kraków

Abstract

Computational EPR spectroscopy provides a combination of a hybrid genetic algorithm for robust and efficient simulation of complex experimental EPR spectra with density functional theory (DFT) calculations of magnetic parameters (g and A tensors, and zero-field splitting). This approach can be used for guiding interpretation of the EPR data of large non-molecular transition-metal containing systems characterised by irregular geometry, profound speciation, and low symmetry features. In calculations of the magnetic parameters it is essential to include spin-orbit coupling which is a relativistic effect. Various levels of theory of relativity treatment can be applied that, along with exchange-correlation functional, seriously influence the results. Thus, trustful experimental EPR parameters may guide the choice of proper calculation scheme and provide a quantitative connection between the molecular structure of investigated paramagnets and their spectroscopic fingerprints.

Keywords: DFT; EPR; computational spectroscopy; simulation, g , A , D tensors

1. Introduction

The chemical properties and reactivity of nanostructured systems are intrinsically connected with their reduced size and dimensionality, pronounced surface reconstruction, presence of structural and morphological defects, etc. The resultant inherent heterogeneity of the exposed surfaces gives rise to low symmetry phenomena and pronounced speciation of the paramagnetic surface species, leading to complicated multi-component powder EPR spectra [1]. They severely restrain recognition of the individual spectral features, which is especially pertinent for electron paramagnetic resonance, since the information herein is often unevenly distributed over broad spectral range. As a consequence, a great deal of significant chemical information about the investigated system can only be recovered with the help of advanced computer analysis of the EPR spectra supported by quantum chemical calculations of their parameters [2,3].

Principal types of surfaces and interfaces which are of our scientific interest are based on porous silica-alumina and calcia-alumina materials such as zeolites, pillared clays, mayenite, and nanostructured oxides. They may be readily rendered chemically active by introduction of transition-metal guest ions to produce paramagnetic surface and cage complexes. A number of important catalytic processes occur with involvement of such centres. Electron transfer from ligand to metal or from metal to ligand, spin pairing and spin crossing

processes accompanying coordination and transformation of the reactants may drastically alter magnetic states and reactivity of active sites constituted by the transition-metal ions [4].

2. Experimental details / Theoretical background

CW-EPR spectra were recorded at liquid nitrogen and room temperatures on a Bruker ELEXSYS 500 spectrometer working at X-band with 100 kHz modulation. The spectra processing was performed with the software provided by Bruker, while for computer simulation of the powder spectra the EPRsim32 [5] program developed in our laboratory was used. DFT modeling for constrained geometry optimization was carried out with DMol [6] and Gaussian03 [7] software. Spectroscopic calculations was carried out with ORCA program [8] based on the concept of spin-orbit mean-field (SOMF) [9] for g tensor and direct spin-spin coupling (SS) together with SOC contribution for zero-field splitting [10].

3. Results and discussion

In a computational EPR spectroscopy we combine a hybrid genetic algorithm for robust and efficient simulation of complex experimental EPR spectra with the density functional theory (DFT) calculations of magnetic parameters. Available experimental EPR parameters may be therefore directly compared with the corresponding calculated values, providing a quantitative connection between the molecular structure of investigated paramagnets and their spectroscopic fingerprints. This approach was used for guiding interpretation of the EPR data of large non-molecular transition metal containing systems. Owing to a progress in the relativistic DFT methods nearly quantitative reproduction of g , A and D tensors is possible at reasonable computing costs. Available experimental EPR parameters may be therefore directly compared with the corresponding calculated values. This approach was used for monitoring and interpretation of changes in the electron and spin states taking place during the interaction of small molecules with surface complexes of transition metals of various electron configurations. Selected examples will demonstrate potential of the computational EPR approach in enhancing interpretation of complex EPR data of heterogeneous systems in low symmetry environments.

There are two reasons why DFT is superior for calculations of large systems over post HF methods. It includes exchange-correlation effects explicitly and scales favorably with the size of the system. However, because of the absence of the universal functional, approximate exchange-correlation functionals should be carefully selected, especially for HFCC calculations. The hierarchy of functionals include simplest local density approximation, where exchange-correlation effects are taken as being proportional to the local electron density,

gradient corrected functionals and hybrid functionals containing admixture of HF exact exchange. The selection of appropriate functional is a delicate problem as we need to account adequately for the polarization effects. The exaggerated exchange may lead to artifacts of spin contamination. Another crucial issue is connected with the choice of the basis set. For satisfactory reproduction of HFCC one need to calculate precisely spatial distribution of the spin density, which usually requires application of large basis sets augmented by polarization functions. Within the standard spin density formulation, the isotropic HFCC depend on the local quality of the wavefunctions at the nuclei, suggesting that Slater-type orbitals (STO) should be preferred as they fulfill the correct cusp condition. However, the majority of studies employ Gaussian-type orbitals which are easier to calculate and the cusp problem can also be satisfactorily resolved.

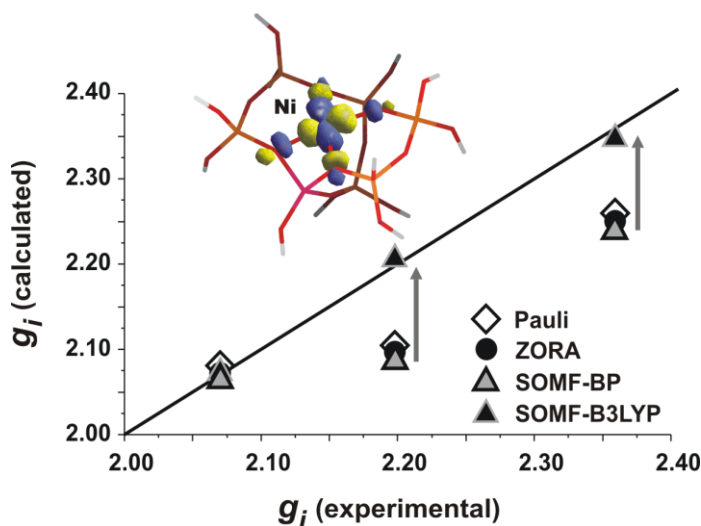


Fig. 1. Influence of the relativity treatment and exchange-correlation functional on the calculated g tensor components of $\text{Ni}^+/\text{M7}$ cluster (density contour of odd electron is shown) mimicking reduced nickel site in ZSM-5 zeolite.

In the case of g tensor calculations it is essential to include spin orbit coupling which is a relativistic effect. Since the exact Dirac equation cannot be solved, calculations for many electron systems are based on the approximate Breit-Pauli Hamiltonian. There are several types of g -tensor calculation schemes which are implemented in the available quantum chemical software. An exemplary result obtained for nickel(I) sites in ZSM-5 zeolite showing influence of the relativity treatment along with exchange-correlation functional on the g tensor components is shown in Fig. 1. A two-component zero order

regular approximation (ZORA) [11] include spin-orbit coupling treated variationally and the magnetic field terms as perturbation. The g -tensor is then calculated as a first-order property. The one component method based on first-order Pauli Hamiltonian [12], obtained by expanding the Dirac equation for large component in terms of $1/c^2$ and retaining only relativistic mass velocity and Darwin term gives the so called scalar relativistic approximations. The spin-orbit coupling and the magnetic field are then treated as perturbations, leading to a second-order g -tensor expression. High-accuracy results can also be obtained using recently developed SOMF (*Spin-Orbit Mean Field*) scheme of Neese. Once the g and A tensors are successfully reproduced, the DFT calculations open the access to vast additional information unavailable from powder experiments, such as molecular interpretation of their nature or orientation of principal magnetic axes. Additional useful information concerning the g tensor can be obtained from the scalar relativistic calculations using Pauli Hamiltonian. The perturbational treatment allows for partitioning of the g tensor into the relativistic, diamagnetic, and paramagnetic components and provide in-depth insight into its character through molecular orbital diagrams, accounting for the most important contributions to the g shift [12].

For HFCC calculations the spin-restricted and spin-unrestricted type of calculations can be used to evaluate, i.a., the spin polarization effects in the isotropic hyperfine constant [13]. In classic approach it is factorized into Fermi contact, spin polarization and pseudocontact terms. Unfortunately the separation of those contributions is difficult because the value of the polarization constant Q_a is hard to be assessed reliably from the reference experimental data, but it can be readily obtained from DFT calculations [4].

Computational EPR spectroscopy was also used by us for investigation of changes in the electron and spin states taking place during the interaction of small molecules like NO, CO, CH₃OH with surface complexes of transition metals of various electron configuration (Cu, Co, Ni, Fe, Mo) engaged in zeolites [3,4]. The results provided not only an in-depth insight into the molecular nature of the g , A and D tensors of the examined systems, but also allowed to account for noncoincidence of axes, spin polarization or structure sensitivity of the magnetic parameters for variety of paramagnetic surface complexes. The SOMF-B3LYP scheme, in turn, was used to resolve the conformational Y vs. T dichotomy of the tricoordinated Ni(I) carbonyls in zeolitic, organometalic, and enzymatic systems [14]. An unusual nature of magnetic coupling between Fe and oxygen and the zero-field splitting for FeO⁺ cores engaged in ZSM-5 zeolites will also be discussed.

Acknowledgements

This work was supported by the Ministry of Science and Higher Education (MNiSW) of Poland, grant no. N N204 239334.

References

- [1] Z. Sojka, Catal. Rev. Sci. Eng. 37 (1995) 461.
- [2] P. Pietrzyk, W. Piskorz, Z. Sojka, E. Broclawik, J. Phys. Chem. B 107 (2003) 6105.
- [3] P. Pietrzyk, Z. Sojka, S. Dźwigaj, M. Che, J. Am. Chem. Soc. 129 (2007) 14174.
- [4] P. Pietrzyk, Z. Sojka, in: “*Past and present in DeNOx catalysis: from molecular modeling to chemical engineering*”, P. Granger, V. I. Parvulescu (Eds.), Stud. Surf. Sci. Catal., vol. 171, Elsevier, 2007, p. 27.
- [5] T. Spalek, P. Pietrzyk, Z. Sojka, J. Chem. Inf. Model. 45 (2005) 18.
- [6] DMol³, Materials Studio 5.0, Accelrys.
- [7] Gaussian03, Gaussian, Inc., Wallingford CT, 2004.
- [8] Neese, F. *ORCA – An Ab Initio, DFT and Semiempirical Electronic Structure Package*, version 2.6-04.2007; Universität Bonn: Bonn, Germany.
- [9] F. Neese, J. Chem. Phys. 115 (2001) 11080.
- [10] F. Neese, J. Chem. Phys. 127 (2007) 164112.
- [11] E. van Lenthe, E. J. Baerends, J. G. Snijders, J. Chem. Phys. 99 (1993) 4597.
- [12] G. Schreckenbach, T. Ziegler, J. Phys. Chem. A 101 (1997) 3388.
- [13] M. Munzarova, M. Kaupp, J. Phys. Chem. A 103 (1999) 9966.
- [14] P. Pietrzyk, K. Podolska, Z. Sojka, Chem Eur.J. 15, 2009, 11802.

Computer program SPM-MC and its applications in EMR studies of transition ions in crystals

I. Stefaniuk^{1)*}, ***C. Rudowicz***²⁾

* *Corresponding author: <istef@univ.rzeszow.pl>*

¹⁾ *Institute of Physics, University of Rzeszów, Rejtana 16a, 35-310 Rzeszów, Poland*

²⁾ *Institute of Physics, West Pomeranian University of Technology, Al. Piastów 17, 70-310 Szczecin, Poland*

Abstract

Development of computer program for superposition model (SPM) calculations is reported. A novel aspect in this our approach is the usage of the Monte Carlo (MC) method to predict the feasible ligands' positions by fitting the experimental electron magnetic resonance (EMR) data to theoretical estimates. The program SPM-MC may be helpful for interpretation of EMR spectra for paramagnetic ions at low (triclinic) symmetry sites and coordinated by up to 13 ligands of arbitrary type. For illustration we consider the case of chromium Cr^{3+} ions in YAlO_3 (YAP) crystal, which exhibits orthorhombic structure ($Pbnm$ space group), whereas the site symmetry is lower than orthorhombic due to structural distortions.

Keywords: Superposition model (SPM); Spin Hamiltonian (SH); Yttrium aluminum perovskite (YAP); YAlO_3 .

1. Introduction

Interpretation of electron magnetic resonance (EMR) spectra is often cumbersome due to low local site symmetry exhibited by paramagnetic centers. For such cases comparative analysis of data obtained from experimental EMR studies and the structural data may be facilitated by theoretical modeling of the zero-field splitting (ZFS) parameters (ZFSPs) - for a review, see, e.g. [1,2]. Various modeling techniques for analysis and interpretation of EMR data for transition ions at low symmetry sites in crystals have recently been discussed in [3]. One major technique is the superposition model (SPM) [4,5], which enables prediction of ZFSPs based on the assumed structural distortions models for a transition (M) ion surrounded by the nearest neighbour n ligands (L) within ML_n complex, see, e.g. [6,7]. Comparison of SPM predictions with experimental ZFSP values enables verification of the structural models and thus provides information about the local distortions around paramagnetic ions.

In this paper we present a computer program SPM-MC for modeling and analysis of the structure of ML_n complexes around paramagnetic centers, which utilizes as input the experimental data extracted from EMR spectra. This program is based on the SPM technique and may also be used for prediction of the ZFSPs based on the structural data. A novel aspect in this approach is the

usage of the Monte Carlo (MC) method to predict the feasible ligands positions by fitting the experimental EMR data to theoretical estimates. The program has been tested for various types of crystal structures and ML_n complexes. Subsequently, we consider its application for SPM analysis for Cr^{3+} and Fe^{3+} ions in yttrium aluminum perovskite $YAlO_3$ (YAP) crystal. The EMR measurements of YAP single crystals containing Cr^{3+} and Fe^{3+} impurity ions as well as the spin Hamiltonian analysis of EMR spectra carried out based on triclinic (C_i) site symmetry were reported in [8]. Capabilities of the program SPM-MC and preliminary results of its application for Cr^{3+} ions in YAP are presented here.

2. Spin Hamiltonian and SPM Analysis of EMR spectra

In this study we adopt the spin Hamiltonian (SH) notation [1,2] outlined in [8]. For clarity we only define the form of SH suitable for arbitrary low (triclinic) symmetry and expressed in terms of the extended Stevens operators (ESO) O_k^q defined in [9,10]:

$$H_s = \mu_B B \cdot g \cdot S + \sum B_k^q O_k^q(S_x, S_y, S_z) = \mu_B B \cdot g \cdot S + \sum f_k b_k^q O_k^q \quad (1)$$

The ZFSPs B_k^q (b_k^q) with $k = 2$ only are required for Cr^{3+} ($S=3/2$), whereas those with $k = 2$ and 4 for Fe^{3+} ($S=5/2$) ions [1,2,8]. For proper relations between the orthorhombic ZFSPs and the conventional ones [1,2] as well as pertinent references, the readers may refer to [8,11].

Low symmetry aspects observed in EMR spectra of Cr^{3+} and Fe^{3+} ions in YAP arise due to structural distortions. YAP has a distorted perovskite structure with the orthorhombic centrosymmetric $Pbnm$ space group [12,13]. The YAP structure forms as a grid of tilted AlO_6 regular octahedra with Y ions occupying voids between them. The YO_8 dodecahedra are considerably distorted since the Y-O bond-length varies from 0.2284 nm to 0.2597 nm for YAP-Nd [13]. The cation ionic radii are: $R_Y = 0.102$ nm and $R_{Al} = 0.053$ nm. The Cr^{3+} ($R_{Cr} = 0.062$ nm), Ti^{3+} ($R_{Ti} = 0.067$ nm), Mn^{4+} ($R_{Mn} = 0.053$ nm), and Fe^{3+} ($R_{Fe} = 0.065$ nm) ions are found to substitute the Al cations in YAP host [14-17].

Superposition model represents the ZFSPs in the form of linear combinations of products of the intrinsic parameters and coordination factors – for definitions see, e.g. [4-7]. The intrinsic parameters depend only on the kind of ligands and their distances from the central ion. The coordination factors $K_k^q(\theta_i, \phi_i)$ depend only on the angular positions of ligands in the coordinate system associated with the paramagnetic ion. Full listing of $K_k^q(\theta_i, \phi_i)$ obtained using the transformation properties of the ESOs for arbitrary symmetry and $k = 2, 4,$ and 6 has been provided in [6]. For illustration we provide the SPM expressions used for the orthorhombic ZFSPs b_k^q suitable for Cr^{3+} ions [18-20]:

$$b_2^0 = \sum_i \left(-A \left(\frac{R_0}{R_i} \right)^n + B \left(\frac{R_0}{R_i} \right)^m \right) \cdot \frac{1}{2} (3 \cos^2 \theta - 1) \quad (2)$$

$$b_2^2 = \sum_i \left(-A \left(\frac{R_0}{R_i} \right)^n + B \left(\frac{R_0}{R_i} \right)^m \right) \cdot \frac{3}{2} (\sin^2 \theta \cos 2\phi)$$

and Fe³⁺ ions [21, 18]:

$$b_2^0 = \sum_i \left((-A + B) \left(\frac{R_0}{R_i} \right)^{t_2} \right) \cdot \frac{1}{2} (3 \cos^2 \theta - 1) \quad (3)$$

$$b_2^2 = \sum_i \left((-A + B) \left(\frac{R_0}{R_i} \right)^{t_2} \right) \cdot \frac{3}{2} (\sin^2 \theta \cos 2\phi).$$

The program (Section 3.1) handles also the general SPM expressions for $k = 2$ and 4 [5,6,22]:

$$b_k^q = \sum_i \bar{b}_k(R_i) \cdot K_k^q(\theta_i, \phi_i), \quad \bar{b}_k(R_i) = \bar{b}_k(R_0) \left(\frac{R_0}{R_i} \right)^{t_k} \quad (4)$$

In Eqs. (2)-(4) (θ, ϕ) are the polar angles, R_i - the distance between the central ion and i^{th} -ligand; the constants $A, B, n, m, t_k, \bar{b}_k$ and the reference distance R_0 depend on the kind of impurity ions and their valence [6,18-21]. The SPM calculations for the 2nd-rank ZFS terms may be carried out in two ways: (i) based on the method [18] using Eqs. (2) or (3) and (ii) using general expressions, Eqs. (4), for all 5 triclinic ZFSPs. For the 4th-rank ZFS terms Eqs. (4) are used together with the selected way for the 2nd-rank ZFS terms. Development of the extended version of the program SPM-MC based on the general SPM expressions for $k = 6$, see, e.g. [22] and references therein, is in progress.

3. Program SPM-MC and its applications

3.1. Program SPM-MC

Basic capabilities of the program SPM-MC are outlined below. The input data, i.e. the unit cell parameters and the number of ligands is first entered in the field 'Structure' (see, Fig. 1). Next, in the field 'Coordinates of ligands' the positions of up to 13 distinct ligands may be entered. The experimental EMR data are provided in the field 'EMR parameter', whereas the rank of ZFSPs to be used for calculations is selected via 'the order'. The values of the model parameters ($A, B, n, m, t_k, \bar{b}_k, R_0$) are entered in the field 'Constant'. At present

two calculation options, i.e. ‘version’ #1 and #2, are available based on the relations (2) or (3) and (4), respectively. The required range and accuracy of calculations are specified in the field ‘Computation range’. Finally, the program may be activated by clicking on the button ‘Start’. The results of calculations based on the Monte Carlo (MC) method, represented in the spherical and Cartesian coordinates together with the values of all EMR parameters are displayed in the two upper-right windows. Additionally, the graphical 3D representation of the ligands positions and the axis systems appears in the lower-right window. Program enables to obtain one set of the values of the ZFSPs b_k^q by clicking on the button ‘1 set’. All numerical output results may be saved into a text file, whereas the graphs are saved as *.bmp files.

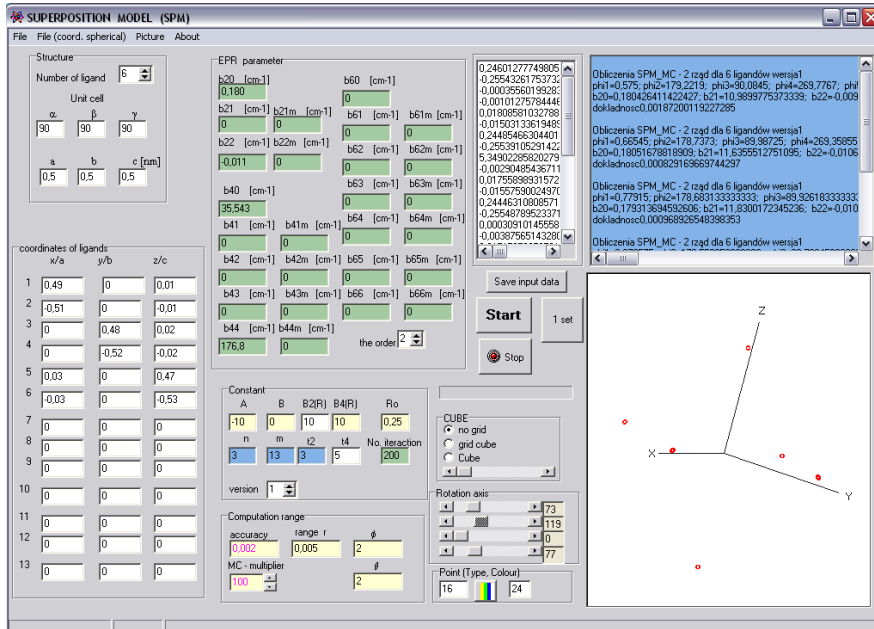


Fig. 1. Sample interface for the SPM-MC showing illustrative input and output data.

3.2. Applications

The parameters A , B , and R_0 for Cr^{3+} ions, which replace Al^{3+} in YAlO_3 , were obtained from the data in [18,21], whereas the crystallographic data from [23]. For illustration, we adopt the following values: $R_0 = 0.195$ nm, $n = 10$, $m = 13$, $A = -10.6$ cm^{-1} , and $B = -8.2$ cm^{-1} . Using the ZFS parameters and the pertinent conversion relations provided in [8,11], the program SPM-MC computes the feasible positions of the oxygen ligands in a given unit cell volume that yield the SPM-predicted ZFSPs consistent with the experimental ZFSPs. The numerical calculations and analysis were carried out for the

complex CrO_6 in YAlO_3 . The angles θ_i and ϕ_i were varied in the range of several degrees from the starting values reported for the undistorted AlO_6 octahedron, whereas the minimum distances R_i were computed from the ionic radii. The averaged values (θ_i , ϕ_i ; R_i) obtained from the program SPM-MC are listed in Table 1 together with the crystallographic data for the AlO_6 octahedron in pure crystal. These values were used to construct the CrO_6 octahedron in YAlO_3 .

Table 1. The positions of the oxygen ligands ($i = 1$ to 6) in the MO_6 octahedra in the polar coordinates.

Ligand's number i :		1	2	3	4	5	6
AlO_6 [23]	R_i [nm]	0.1901	0.1901	0.1910	0.1910	0.1921	0.1921
	θ_i [°]	14.2	165.8	80.2	99.8	80.2	99.8
	ϕ_i [°]	196.7	16.7	56.0	236.0	324.4	144.4
CrO_6	R_i [nm]	0.2010	0.1967	0.2041	0.2033	0.2088	0.2162
	θ_i [°]	16.3	86.5	88.1	101.2	175.6	100.1
	ϕ_i [°]	205.1	57.2	331.7	241.6	22.0	154.1

4. Conclusions

Computer program SPM-MC based on the superposition model (SPM) approach and incorporating the Monte Carlo (MC) method has been developed for interpretation of EMR spectra for paramagnetic ions coordinated by up to 13 ligands of arbitrary type. The extended version of this program will be suitable for low (triclinic) symmetry sites. This program enables prediction of the feasible ligands' positions by fitting the experimental EMR data to the theoretical estimates. Preliminary results for the impurity Cr^{3+} ions in YAlO_3 are presented. SPM analysis confirms the most probable model of distortions around Cr^{3+} ions occupying the Al positions. The predicted small radial distortions of the $\text{Cr}(\text{Al})\text{O}_6$ complex correlate well with the size of the ionic radii of the dopant ions.

Acknowledgements

This work was partially supported by a grant from the Polish Ministry of Science and Education for the years 2009-2010 to CZR. Thanks are due to Mr P. Gnutek for helpful comments.

References

- [1] C. Rudowicz, Magn. Res. Rev. 13 (1987) 1; Erratum, *ibidem* 13 (1988) 335.
- [2] C. Rudowicz and S. K. Misra, Appl. Spect. Reviews 36 (2001) 11.
- [3] C. Rudowicz and P. Gnutek, Physica B 404 (2009) 3582.
- [4] D. J. Newman and W. Urban, Adv. Phys. 24 (1975) 793.
- [5] D. J. Newman and B. Ng, Rep. Prog. Phys. 52 (1989) 954.
- [6] C. Rudowicz, J. Phys. C: Solid State Phys. 20 (1987) 6033.
- [7] T. H. Yeom, Y. M. Chang, S. H. Choh, and C. Rudowicz, Phys. Stat. Sol. (b) 185 (1994) 409.
- [8] I. Stefaniuk, C. Rudowicz, P. Gnutek, and A. Suchocki, Appl. Magn. Res. 36 (2009) 371.
- [9] C. Rudowicz, J. Phys. C: Solid State Phys. 18 (1985) 1415; Erratum, *ibidem* 18 (1985) 3837.
- [10] C. Rudowicz and C. Y. Chung, J. Phys.: Condens. Matter 16 (2004) 5825.
- [11] C. Rudowicz, J. Phys.: Condens. Matter 12 (2000) L417.
- [12] S. Geller and E. A. Wood, Acta Crystallogr. 9 (1956) 563.
- [13] L. Vasylechko, A. Matkovskii, D. Savvitski, A. Suchocki, and F. Wallrafen, J. Alloys Compds. 291 (1999) 57.
- [14] M. Yamaga, H. Takeuchi, T. J. Han, and B. Henderson, J. Phys.: Condens. Matter 5 (1993) 8097.
- [15] R. F. Belt, J. R. Latore, and R. Uhrin, Appl. Phys. Lett. 25 (1974) 218.
- [16] R. R. Rakhimov, A. L. Wilkerson, G. B. Loutts, M. A. Noginov, N. Noginova, W. Lindsay, and H. R. Ries, Solid State Comm. 108 (1998) 549.
- [17] M. Yamaga, T. Yosida, B. Henderson, K. O'Donnell, and M. Date, J. Phys.: Condens. Matter 4 (1992) 7285.
- [18] K. A. Müller and W. Berlinger, J. Phys. C: Solid State Phys. 16 (1983) 6861.
- [19] K. A. Müller, W. Berlinger, and J. Albers, Phys. Rev. B 32 (1985) 5837.
- [20] J. Kuriata, J. M. Baker, L. Sadlowski, I. Stefaniuk, and T. Bodziony, J. Phys.: Condens. Matter 10 (1998) 407.
- [21] E. Siegel and K. A. Müller, Phys. Rev. B 20 (1979) 9.
- [22] P. Gnutek, M. Acikgoz, and C. Rudowicz, Opt. Mat. (2010) - *in press*
- [23] R. Diehl and G. Brandt, Mat. Res. Bull. 10 (1975) 85.

Ferroic materials studied by EPR

S. Waplak

*Institute of Molecular Physics, Polish Academy of Sciences,
Mariana Smoluchowskiego 17, 60-179 Poznań, Poland
Email: stefan.waplak@ifmpan.poznan.pl*

We can call crystal as „ferroic” if it has two or more orientational (energy) states and can be transformed to one of them by an external forces like magnetic, electric, mechanical etc. Especially the phase transition phenomena which are realized by jumpwise and/or tiny changes in atoms positions could be tracked by EPR. The emphasis is now on collective phenomena in systems where disorder and/or nonlinearity are the major ingredients: mixed crystals, incommensurate structure, proton-glasses, charge density wave, superparaelectric, nanosized etc. In these cases, magnetic resonance techniques have provided unique microscopic information especially powerful if used commonly with traditional bulk methods.

Historical evolution of EPR devoted to study of ferroics in laboratories of Institute of Molecular Physics Polish Academy of Sciences will be done in this presentation.

Electric Current Induced Spin Excitation due to Rashba Field
Z. Wilamowski,^{*1,2)}, W. Ungier¹⁾, M. Havlicek³⁾, and W. Jantsch³⁾,

* Corresponding author: wilamz@ifpan.edu.pl

¹⁾ Institute of Physics Polish Academy of Sciences, 02-668 Warsaw, Poland

²⁾ Faculty of Mathematics and Computer Sciences, UWM Olsztyn, Poland

³⁾ Institut für Halbleiter- und Festkörperphysik, JKU, 4040 Linz, Austria

We discuss resonant spin excitation by a high frequency electric current in the presence of Rashba spin orbit coupling. We review experimental data for asymmetric Si quantum wells and ZnO bulk crystals. Evidence for this mechanism is based on the anisotropy of the spin resonance signal and on the amplitude of the absorption signal. We demonstrate that for high mobility carriers the driving force of the current induced mechanism strongly exceeds that caused by magnetic dipole transitions. The current induced ESR signal is characterized by a specific line shape – it changes from absorptive to dispersive, depending on the electron mobility and the experimental geometry. We explain the rich dependence in terms of two contributions: the transfer of microwave energy to (i) the magnetic energy and (ii) to Joule heating. The latter shows a resonant effect due to the spin dependent carrier velocity.

Keywords: Rashba splitting, spin orbit coupling, Electron Spin Resonance

Posters

Dyson line and modified Dyson line in the EPR measurements

M. Bester, I Stefaniuk, M. Łabuz, M. Kuźma

Institute of Physics, University of Rzeszow, Rejtana 16A, 35-959 Rzeszow, Poland

In many measurements, EPR resonance line is observed in a very broad form. We might point on the broad line if its half-width is comparable with the resonance field (eg, $\Delta B=100mT$ i $B_0=330mT$ in the measurements of X-band). In such cases, the measurement accuracy of line parameters such as, position, width and shape deteriorates. For polycrystalline samples with magnetic admixtures we assume that the line is Lorentz type with the exception of banks (called wings) where the line is Gaussian or exponential. This line shape is mainly due to exchange narrowing. Gaussian shape of the line tail has been described in the work of Dyson [1], while exponential tail has been described in the Feher's paper [2]. It can be assumed that the line is of Lorentz shape in the range of magnetic field $B=B_0\pm a$, where $2a/\Delta B>1$. Gaussian tails are usually covered by noise, that is why narrowed by exchange interaction signal may be adjusted with the Lorentz function with a good accuracy.

In most cases, the signals are symmetric, averaging the EPR magnetic anisotropy and other impacts. Often, however, in the studies of magnetic materials by EPR, lines are asymmetric. Then the line is well described by the function of Dyson [1-3]. The parameters describing the Dyson line and its derivative are the same as for the Lorentz line: B_{pp} , B_0 , I , and additional A/B parameter which is the ratio of amplitude of the left peak A, to the right peak B: $A/B=I_L/I_R$. Alternate shall be equivalent to the so-called α parameter, asymmetry parameter which is the ratio of dispersion and absorption. Dyson line parameters can be determined either by the graphical method of direct measurement of the spectrum, or by computer fitting of Dyson function with four parameters A , α , ΔH , H_0 to the experimental spectrum. There is another, alternative way, by fitting the experimental spectrum of the polynomial variable x [4, 5]:

$$F(x) = \frac{(I - Cx - x)}{(I + x^2)^2} \quad (1)$$

where $x=(H-Hr)/\Delta H$. The procedure for the designation of the parameters in this way is described in paper of Peter *et al.* [4]. For the broad EPR line one must take into account the contribution of the component field in the part which rotates in the opposite direction than the Larmor precession. In fact one can notice that for a circularly polarized microwave field, where the factor g is anisotropic and contains components of the positive and negative sign, the EPR signal appears on both sides of $B=0$. This phenomenon is described in the book

of Bleaney and Abragam. The impact of this effect on the shape of the broad EPR line was given attention in the work of Ivanshin [6] and is expressed in equations for Lorentz and Dyson broad lines [7]:

$$P_L = \left[\frac{\Delta B}{4(B - B_0)^2 + \Delta B^2} + \frac{\Delta B}{4(B + B_0)^2 + \Delta B^2} \right] \quad (2)$$

$$P_D = \left[\frac{\Delta B + \alpha(B - B_0)}{4(B - B_0)^2 + \Delta B^2} + \frac{\Delta B + \alpha(B + B_0)}{4(B + B_0)^2 + \Delta B^2} \right]$$

In these formulas there is an asymmetry against a field $B=0$, although from a physical point of view, the asymmetry should not exist because the reversal field B in the spectrometer should not change the properties of the investigated system. Such an asymmetry can be explained basing on the components of absorption and dispersion of the broad EPR line [7]. In our experiments with electrically conductive ferromagnetic samples, EPR line shifts towards low fields as a result of large internal magnetic field. This shift is so large that only right half of the signal derivative is fully visible. Then it is necessary to determine the parameters solely from that part of the curve by computational fitting of the analytical functions to experimental data. One can observe that the parameters derived from the part of the curve differ from those which would be derived from the whole curve. In this paper we analyze the accuracy of the determination of the parameters of asymmetric line from its registered component.

References

- [1] Dyson F J 1955 *Phys.* **98** 349
- [2] Feher G and Kip A F 1955 *Phys.* **98** 337
- [3] Webb R H 1967 *Phys.* **158** 225
- [4] Peter M, Shaltiel D, Wernicke J H, Williams H J, Mock J B and Sherwood R C 1962 *Phys.* **126** 1395
- [5] Burgardt P and Seehra M S 1977 *Phys. B* **1916** 1802
- [6] Ivanshin V A, Deisenhofer J and Krug von Nidda H A 2000 *Phys. B* **1961** 6213
- [7] J P Joshi and S V Bhat 2004 *J. Magnetic. Res.* **168** 284

Magnetic properties of transition metal doped zinc-oxide.

I.Stefaniuk**, *B.Cieniek*, *I. Virt

** Corresponding author: istef@univ.rzeszow.pl*

Institute of Physics, University of Rzeszow, Rejtana 16a, 35-310 Rzeszow, Poland

Diluted Magnetic Semiconductors (DMS) are of interest for study mainly due to the spin-spin exchange interaction between the localised magnetic moments and the band electrons [1]. This property of DMS has potential applications in the spin-dependent semiconductor electronics [2].

Zinc-oxide have attracted intense attention in the searching for high T_C ferromagnetic DMS materials, since Dietl *et al.* [3] predicted that GaN- and ZnO-based DMSs could exhibit ferromagnetism above room temperature upon doping with transition elements, such as Mn, (on the order of 5% or more) in *p*-type materials.

We report on the magnetic properties of zinc-oxide (ZnO) doped with Co, Cr and Mn. Electron paramagnetic resonance (EPR) spectra have been measured and analysed to extract information on the incorporation of the ions in the lattice.

The EPR measurements were performed on the X-band. The temperature of the samples was controlled in the range of 92–370 K using the BRUKER liquid N gas flow cryostat.

Mn, Co and Cr -doped ZnO thin films were grown by pulsed laser deposition (PLD) method.

As an example, we show in this abstract the EPR spectra for the sample ZnO:Mn (Fig. 1).

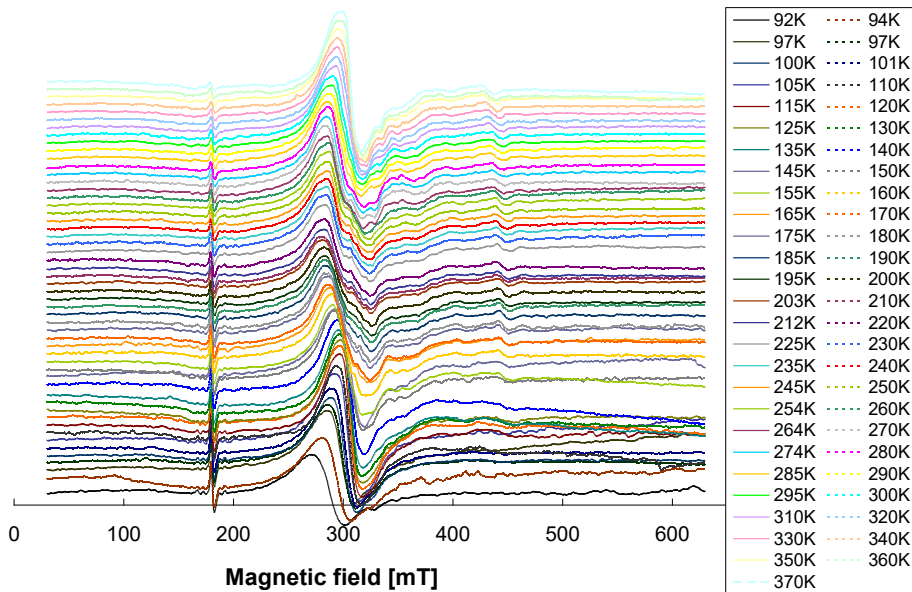


Fig.1. EPR spectra of ZnO:Mn in temperature range 92-370K.

We performed a fitting of a Lorentz-type curve to the EPR spectra. In this way we found parameters for EPR lines such as the peak-to-peak line width (ΔH_{pp}), the intensity (I) as well as the resonance field (H_r). Basing on these data we have obtained the temperature dependences $\Delta H_{pp}(T)$, $I(T)$, and $g(T)$. We used Curie-Weiss law to analyse the temperature dependences of integral intensity.

References

- [1] Dobrowolski W., Kossut J., Story T *II-VI and IV-VI Diluted Magnetic Semiconductors—new bulk materials and low dimensional quantum structures* (Handbook of Magnetic Materials vol. 15) ed. K.H.J. Bushow (Elsevier) (2003)
- [2] Awshalom D D., Loss D., Samarth N Eds. *Semiconductors Spintronics and Quantum Computation* (Springer) (2002)
- [3] T. Dietl, H. Ohno, F . Matsukura, J . Cibert and D. Ferrand, *Science* 287 (2000) 1019.

Studies on Antioxidants Structure in Glycerol Fractions from Biodiesel Production: Spin Trapping EPR and DFT Investigations

Irmina Ćwieląg-Piasecka*, Maciej Witwicki, Maria Jerzykiewicz

* irminac@eto.wchuwr.pl

Faculty of Chemistry, Wrocław University, 14 F. Joliot-Curie St., 50-383 Wrocław, Poland

Abstract

Spin trapping electron paramagnetic resonance (EPR) spectroscopy and density functional theory (DFT) were employed to investigate antioxidant properties of glycerol fractions (GF) obtained in biodiesel production process. The structure of antioxidant species was examined *via* the EPR measurement of trapped radical derived from the H₂O₂ and GF reaction. As reference chemical systems pure glycerol, α - and δ -tocopherol along with oil were used, since they are potential constituents of GF. The parameters of glycerol fraction-PBN adduct EPR spectra ($a_{iso}(^{14}N) = 15.3$ G and $a_{iso}(^1H) = 3.8$ G) indicate the α -tocopherol origin of PBN trapped radicals.

Results obtained from the DFT calculations of EPR parameters stay in good accordance with experimental ones when the solvent effects are included - PCM formalism and two explicit ethanol molecules interacting with the radical center. Surprisingly, DFT results exclude trapping of oxygen centered radical and suggest carbon centered type.

Keywords: EPR, tocopherol, PBN, spin trap, DFT

1. Introduction

Glycerol fraction (bioglycerol, GF) is a product of transesterification reaction of edible oils and animal fats. Presence of antioxidants and anticorrosive properties of glycerol fractions were established, however no attempts to structural investigation of compounds responsible for these features were made. Our previous studies based on the reaction with galvinoxyl radical proved existence of phenolic systems [1].

One of the most important and reliable technique for detection as well as qualitative and quantitative characterization of antioxidants is the electron paramagnetic resonance spectroscopy (EPR) [2-4]. Spin trapping is an approach to the study of unstable free radicals, in which short-living radical is allowed to react with diamagnetic compound (spin trap), to obtain a relatively long-living product called a spin adduct [5-7]. The EPR parameters are known to be conditional upon adduct type. Therefore, obtained EPR spectra allow to study and characterize initial radical and its nature (oxygen-, nitrogen-, carbon-centered) based on the parameters from the simulation of spectra such (e. g. isotopic hyperfine splittings ($a_{iso}(^{14}N)$ and $a_{iso}(^1H)$ or g factor) [8].

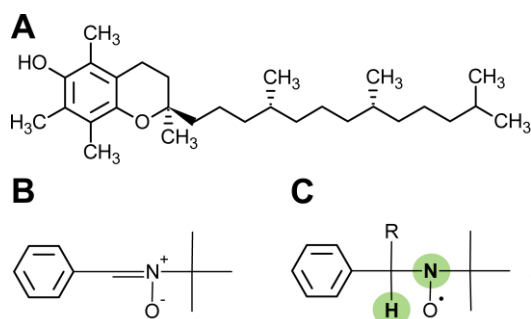


Fig. 1. Structures of chemical systems under investigation: (A) α -tocopherol; (B) N-t Butyl- α -phenylnitrone (PBN); (C) PBN spin adduct of R• radical (nucleus giving isotropic hyperfine splittings are highlighted)

The aim of this work is to determine the structures of antioxidants present in the glycerol fraction and their paramagnetic PBN adducts. To complete the spin trapping research of phenolic species in bioglycerol theoretical DFT studies were used. We have expected that the comparison of EPR parameters obtained for the PBN spin adducts of GF and different antioxidants potentially present in it would reveal which them are present and active in bioglycerol. Furthermore, the relationship between theoretically predicted EPR properties of various spin adducts and values experimentally obtained have been envisaged to point out the realistic structure of PBN trapped radical.

2. Experimental and computational details

EPR spectra were obtained at room temperature using Bruker ESP300E spectrometer with a 100 kHz magnetic field modulation, equipped with a Bruker NMR gaussmeter ER 035M and a Hewlett-Packard microwave frequency counter HP 5350B operating at X-band frequency (~ 9.7 GHz). Microwave power 20 mW and modulation amplitude 1 G were used. Samples were measured 10 minutes and 1 hour after H_2O_2 was added. In the first week reaction was sampled and measured each day, than after every few days and finally every week till the PBN adduct signal disappearance. Samples were dissolved in PBN ethanol solution except oils that were dissolved in acetone.

All computations were performed with GAUSSIAN 09 suite of programs. Geometries were optimized at the UB3LYP/6-31G(d,p) theory level. The UB3LYP/EPR-II and UPBE0/EPR-II methods were employed to calculate the EPR properties. To caption the major effects of solvation Tomasi's polarized continuum method (PCM) was employed using its integral equation formalism variant (IEFPCM) to mimic ethanol ($\epsilon = 24.852$) as a solvent. Furthermore, to take into account the specific interactions between the solvent molecules and solute, the more elaborated computations including the PCM and two ethanol molecules interacting with the nitric oxide radical center were performed.

3. Results and discussion

3.1. Formation of different PBN adducts

The g parameter for the PBN adducts remained constant through whole experiment. Its value was ranged between 2.0058 and 2.0059 for GF and tocopherols while for the oil sample it was slightly higher (~ 2.0060). The hyperfine splittings were different depending on the investigated sample and time of the measurements. However, for different GT fractions only the hydrogen hyperfine splittings were found to be meaningful indicators of the structure. Within first days of measurements the sample of α -tocopherol exhibited the well-known α -tocopherol radical [9] (see Fig. 2A). One week after reaction has been started the formation of PBN spin adduct was confirmed by recording of its EPR spectrum (Fig. 2B). In the end only the PBN- α -tocopherol adduct was observed (Fig. 2C).

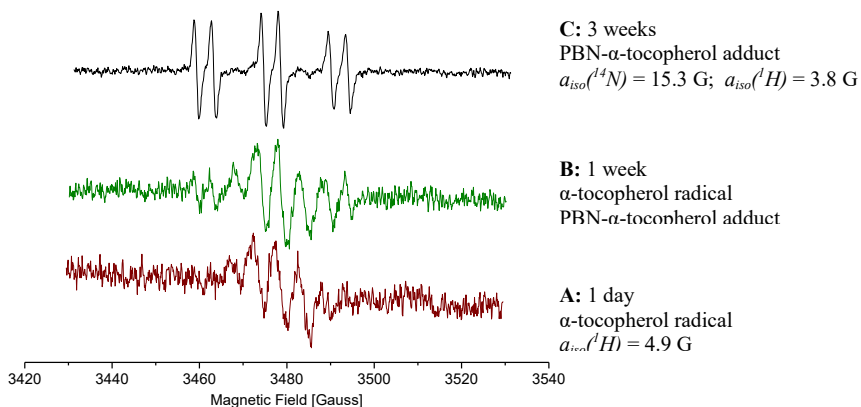


Fig. 2. EPR spectra of α -tocopherol radical (A); α -tocopherol radical and received PBN adduct (B); PBN- α -tocopherol adduct (C)

It is essential that hyperfine splitting observed for GT fractions were like for α -tocopherol ($a_{iso}(^{14}N)=15.3$, $a_{iso}(^1H)=3.8$). That proves presence of antioxidant similar to α -tocopherol in discussed glycerol fractions.

3.2. DFT computations

The $a_{iso}(^{14}N)$ and $a_{iso}(^1H)$ isotropic hyperfine splittings as well as g tensors were calculated for the potentially possible PBN spin adducts received as shown below:



For every R various hydrogen atoms abstracted by the $\cdot OH$ radical were considered giving different $R\cdot$ radicals to be trapped by PBN.

The crucial aspect of our DFT calculations was to establish solvent effect on the properties under investigation. The inclusion of explicit ethanol molecules H-bonded to the radical center was found to be essential and the impact of functional used in the calculations was found to be minor. The comparison of experimental and theoretical $a_{iso}(^{14}N)$ and $a_{iso}(^1H)$ implied strongly that the spin adducts in investigated systems are formed from the carbon centered radicals, that can be formed both at the methyl groups of aromatic ring and aliphatic chain of α -tocopherol.

4. Conclusions

Parameters simulated from PBN-adduct EPR spectra define unequivocally that antioxidants present in glycerol fraction from biodiesel production have structure of α – tocopherol. Hyperfine splitting constants of bioglycerol samples remained unchanged during the whole experiment and were the same as for α – tocopherol ($a_{iso}(^1H) = 3.8G$ $a_{iso}(^{14}N) = 15.3G$).

The DFT calculations showed that accurate inclusion of solvent effects (combination of PCM method and explicit ethanol molecules) is mandatory for correct prediction of $a_{iso}(^1H)$, $a_{iso}(^{14}N)$ and g-tensor in radical systems under studies. Moreover, the comparison of experimental and DFT predicted $a_{iso}(^1H)$ values reveals that the carbon centered α – tocopherol radical is trapped by PBN. However, this fact cannot be unambiguously associated with the antioxidant activity. Though it was shown that antioxidant activity of α -tocopherol against hydroxyl radicals is not selective and can take place at several positions [10]. Moreover one should keep in mind that in experiments reported herein α -tocopherol was exposed to hydroxyl radicals constantly, even after exhaustion of its antioxidant capability, therefore the probability of formation and trapping of carbon centered radical was additionally increased.

Acknowledgements

This work was supported by the Polish Ministry of Science and Higher Education (MNiSW), project no. N N204 124038. All computations were performed using computers of the Wrocław Center for Networking and Supercomputing (Grant No. 48).

References

- [1] M. Jerzykiewicz, I. Cwiela, W. Jerzykiewicz, J. Chem. Technol. Biotechnol. 84 (2009) 1196.
- [2] M. Rohrer, F. MacMillan, T. Prisner, A. Gardiner, K. Möbius, W. Lubitz, J. Phys. Chem. B 102 (1998) 4648.
- [3] J.A. Pedersen, Spectrochim. Acta A 58 (2002) 1257.
- [4] K.C. Christoforidis, S. Un, Y. Deligiannakis, J. Phys. Chem. A 111, 2007, 11860.
- [5] E.G. Janzen, Methods Enzymol. 105 (1994) 188.

- [6] E.G. Janzen, D.L. Haire, *Advances in Free Radical Chemistry Vol. 1*, D.D. Tanner, Greenwich Ed., CT, U.S.A. 1990, pp. 253–295.
- [7] D. Rehorek, *Chem. Soc. Rev.* 20 (1991) 341.
- [8] G. Buettner, *Free Radic. Biol. Med.* 3 (1987) 259.
- [9] L. Vicente, N. Deighton, S.M. Glidewell, J.A.I. Empis, B.A. Goodman, *Z Lebensm. Unters. Forsch* 200 (1995) 44.
- [10] M. Navarrete, C. Rangel, J.C. Corchado, J. Espinosa-Garcia, *J. Phys. Chem. A.* 109 (2005) 4777.

EPR spectroscopy of tetraborate glasses, doped with Cu and Mn

B.V. Padlyak^{1,2}, *A. Drzewiecki*^{1*}, *O.O. Smyrnov*¹

¹*Division of Spectroscopy of Functional Materials, Institute of Physics, University of Zielona Góra, 4a Szafrana Str., 65-516 Zielona Góra, Poland*

²*Institute of Physical Optics, 23 Dragomanov Str., 79-005 Lviv, Ukraine*

The lithium and potassium-lithium tetraborate glasses ($\text{Li}_2\text{B}_4\text{O}_7$ and KLiB_4O_7 or LTB and KLTB), doped with Cu and Mn were obtained in the air from corresponding crystalline compounds by standard glass technology according to [1]. The Cu and Mn impurities were added to the basic melt composition in the form of the corresponding oxide compounds (CuO and MnO) in amounts 0.4 and 1.6 mol. %. On the basis of analysis of electron paramagnetic resonance (EPR) $\text{Li}_2\text{B}_4\text{O}_7$ and KLiB_4O_7 glasses, doped with Cu and Mn it was shown the following results.

The Cu impurity is incorporated into the tetraborate glass network as Cu^{2+} ($3d^9$) paramagnetic ions. The EPR spectra of Cu^{2+} centres are almost identical in glasses with $\text{Li}_2\text{B}_4\text{O}_7:\text{Cu}$ and $\text{KLiB}_4\text{O}_7:\text{Cu}$ compositions and are characteristic for glassy compounds. The parameters of the Cu^{2+} EPR spectra (g -values, hyperfine constants and peak-to-peak linewidths) in the $\text{Li}_2\text{B}_4\text{O}_7:\text{Cu}$ and $\text{KLiB}_4\text{O}_7:\text{Cu}$ glasses with different Cu content are determined at $T = 300$ K and 77 K. The obtained g_{\parallel} and g_{\perp} values are characteristic for a Cu^{2+} ($3d^9$) Jahn-Teller ions coordinated by six O^{2-} ligands that form an oxygen octahedron, elongated along the z -axis. The ground state for unpaired electron of the Cu^{2+} ion is ${}^2\text{B}_{1g}$ ($d_{x^2-y^2}$ orbital), because $g_{\parallel} > g_{\perp} > g_e = 2.0023$.

The Mn impurity is incorporated into the tetraborate glass network as Mn^{2+} ($3d^5$) paramagnetic ions. Characteristic for glassy compounds EPR spectra of the Mn^{2+} paramagnetic centres are almost identical in glasses with $\text{Li}_2\text{B}_4\text{O}_7:\text{Mn}$ and $\text{KLiB}_4\text{O}_7:\text{Mn}$ compositions and have been attributed to the isolated Mn^{2+} ions with broad distribution of crystal field parameters in the trigonally-distorted octahedral sites and small clusters of the Mn^{2+} ions in the tetraborate glass network. The parameters of the Mn^{2+} EPR spectra in the LTB:Mn and KLTB:Mn glasses with different Mn content are determined at $T = 300$ K and 77 K.

References

- [1] B.V. Padlyak, W. Wojtowicz, V.T. Adamiv, Ya.V. Burak, I.M. Teslyuk, Acta Phys. Pol. A, 117 (2010) 122-125.

* Corresponding and presenting author, e-mail: A.Drzewiecki@ztpnet.pl

Multiplication of Qubits in a Doubly Resonant Bichromatic Field: A transient nutation EPR study

R. Fedaruk^{*1)}, ***A. P. Saiko***²⁾, ***S. A. Markevich***²⁾

* *Corresponding author: fedaruk@wmf.univ.szczecin.pl*

¹⁾ *Institute of Physics, University of Szczecin, Szczecin, Poland*

²⁾ *Scientific-Practical Materials Research Centre NAS of Belarus, Minsk, Belarus*

Abstract

We demonstrate theoretically and experimentally that multiplication of spin qubits arises at double resonance in a bichromatic field when the frequency of the radio-frequency field is close to that of the in the microwave field, provided its frequency equals the Larmor frequency of the initial qubit. The effect is investigated beyond the rotating wave approximation using transient nutations in the pulse EPR of E' centers in crystalline quartz. It is show that the operational multiphoton transitions of qubits dressed by the bichromatic field can be selected by the choice of both the rotating frame and the radio-frequency phase.

Keywords: pulse EPR; transient nutation; double resonance; bichromatic field; spin qubit; Rabi oscillation

1. Introduction

It is known [1] that the resonant interaction between electromagnetic radiation and two-level quantum system (qubit) induces Rabi oscillations, which are the basis for quantum operations. The Rabi frequency ω_R is defined by the amplitude of the electromagnetic field and usually is much smaller than the energy difference ω_0 (in frequency units) between the qubit's states. The "dressing" of qubit by the electromagnetic field splits each level into two giving rise to two new qubits with energy difference ω_R . The spectrum of the multilevel "qubit + field" system consists of three lines at the frequencies ω_0 and $\omega_0 \pm \omega_R$. The second low-frequency electromagnetic field with the frequency close to the Rabi frequency ω_R could induce an additional Rabi oscillation on dressed states of new qubits. These qubits are attracting interest because their coherence time is longer than that of the initial qubit [2,3]. The results of studies of qubits dressed by bichromatic radiation formed by fields with strongly different frequencies are important for a wide range of physical objects, including, among others, nuclear and electron spins, double-well quantum dots, flux and charge qubits in superconducting systems. In NMR [4,5] and EPR [3,6,7] such investigations are used in the development of line-narrowing methods. In this report, we study the dynamics of spin qubits at double resonance in a bichromatic field when the frequency of one (transverse

microwave) field is equal to the Larmor frequency of the spin system and the frequency of the other (longitudinal radio-frequency) field is close to the Rabi frequency in a microwave field. The peculiarities of Rabi oscillations are investigated beyond the rotating wave approximation using pulse EPR in the rotating frame.

2. Theoretical background

Let an electron spin qubit be in three fields: a microwave (mw) one directed along the x axis of the laboratory frame, a radio-frequency (rf) one directed along the z axis, and a static magnetic one also directed along the z axis. The Hamiltonian of the qubit in these fields can be written as follows:

$$H = H_0 + H_{\perp}(t) + H_{\square}(t). \quad (1)$$

Here $H_0 = \omega_0 s^z$ is the Hamiltonian of the Zeeman energy of a spin in the static magnetic field B_0 , where $\omega_0 = \gamma B_0$, and γ is the electron gyromagnetic ratio. Moreover, $H_{\perp}(t) = 2\omega_1 \cos(\omega t + \varphi) s^x$ and $H_{\square}(t) = 2\omega_2 \cos(\omega_{rf} t + \psi) s^z$ are the Hamiltonians of the spin interaction with linearly polarized mw and rf fields, respectively. B_1 and B_2 , ω and ω_{rf} , and φ and ψ denote the respective amplitudes, frequencies, and phases of the mw and rf fields. Finally, $\omega_1 = \gamma B_1$ and $\omega_2 = \gamma B_2$ stand for the Rabi frequencies, whereas $s^{x,y,z}$ are the components of the spin operator. The mw phase $\varphi = 0$ and the counter-rotating component of the mw field is neglected. We also assume that the exact resonance condition is fulfilled $\omega_0 - \omega = 0$, and that $\omega_1, \omega_{rf} \ll \omega_0$. We obtained the following expression for the absorption signal in the laboratory frame (LF):

$$\begin{aligned} v_{LF}(t) = & (1/2) \sin \xi \cos \xi \cos \psi \sin \omega t - \\ & (1/4) \sin \xi \cos \xi \cos \psi [\sin(\omega - \varepsilon)t + \sin(\omega + \varepsilon)t] + \\ & + (1/4) \sin \xi \sin \psi [\cos(\omega + \varepsilon)t - \cos(\omega - \varepsilon)t] + \\ & + (1/8) \sin^2 \xi \sin 2\psi [\cos(\omega + \omega_{rf})t + \cos(\omega - \omega_{rf})t] + \\ & + (1/16) \left((\cos \xi - 1)^2 + (\cos^2 \xi - 1) \cos 2\psi \right) [\sin(\omega + \omega_{rf} - \varepsilon)t - \sin(\omega - \omega_{rf} + \varepsilon)t] + \\ & + (1/16) (\cos^2 \xi - 1) \sin 2\psi [\cos(\omega - \omega_{rf} + \varepsilon)t + \cos(\omega + \omega_{rf} - \varepsilon)t] + \\ & + (1/16) \left((\cos \xi + 1)^2 + (\cos^2 \xi - 1) \cos 2\psi \right) [\sin(\omega + \omega_{rf} + \varepsilon)t - \sin(\omega - \omega_{rf} - \varepsilon)t] + \\ & + (1/16) (\cos^2 \xi - 1) \sin 2\psi [\cos(\omega - \omega_{rf} - \varepsilon)t + \cos(\omega + \omega_{rf} + \varepsilon)t]. \quad (2) \end{aligned}$$

Here $\varepsilon = ((\omega_1 - \omega_{rf} + \Delta_{BS})^2 + \omega_2^2)^{1/2}$ is the frequency of the Rabi oscillations between the spin states dressed simultaneously by the mw and rf field while $\sin \xi = -\omega_2 / \varepsilon$, $\cos \xi = (\omega_1 - \omega_{rf} + \Delta_{BS}) / \varepsilon$, and $\Delta_{BS} \approx \omega_2^2 / 4\omega_{rf}$ is the Bloch–Siegert-like frequency shift. This shift of the dressed-state frequency is due to effect of the counter-rotating (antiresonance) component of the rf field

It follows from Eq. (2) that the resonant interaction between the mw field and the qubit creates its dressed states and two new qubits with energy splitting equal to the Rabi frequency ω_1 . The rf field with the frequency ω_{rf} , which is close to the Rabi frequency ω_1 of the new qubits, “dresses” these qubits, giving rise to four qubits with the energy splitting ε . Allowed multiphoton transitions between states of these qubits afford nine spectral lines observed in the laboratory frame.

There is the possibility of selecting the observed transitions of four qubits by employing the rotating frame. In the singly rotating frame (SRF), which rotates with frequency ω around the z axis of the laboratory frame, the absorption signal can be written as

$$\begin{aligned} \nu_{SRF}(t) = & (1/8) \left[2 \sin^2 \xi \left(\sin \omega_{rf} t + \sin (\omega_{rf} t + 2\psi) \right) + \right. \\ & + (1 + \cos \xi)^2 \sin (\omega_{rf} + \varepsilon) t - (1 - \cos^2 \xi) \sin ((\omega_{rf} + \varepsilon) t + 2\psi) + \\ & \left. + (1 - \cos \xi)^2 \sin (\omega_{rf} - \varepsilon) t - (1 - \cos^2 \xi) \sin ((\omega_{rf} - \varepsilon) t + 2\psi) \right]. \end{aligned} \quad (3)$$

For the random rf phase, the absorption signal has three comparable oscillating components with frequencies ω_1 and $\omega_1 \pm (\omega_2^2 + \Delta_{BS}^2)^{1/2}$. For the rf phase $\psi = 0$, the sidebands are smaller than those at the random rf phase by the factor $\Delta_{BS} / (\omega_2^2 + \Delta_{BS}^2)^{1/2}$. When we use $\psi = \pi / 2$, the component with frequency ω_1 vanishes and the sidebands are comparable to those at the random rf phase. Note that in the strong-field regime the counter-rotating component of the rf field gives rise to the Bloch–Siegert effect, and the high-frequency sideband is always more intensive than the low-frequency one.

Upon the rotating wave approximation ($\Delta_{BS} \rightarrow 0$), it follows from Eq. (3) that for $\psi = 0$ only the component with frequency ω_1 remains. At the same time, for both $\psi = \pi / 2$ and the random rf phase, the intensities of the sidebands are equal. The equalization of sidebands can be used to indicate the validity of the rotating wave approximation. On the contrary, their asymmetry reveals the effect of the counter-rotating component of the rf field.

In the doubly rotating frame (DRF), in which the Hamiltonian is diagonalized to the form $H_{diag} = \varepsilon s^z$, the absorption signal can be written as follows:

$$\nu_{DRF}(t) = (\cos \xi \cos \psi \sin \varepsilon t - \sin \psi \cos \varepsilon t) / 2. \quad (4)$$

According to Eq. (4), the absorption signal in the doubly rotating frame is caused by the transitions between spin states dressed simultaneously by the mw and rf fields. At the exact resonance ($\omega_1 = \omega_{rf}$), the signal for $\psi = 0$ is smaller than the signal for $\psi = \pi / 2$ by the factor $\Delta_{BS} / (\omega_2^2 + \Delta_{BS}^2)^{1/2}$. If $\Delta_{BS} \rightarrow 0$, the signal for $\psi = 0$ disappears. In this case, for $\psi = \pi / 2$, the absorption signal oscillates with the Rabi frequency ω_2 .

3. Results and discussion

The predicted effects are confirmed by observations of the transient nutations (Rabi oscillations) in the pulse EPR of E' centers in crystalline quartz. We used the experimental method and the sample described in [3]. The experiments were carried out at room temperature. The duration, amplitude, and repetition period of the magnetic-field pulses were equal to 10 μ s, 0.12 mT, and 1.25 ms, respectively. To improve the signal-to-noise ratio, the digital summation (up to 10^3) of the nutation signals obtained during each pulse was used.

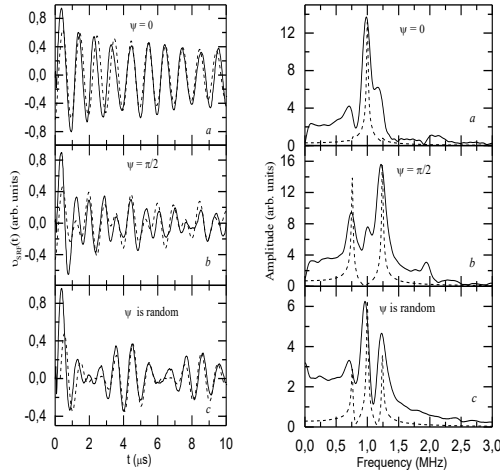


Fig. 1. Time evolution of the absorption EPR signals in the singly rotating frame. Here, $\omega = \omega_0$, $\omega_1 = \omega_{rf} = 2\pi$ 1.0 MHz, $\omega_2 = 2\pi$ 0.24 MHz. The solid and dashed lines correspond to the experiment and theory, respectively.

Fig. 2. Fourier spectra of the absorption signals shown in Fig. 1. The solid and dashed lines correspond to the experiment and theory, respectively.

Fig. 1 shows the time evolution of absorption signals observed in the singly rotating frames. The signals were obtained for the following parameters of the bichromatic field: $\omega = \omega_0$, $\omega_1 = \omega_{rf} = 2\pi \cdot 1.0$ MHz, $\omega_2 = 2\pi \cdot 0.24$ MHz, for the rf phase $\psi = 0$ (Fig. 1a), $\psi = \pi/2$ (Fig. 1b) and the random rf phase (Fig. 1c). The signal shown in Fig. 1c is the result of the averaging of nutation signals at the uniform distribution of random phases of the rf field over the interval from 0 to 2π . The Fourier spectra of obtained signals are presented in Fig. 2.

The fitting of the observed signals by Eq. (3) shown by the dashed lines in Figs. 1 and 2 demonstrates a good agreement between the theory and experiment and confirms that the observed signal has three oscillating components with frequencies ω_1 and $\omega_1 \pm (\omega_2^2 + \Delta_{BS}^2)^{1/2}$. The predicted dependence of these components on the rf phase is also observed. The approximation of the damping of the signals was done using in Eq. (3) the exponential decay function with $T = 14 \mu\text{s}$.

Same difference between observed and calculated signals is due to inhomogeneous broadening of EPR line of our sample, which was not taken into account in the theoretical description. In the Fourier spectra, the broadening of observed lines in comparison with the calculated those is due to the limited time interval of the observation of the nutation signals.

It is seen in the signal shown in Fig. 2 that the violation of the rotating-wave approximation is manifested in the asymmetry of the amplitudes of signals at the frequencies $\omega_1 \pm (\omega_2^2 + \Delta_{BS}^2)^{1/2}$.

4. Conclusions

We have shown theoretically and experimentally that multiplication of spin qubits arises at double resonance in a bichromatic field ($\omega = \omega_0$ and $\omega_1 = \omega_{rf}$). We show that the operational multiphoton transitions of dressed qubits can be selected by the choice of both the rotating frame and the rf phase. The experimental results obtained in the two-level EPR system in the rotating frame demonstrate that the theory correctly describes the dynamics of spin qubits dressed by the bichromatic field. The effects predicted beyond the rotating wave approximation are also confirmed by the observation of transient nutations.

References

- [1] M. de Belas, Short Introduction to Quantum Information and Quantum Computation, Cambridge University Press, Cambridge, 2006.
- [2] Ya. S. Greenberg, Phys. Rev. B 76 (2007) 104520.
- [3] A. P. Saiko, G. G. Fedoruk, JETP Lett. 87 (2008) 128.
- [4] A.G. Redfield, Phys. Rev. 98 (1955) 1787.
- [5] H. Hatanaka, M. Sugiyama, N. Tabuchi, J. Magn. Res. 165 (2003) 293.
- [6] G. Jeschke, Chem. Phys. Lett. 301 (1999) 524.
- [7] G. G. Fedoruk, Phys. Solid State 46 (2004) 1631.

Superposition model analysis of the zero-field splitting parameters of Fe^{3+} : TlBX_2 crystals – insight into local distortions and low symmetry aspects

Paweł Gnutek¹⁾, Muhammed Açıkgöz²⁾ and Czesław Rudowicz^{*1)}

* Corresponding author: crudowicz@zut.edu.pl

¹⁾ Modeling in Spectroscopy Group, Institute of Physics, West Pomeranian University of Technology, Al. Piastów 17, 70–310 Szczecin, Poland

²⁾ Bahcesehir University, Faculty of Art and Sciences, Beşiktaş, Istanbul, Turkey

Abstract

In this presentation we report on our recent studies of the Fe^{3+} centers in single crystals of wide-band gap semiconductors TlInS_2 , TlGaS_2 , and TlGaSe_2 . Superposition model (SPM) calculations were carried out to investigate the local environment around the Fe^{3+} centers. A novel approach based on the ascent in symmetry method is applied to the crystallographic data to quantify the structural approximation from triclinic to orthorhombic and to tetragonal site symmetry. Electron magnetic resonance (EMR) data are reconsidered to provide more meaningful interpretation of the zero-field splitting (ZFS) parameters obtained by fitting EMR spectra. The values of the experimental ZFS parameters are matched with the SPM obtained values to obtain better insight into the local distortions and low symmetry aspects. The SPM results indicate that Fe^{3+} ions substitute for the B^{3+} ions in TlBX_2 ($\text{B} = \text{In}, \text{Ga}, \text{X} = \text{S}, \text{Se}$) crystal.

Keywords: Electron magnetic resonance (EMR); Superposition Model (SPM), Zero-field splitting (ZFS) parameters; TlInS_2 ; TlGaS_2 ; TlGaSe_2 ; Fe^{3+} ions.

1. Introduction

The Fe^{3+} paramagnetic centers in the ternary thallium chalcogenides TlBX_2 ($\text{B} = \text{In}, \text{Ga}, \text{X} = \text{S}, \text{Se}$) have recently been intensively investigated [1-6] in view of potential applications. Single TlBX_2 crystals belong to the class of ferroelectric wide-band gap semiconductors in which a complex sequence of structural phase transitions occurs with decreasing temperature [7,8]. Recently we have embarked on theoretical modeling of second- B_2^q (b_2^q) and fourth-rank ZFSPs B_4^q (b_4^q) zero-field splitting (ZFS) parameters (ZFSPs) and structural distortions in these systems [9,10] using the superposition model (SPM) [11-14]. In the previous studies, the SPM analysis was carried out for the ZFS parameters for Fe^{3+} ions in TlInS_2 [9] and TlGaS_2 [10] crystals. Following the procedure worked out in [9], SPM and crystallographic data were employed to determine the ZFS parameters for Fe^{3+} ions at the two substitutional structurally different Ga sites (hereafter denoted 1 and 2) in TlGaSe_2 crystal. In this

presentation preliminary results of this study are provided. Comprehensive SPM results together with their analysis will be presented in the full paper [15].

2. Crystal structure of TlGaSe₂ single crystals

The single crystals of TlGaSe₂ have the monoclinic space group $C2/c$ (No. 15, C_{2h}^6) at room temperature [16-18]. The atomic positions of TlGaSe₂ determined in [17] and [18] and the unit cell parameters [16-18] are listed in [15]. Fe³⁺ ions doped into TlGaSe₂ crystal occupy one of the two crystallographically inequivalent sites Ga³⁺ sites denoted Ga(1) and Ga(2) [1,3,6]. For SPM calculations, a modified crystallographic axis system (CAS*) is adopted as: $x||a$, $y||b||C_2$, and $z||c^*$ with the c^* -axis perpendicular to the plane (ab) (see Fig. 2 in [9]). The ligand bond length (R_i) and angular positions of ligands (θ_i , ϕ_i) for the Ga(1) and Ga(2) sites were calculated based on two sets of crystallographic data and used for the SPM modeling of the ZFS parameters for Fe³⁺ ions in TlBX₂ [9,10,15].

3. Superposition Model analysis

The Fe³⁺ ions doped into TlGaSe₂ crystal substitute at the Ga³⁺ sites [1,3,6]. The spin Hamiltonian [19,20] expressed in the extended Stevens (ES) operator O_k^q notation [21] is employed:

$$\begin{aligned} H = H_{Ze} + H_{ZFS} &= \mu_B \mathbf{B} \cdot \mathbf{g} \cdot \mathbf{S} + \sum B_k^q O_k^q(S_x, S_y, S_z) = \\ &= \mu_B \mathbf{B} \cdot \mathbf{g} \cdot \mathbf{S} + \sum f_k b_k^q O_k^q(S_x, S_y, S_z). \end{aligned} \quad (1)$$

The general SPM equations and details of the procedure were provided in [9,10]. Here we report some preliminary results for Fe³⁺:TlGaSe₂. Two sets of the model parameters are considered in [9,10,15]. For illustration, the ZFS parameters for one SPM parameter set is presented in Table 1.

Table 1. The triclinic ZFS parameters b_k^q (in 10^{-4} cm $^{-1}$) calculated using the SPM for the Fe $^{3+}$ ions at the Ga sites (1) and (2) in TlGaSe $_2$; for selection of the SPM parameters, see, [15].

Set	1	2		1	2		1	2
b_2^0	-817.3	-98.8	b_4^0	-3.59	-3.92			
b_2^1	-5288.4	-313.2	b_4^1	-0.86	1.83	b_4^3	-6.32	13.48
b_2^{-1}	4433.5	-1355.6	b_4^{-1}	0.42	2.40	b_4^{-3}	-3.61	-14.97
b_2^2	1197.7	1272.5	b_4^2	0.55	0.63	b_4^4	-19.16	-19.57
b_2^{-2}	1805.1	3538.0	b_4^{-2}	-3.16	4.91	b_4^{-4}	0.44	0.3
b_2^2/b_2^0	-1.47	12.88	b_4^2/b_4^0	-0.153	-0.161	b_4^4/b_4^0	5.34	4.99

Since the EMR spectra indicate nearly orthorhombic site symmetry [1], next we employ the orthorhombic approximation [9] of the structural data for the two centers in TlGaSe $_2$. The details of the ascent in symmetry method may be found in [9]. In short, using the averages of the ligands spherical polar coordinates in Table 2, we obtained the ‘orthorhombic-like’ coordinates denoted as the set OR1 and OR2. Subsequently, these coordinates are used to obtain the best matched sets aOR1 and aOR2 by changing iteratively θ_i and then ϕ_i and comparing b_2^0 and b_2^2 in the approximated sets with the experimental ZFSPs [1]. For illustration one set of the best matched ZFSP sets and the corresponding structural parameters are listed in Table 3 and 2, respectively. Accordingly, the fourth-rank ZFSPs were calculated for each pertinent structural data set for Fe $^{3+}$: TlBX $_2$ [9,10,15].

Table 2. The spherical polar coordinates of ligands in TlGaS $_2$ (R_i , θ_i , ϕ_i) for the local site symmetry approximated to orthorhombic.

OR1	$R = R_{av} =$ 0.24124	$\theta = \theta_{av} =$ 55.56	$\phi = \phi_{av} =$ 44.24
OR2	$R = R_{av} =$ 0.24065	$\theta = \theta_{av} =$ 54.85	$\phi = \phi_{av} =$ 44.24
aOR1	$R = 0.2410$	$\theta = 48.38$	$\phi = 41.44$
aOR2	$R = 0.2400$	$\theta = 48.58$	$\phi = 41.58$

Table 3. The ZFS parameters b_k^q (in 10^{-4} cm $^{-1}$) for Fe $^{3+}$ ions at the two Ga sites in TlGaSe $_2$ calculated using the SPM for the local site symmetry approximated to orthorhombic.

Set	OR1	aOR1	OR2	aOR2	Exp. [Błąd! Nie zdefiniow ano zakładki.]
b_2^0	-910	7272	-131	7277	7274
b_2^2	1217	4673	1237	4670	4672
b_4^0	-3.68	-4.18	-4.01	-4.43	—
b_4^2	0.55	3.53	0.61	3.58	—
b_4^4	-19.73	-12.93	-20.21	-13.91	—

Comprehensive SPM results together with their analysis will be presented in the full paper [15].

4. Conclusions

A novel approach based on the ascent in symmetry method applied to the crystallographic data to quantify the structural approximation from triclinic to orthorhombic and to tetragonal site symmetry may be useful to study the triclinic second-rank (b_2^q) and fourth-rank (b_4^q) zero-field splitting (ZFS) parameters (ZFSPs) for the transition ions in low symmetry crystals. Current applications of this method comprise Fe $^{3+}$ ions at the two Ga sites in TlInS $_2$ [9], TlGaS $_2$ [10], and TlGaSe $_2$ [15] single crystals. The results of our SPM analysis provide adequate interpretation of the ZFS parameters obtained by fitting EMR spectra and indicate that Fe $^{3+}$ ions substitute for the Ga $^{3+}$ ions in TlGaSe $_2$ crystal. More accurate modelling for Fe $^{3+}$ ions in TlGaSe $_2$ may be carried out when better quality EMR results taking into account the low symmetry effects in EMR spectra and the values of the fourth-rank ZFSPs become available.

Acknowledgements

This work was partially supported by a grant from the Research Fund of Bahcesehir University to MA and the Polish Ministry of Science and Education for the years 2009-2010 to PG and CZR.

References

- [1] F. A. Mikailov, B. Z. Rameev, S. Kazan, F. Yildiz, T. G. Mammadov, B. Aktas, *Solid State Commun.* 133 (2005) 389.
- [2] F. A. Mikailov, S. Kazan, B. Z. Rameev, M. Acikgoz, B. Aktas, *Phys. Stat. Sol. (a)* 203 (2006) 1580.
- [3] M. Acikgoz, S. Kazan, F. A. Mikailov, T. G. Mammadov, B. Aktas, *Solid State Comm.* 145 (2008) 539.
- [4] M. Acikgoz, S. Kazan, F. A. Mikailov, E. Kerimova, B. Aktas, *Cryst. Res. Technol.* 43 (2008) 863.
- [5] F. A. Mikailov, S. Kazan, B. Z. Rameev, A. M. Kulibekov, E. Kerimova, B. Aktas, *Solid State Comm.* 138 (2006) 239.
- [6] M. Acikgoz, S. Kazan, F. A. Mikailov, *Appl. Spectr. Reviews* 44 (2009) 181.
- [7] S. N. Mustafaeva, M. M. Asadov, A. A. Ismailov, *Phys. Solid State* 51 (2009) 2269.
- [8] M. H. Yu Seyidov, R. A. Suleymanova, F. Salehli, *Phys. Solid State* 51 (2009) 2513.
- [9] P. Gnutek, M. Acikgoz, C. Rudowicz, *Opt. Mat.* (2010), in press
- [10] M. Acikgoz, P. Gnutek, C. Rudowicz, *Solid State Commun.* (2010); doi:10.1016/j.ssc.2010.03.008.
- [11] D. J. Newman, W. Urban, *Adv. Phys.* 24 (1975) 793.
- [12] C. Rudowicz, *J. Phys. C: Solid State Phys.* 20 (1987) 6033.
- [13] T. H. Yeom, Y. M. Chang, S. H. Choh, C. Rudowicz, *Phys. Stat. Sol. (b)* 185 (1994) 409.
- [14] J. F. Clare, S. D. Devine, *J. Phys. C: Solid State Phys.* 13 (1980) 865.
- [15] M. Acikgoz, P. Gnutek, C. Rudowicz, *in preparation*
- [16] D. Müller, H. Hahn, *Z. Anorg. Allg. Chem.* 438 (1978) 258.
- [17] W. Henkel, H. D. Hochheimer, C. Carlone, A. Werner, S. Ves, H. G. Schnering, *Phys. Rev. B* 26 (1982) 3212.
- [18] G. E. Delgado, A. J. Mora, F. V. Perez, J. Gonzalez, *Cryst. Res. Technol.* 42 (2007) 663.
- [19] C. Rudowicz, *Magn. Res. Rev.* 13 (1987) 1; Erratum, *ibidem* 13 (1988) 335.
- [20] C. Rudowicz, S. K. Misra, *Appl. Spect. Reviews* 36 (2001) 11.
- [21] C. Rudowicz, *J. Phys. C: Solid State Phys.* 18 (1985) 1415; Erratum, *ibidem* 18 (1985) 3837

The stress influence on the generation of long lived radicals in wheat leaves

Maria Łabanowska¹, Maria Filek², Ewa Bidzińska¹, Katarzyna Obal¹

¹Faculty of Chemistry, Jagiellonian University, Ingardena 3, 30-060 Kraków, Poland,

²Institute of Plant Physiology, Polish Academy of Sciences, Niezapominajek 21, 30-239 Kraków, Poland

The EPR technique was applied to investigation of the character and amounts of long lived radicals present in raw leaves of wheat. It was found that healthy plants exhibited the EPR spectrum in which two kinds of signals of Gaussian shape could be separated. The intensive narrow signal, easily saturated, with $g_{av} = 2.0026$, was attributed to primary donor P^+ of photosystem PS I. The remaining signals of the spectrum showing the unusual stability were ascribed to long lived radicals. These signals were concentrated around g equal to about 2.006 and their characteristic feature was the splitting of particular signals on two lines of hyperfine structure. On the basis of g factor value as well the HFS constants the signals were attributed to sugar radicals with an unpaired electron localized at carbon atom of glucose molecule. The high stability of the species suggested their bonding to molecules with high molecular weight. The similarity of the EPR parameters of long lived radicals present in raw leaves to those observed for species generated thermally in wheat starch spoke in favour for such assignment. In the leaves of wheat influenced by the cadmium stress, the strong increase in the signal intensity of long lived radicals was observed. This increase was accompanied with simultaneous increase of the content of starch, found by electron microscopy. The comparison of two genotypes of wheat with different susceptibility towards the stress, showed that EPR methods could be very useful to the investigation of the plant answer to various disturbances. The studies of the Finnish and the Camilla wheat revealed that selenium stress led to double increase of amounts of long lived radicals. Moreover, in the case of the Camilla wheat the increase of signal of primary donor P^+ was observed. The effect of such protective activity of selenium on photosystem I was observed for rape leaves stressed by cadmium.

Acknowledgement

The investigations were partially supported by the grant No DPN/N110/COST/2009

Spin trapping study of the influence of taxifolin on Fenton reaction in ethanol and methanol

Katerina Makarova^{*1,2)}, **Katarzyna Łastawska**¹⁾, **Katarzyna Zawada**¹⁾, **Iwona Wawer**¹⁾

* Corresponding author: katerina.makarova@wur.nl

¹⁾ Department of Physical Chemistry, Faculty of Pharmacy, Medical University of Warsaw, 1 Banacha Street, 02-097 Warsaw, Poland

²⁾ Laboratory of Biophysics, Wageningen NMR Centre, Wageningen University, Dreijenlaan 3, 6703 HA Wageningen, The Netherlands

Abstract

To examine the effect of solvents on the nature and amount of the spin adducts, spin trapping experiments with 4-POBN, the Fenton reagents and taxifolin were performed in solutions of ethanol or methanol and water. The addition of taxifolin resulted in a decrease of the spectrum intensity of the spectrum that was dependent on taxifolin concentration. Computer simulation revealed that 4-POBN/ \bullet CH(CH₃)OH adduct dominated in ethanol whereas 4-POBN/ \bullet OH and 4-POBN/ \bullet CH₂OH adducts are present in methanol.

Keywords: ESR; spin trapping; simulation; taxifolin

1. Introduction

Flavonoids are a group of compounds abundant in plants and also present in human diet. Many studies confirm the role of flavonoids in preventing diseases like coronary heart disease, cancer and age-related neuropathologies. Flavonoids are able to scavenge free radicals, chelate transition metal ions and interact with other antioxidants [1]. Taxifolin, which is present in the plants from pinus genus (in pinus maritima), in the milk thistle seeds [2], and in citrus fruits, has a flavanonol structure and can act as an antioxidant due to reducing properties of its hydroxyl groups.

The aim of this research was to study the radicals produced in Fenton reaction with methanol or ethanol and the mechanism of their reaction with taxifolin. The ESR technique, coupled with spin trapping methods and computer simulation has been extensively used for the detection and identification of short-lived free radicals. The method of spin trapping is based on the scavenging of the radicals by a spin trap, leading to the formation of a spin adduct with higher stability. In this work a 4-POBN spin trap was chosen due to its stability and its selectivity toward trapping of carbon-centered radical species. Normally, it is easy to establish the presence of the radical and more of a challenge to identify it. Computer simulation is the most powerful technique in the analysis of multi component ESR spectra.

2. Experimental details

2.1. ESR spectroscopy

ESR spectra were measured on a MiniScope MS 200 spectrometer from Magnetech at room temperature (23-24C) in 50 μ l capillary tubes. Typical instrument settings were: microwave attenuation 10 dB, modulation amplitude of 0.5G, sweep time 20s. Measurements of kinetics were performed every 3 minutes unless indicated otherwise. The simulations of fast motion ESR spectra were performed with routines implemented in EasySpin toolbox [3] for Matlab. The ESR spectra of 4-POBN spin adducts exhibit hyperfine splittings from one ^{14}N and one ^1H – nuclei. The hyperfine data provided a good initial guess for the fitting [4-6].

2.2. Generation of free radicals for ESR

α -(4-Pyridyl N-oxide)-N-tert-butyl nitron (4-POBN) was purchased from Sigma Aldrich. Solutions were prepared using distilled and degassed water. Taxifolin solutions (0.010 M) in methanol and (0.012 M) in 96% ethanol were prepared, kept in a refrigerator and protected from light. Samples were prepared using 20 μ l of 20mM 4-POBN dissolved in water. POBN was mixed with 20 μ l of 5mM FeSO_4 prepared freshly from 0.1M stock solution and 20 μ l of 25mM H_2O_2 solution, prepared from 30% solution. Finally, 20 μ l of taxifolin sample (or solvent only) was added. The taxifolin concentration varied from 0.1mM to 2mM.

3. Results and discussion / Methods and results

The Fenton reaction was the method for generating free radicals. To examine the effect of solvents on the nature and amount of the spin adducts, spin trapping experiments in the Fenton reagents in ethanol, methanol and water were performed first. The second set of experiments was performed in the presence of taxifolin solutions.

3.1 Spin Trapping in solvents.

The 4-POBN/ $\bullet\text{OH}$ radical adduct was the only species obtained in the Fenton reactions based on Fe(II) in water. The 4-POBN/ $\bullet\text{OH}$ adducts were unstable and decayed fast to ESR silent products. The hyperfine splittings obtained by computer simulations are $a_{\text{N}} = 14.9\text{G}$ and $a_{\text{H}} = 1.63\text{ G}$. These values are in agreement with previous data [4] and were used for further simulations.

A 6-line ESR spectrum due to 4-POBN radical adducts was recorded when mixing Fe^{2+} (as FeSO_4), H_2O_2 , 4-POBN and methanol. The spectra were registered every 3 minutes, starting from the 4th minute after the addition of H_2O_2 to the sample. Computer simulation of the spectrum (Fig. 1) revealed a

species having hyperfine coupling constants of $a_N = 15.5$ G and $a_H = 2.8$ G and $a_N = 15.0$ G and $a_H = 1.6$ G (Table 1) values reasonably close to 4-POBN/ \bullet CH₂OH and 4-POBN/ \bullet OH adducts in aqueous solution [6]. The ESR spectrum measured 4 minutes after the addition of H₂O₂ to the sample and the spectrum measured after 140 minutes of the reaction had a similar (30%) ratio of 4-POBN/ \bullet OH (Fig. 1). The ESR signal measured 20-80 minutes after H₂O₂ addition to the sample was dominated by 4-POBN/ \bullet CH₂OH radical adduct (Fig. 1).

The Fenton reaction in ethanol can generate a number of radicals [7]. Computer simulation of radicals that were trapped by 4-POBN revealed a mixture of C-centered radical adducts. The 4-POBN/ \bullet CH(CH₃)OH adduct, the most commonly detected, dominates the spectrum with hyperfine splittings: of $a_N = 15.5$ G and $a_H = 2.5$ G (Table 1). However, the 4-POBN/ \bullet OH radical adduct was not detected in Fenton reaction with ethanol. This result suggested that \bullet OH radicals rather react with ethanol producing \bullet CH(CH₃)OH radicals, and then they are trapped by 4-POBN. It is important to note that the reaction of ferryl radical, usually produced in Fenton reaction, with ethanol [8] is another mechanism of \bullet CH(CH₃)OH radicals production.

3.2 Spin trapping in Fenton reagents in the presence of taxifolin solutions.

Taxifolin concentration had a significant effect on the intensity of the ESR signal and kinetics of its decay. The taxifolin concentration of 0.1mM decreased the intensity by about 50% in comparison with the reference. The concentration of 2mM caused signal decay during 15 minutes. The spin adducts which were detected in the presence of taxifolin in methanol were similar to the situation in the absence of taxifolin, i.e. 4-POBN/ \bullet OH and 4-POBN/ \bullet CH₂OH appeared. The first stage of the reaction, where \bullet OH radicals were formed and trapped by 4-POBN remained unchanged, however higher concentrations of taxifolin decreased the intensity of carbon-centered radical adduct signal and shortened the period of carbon-centered radical domination in the spectrum (Fig. 2).

The same dominating adduct (4-POBN/ \bullet CH(CH₃)OH) was identified in the presence of taxifolin in ethanol. The effect of taxifolin concentration on the ESR signal intensity was similar to the system with methanol. The taxifolin concentration of 0.1mM decreased the intensity by about 50 % in comparison with the reference, higher concentrations (1mM and 11.7mM) caused a very fast decay of the ESR signal (Fig.3).

The general conclusion is that the presence of taxifolin affects the intensity of carbon-centered 4-POBN adduct component. There are several possible explanations for this effect: (i) taxifolin could react with 4-POBN radical adducts resulting in ESR silent products; (ii) taxifolin could react with radicals formed in the experimental systems (scavenging), and (iii) the reaction of

taxifolin with Fe(II) or intermediate radicals that are involved in 1-hydroxyethyl or hydroxymethyl radical production.

Table 1. Isotropic hyperfine splitting of 4-POBN adducts in solutions

system	adduct	hyperfine splitting, G	
		a_N	a_H
Fe(II)/H ₂ O/4-POBN	4-POBN/ OH	14.9	1.6
Fe(II)/MeOH/4-POBN	4-POBN/ OH	15.0	1.6
	4-POBN/ CH ₂ OH	15.4	2.8
Fe(II)/EtOH/4-POBN	4-POBN/ CH ₂ (OH)CH ₃	15.5	2.5

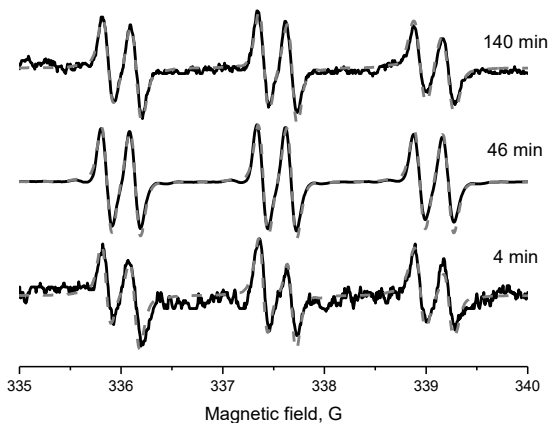
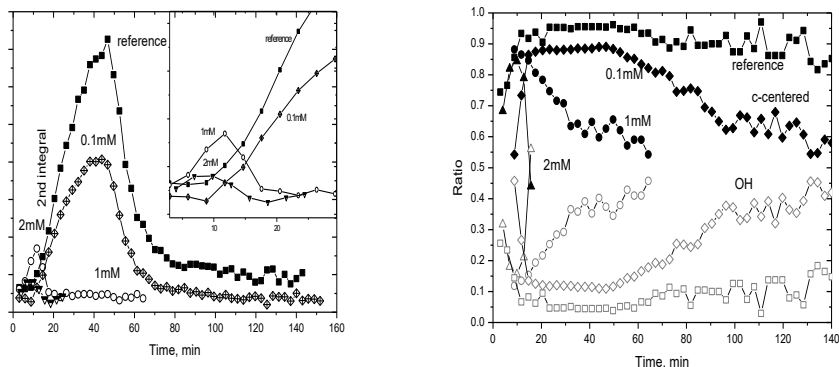


Fig. 1. X-band ESR spectra of 4-POBN/•OH and 4-POBN/•CH₂OH spin adduct in Fenton reaction with methanol recorded after 4, 46 and 140 minutes of reaction (solid line). The dotted lines are calculated spectra using hyperfine splitting constants from Table 1.



a

b

Fig. 2. (a) 2nd integral of ESR signal intensity of 4-POBN radical adducts from Fenton reaction with methanol (■) in the presence of 0.1mM (◇), 1mM (○) and 2mM (▼) of taxifolin. (b) ratio between 4-POBN/OH (grey symbols) and 4-POBN/CH₂OH (black symbols) components in reference (■) system and in the presence of 0.1mM (◇), 1mM (○) and 2mM (▼) of taxifolin.

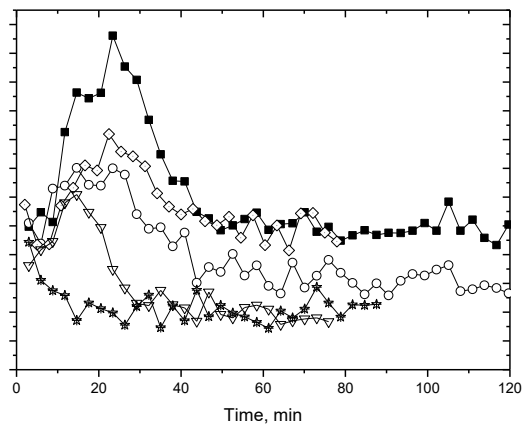


Fig. 3. 2nd integral of ESR signal intensity of 4-POBN radical adduct from Fenton reaction with ethanol (■) in the presence of 0.05mM (◇), 0.1mM (○), 1mM (▼) and 11.7mM (★) of taxifolin.

4. Conclusions

The radicals formed in the Fenton reaction with methanol and ethanol were studied with ESR spin trapping technique and analyzed with the aid of computer simulations. The fitting of experimental spectra made it possible to

identify radical adducts that were formed in these reactions and to follow the kinetics of each component. It was shown that the presence of taxifolin decreased the ESR signal intensity, affecting mainly the c-centered radical adduct component. Taxifolin mechanism of the reaction with free radicals requires further investigation. Further experiments are in progress.

Acknowledgements

EPR measurements were accomplished at the Structural Research Lab., Medical University of Warsaw, Faculty of Pharmacy, Poland. SRL was established with financial support from European Regional Development Fund in the Sectoral Operational Programme "Improvement of the Competitiveness of Enterprises, years 2004-2006" project no: WKP_1/1.4.3./1/2004/72/72/165/2005/U

References

- [1] S. Teixeira, Ch. Siquet, C. Alves, I. Boal, M. P. Marques, F. Borges, J.L.F.C. Lima, S. Reis, *Free Rad. Biol. Med.* 39 (2005) 1099 – 1108
- [2] N.C. Kim, T.N.Graf, C.M. Sparacino, M.C. Wani, M.E. Wall, *Org. Biomol. Chem.* 1 (2003) 1684-1689
- [3] S. Stoll, A. Schweiger, *J. Magn. Reson.* 178(2006) 42-55
- [4] E.G. Janzen, Y.Y. Wang, R.V. Shetty, *J. Am. Chem. Soc.* 100,9 (2006), 2923-2925
- [5] E. Finkelstein, G. M. Rosen, E. J. Rauckman, *Mol. Pharmacol.* 21 (1982) 262–265
- [6] R. Sridhar, P. Beaumont, E. Powers, *J. Radioanal. Nucl. Chem.* 101, 2 (1986) 227-237
- [7] A. Bosnjakovic, S. Schlick, *J. Phys. Chem. B* 110, 22 (2006) 10720-10728
- [8] I. Yamazaki, L.H. Piette, *J. Biol. Chem.* 265 (1990) 13589-13594

Effects of genistein on dipalmitoylphosphatidylcholine membranes

Bożena Pawlikowska-Pawłęga^{*1)}, Lucjan E. Misiak²⁾, Wiesław I. Gruszecki²⁾, Antoni Gawron¹⁾

* Corresponding author: bozka1996@o2.pl

¹⁾ Department of Comparative Anatomy and Anthropology, Maria Curie-Skłodowska University, Akademicka 19, 20-033 Lublin, Poland

²⁾ Institute of Physics, Maria Curie-Skłodowska University, Akademicka 19, 20-033 Lublin, Poland

Abstract

Genistein is a naturally occurring flavonoid that has a lot of beneficial properties on human health. Ability to interact with the cell membranes is of crucial importance in some biological effects of flavonoids such as antioxidant or anticancer activity. We have investigated the interaction of isoflavone - genistein with multilamellar DPPC liposomes. The results showed that genistein (5mol%) induced increase of the maximum splitting parameter value ($2T'_{\parallel}$) at the depth penetrated by 5-SASL. Modulation of DPPC liposomes with flavonoid had no effect on the fluidity at the hydrophobic core of the membrane at the depth monitored by 16-SASL. At the same time the results showed that incorporation of genistein into DPPC liposomes did not cause any changes in the partition coefficient of the Tempo spin label between the water and polar head group phases.

EPR data indicated rigidifying effect of flavonoid in the region penetrated by 5-SASL. Alteration of the membrane fluidity by genistein might generate multiple effects, leading to the final anticancer action of this compound.

Keywords: DPPC liposomes; EPR; flavonoids; genistein; spin labels;

1. Introduction

Flavonoids occur widely in plants and are a biologically major and chemically diverse group of secondary metabolites. Genistein, a known isoflavone, has received increased attention because of its possible role in cancer prevention [1]. It constitutes an important component in the majority of people's daily diets. The common source of it is soybean [2]. It is known from its antioxidant and radical scavenging activity, and antimicrobial activities as well. It has also estrogenic, growth stimulatory quality. Genistein has been found to interact not only with lipids but also with membrane proteins [3, 4]. Thus within a cell, the membrane seems to be one of the targets for its activity.

2. Methods

2.1. Chemicals

Genistein (Sigma Chemical Co., USA) dissolved in ethanol (Merck, Germany) was used in the studies. The solution was kept in the dark. Spin labels: 2-(14-carboxytetradecyl)-2-ethyl-4,4-dimethyl-3-oxazolidinyloxy free radical (16-

SASL), 2,2,6,6-tetramethyl-1-piperidinyloxy (Tempo), 2-(3-carboxypropyl)-4,4-dimethyl-2-tridecyl-3-oxazolidinyloxy free radical (5-SASL), 1,2-dipalmitoyl-sn-glycero-3-phosphocholine (DPPC) were purchased from Sigma Chemical Co. Spin labels were dissolved in absolute ethanol and stored at 4 °C.

2.2. *Electron paramagnetic resonance (EPR) measurements*

Multilamellar liposomes were obtained by shaking. We used saturated DPPC liposomes, which resulted in an ordered phase that was interrupted by an insertion of the flavonoid. The concentration of the lipid DPPC in phosphate buffer was 10^{-5} M. The concentration of flavonoids was 5 mol% and of the spin label 1 mol% with respect to the lipid. Dispersion of multilamellar liposomes of DPPC (73 mg/ml of chloroform) was prepared by mixing solutions of respective compounds, evaporation of solvent, first in a stream of nitrogen and subsequently by vacuum (2 h). The samples were hydrated with phosphate buffer (100 mM, pH 7) by vigorous shaking at a temperature above the main phase transition of lipid (41 °C) until optical homogeneity of the mixture was observed. The samples, to be measured, were placed in a 1.3-mm diameter capillary (Hyland Lab. Inc) and sealed with miniseal wax. EPR spectra were recorded with a SE/X-2547 (Radiopan, Poznań) spectrometer working in the X band and equipped with variable temperature - stabilizing unit under the following conditions: modulation amplitude 5 G in the case of spectra scanning and 10 G for determining an accurate position of the maxima time constant 0.3 s, scan time 2 min, scan range 3200–3300 G.

3. Results and discussion

3.1. *The effect of genistein on structural and dynamic properties of model phosphatidylcholine membranes*

To assess the fluidity of membranes spin labels were introduced to multilamellar DPPC liposomes and examined by EPR technique. Spin labels of n-SASL are commonly used to monitor structural and dynamic properties of lipid bilayer because the shape of their EPR spectra is strongly dependent on the motional freedom of the free radical segment of a spin label molecule within membrane. The lower the maximum splitting ($2T'_{\parallel}$, the parameter closely related with order parameter within the membrane) the higher the fluidity of the membrane in the vicinity of free radicals. With the use of the polar spin label Tempo we have also examined the changes of partition coefficient B/A. High-field EPR spectra of Tempo spin label show two peaks: one correspondent to a relatively mobile fraction of spin label in the water phase (A) and the fraction of spin label immobilized within membrane (B).

The results showed that modification of DPPC liposomes with genistein (5 mol%) had effect on the fluidity of hydrophobic core of the membrane at the depth monitored by 5-SASL. Genistein induced increase of the $2T'_{\parallel}$ value at the depth penetrated by 5-SASL. The values of the maximum splitting $2T'_{\parallel}$ for 5 –

SASL in liposomes with genistein were generally about 1.5 - 3,5 G higher (Fig. 1a). Modulation of DPPC liposomes with flavonoid had no effect on the fluidity at the hydrophobic core of the membrane at the depth monitored by 16-SASL (Fig. 1b). At the same time the results showed that incorporation of genistein into DPPC liposomes did not cause any changes in the partition coefficient of the Tempo spin label between the water and polar head group phases (Fig.1c).

3.2. Discussion

Membrane function is of vital importance to normal processes and can be influenced by a wide range of factors. One such factor is the modulation of membrane function by dietary components such as flavonoids. An understanding of the effects of flavonoids on biophysical properties of membranes may help to better elucidate their mechanism of action as anticancer agents as well as antioxidants. The term “fluidity” refers to the relative motional freedom of the lipid molecules in the membrane bilayer. By the use of 5-SASL, 16-SASL and Tempo spin label it was possible to determine fluidity of the membrane as a function of depth within membrane. The results suggest that genistein partitioned into the hydrophobic core of the model membrane, where it modifies the lipid packing order within the bilayer. Genistein decreased membrane fluidity in the interior region of the membrane penetrated by 5-SASL. Reports based on fluorescence anisotropy have supported genistein localization in this hydrophobic region of vesicles as well as membrane fluidity decrease [5, 6]. In cells e.g. human colon tumor (HCT) genistein was also able to reduce fluidity of membranes [7]. By imposing a greater degree of structural order and rigidity to the membrane, genistein could reduce the mobility of free radicals in the lipid bilayer. In consequence, this would result in inhibition of lipid peroxidation due to a slow down of free radical reactions.

4. Conclusions

Localization of genistein in membranes and resulting restrictions on fluidity of membranes might generate multiple effect, leading to the final anticancer or/and antioxidant action of these compounds.

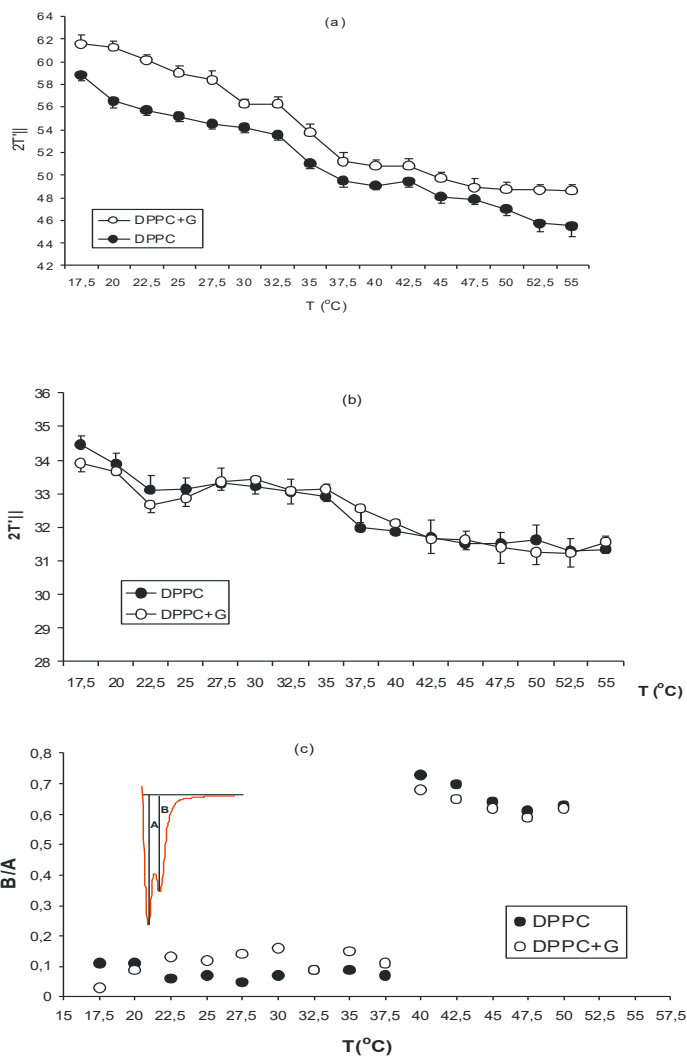


Fig. 1. The effect of genistein on liposomes of DPPC (a) the effect of genistein on a maximum splitting parameter ($2T'_{||}$) as a function of temperature of 5-doxylstearic acid (5-SASL) spin label doped into liposomes (b) the effect of genistein on a maximum splitting parameter ($2T'_{||}$) as a function of temperature of 16-doxylstearic acid (16-SASL) spin label doped into liposomes (c) temperature dependence of partition coefficient B/A of Tempo spin label between lipid and water phases doped into liposomes. The measurements were performed at various temperatures (17,5 $^{\circ}\text{C}$ -57,5 $^{\circ}\text{C}$).

References

- [1] D. Chodon, A. Arumugam, D. Rajasekaran, S. Dhanapal (2008) *J Health Sci* 54 (2008) 137.
- [2] A. Hendrich, *Acta Pahrmacol Sinica* 27 (2006) 27.
- [3] L. Al-Nakkash , S. Hu, T. Hwang, *J Pharmacol Exp Ther* 296 (2001) 464.
- [4] B. Lania-Pietrzak, A. Hendrich, J. Zugaj, K. Michalak, *Arch Biochem Biophys* 433 (2005) 428.
- [5] A. Arora, T. Byrem, M. Nair, G. Strasburg, *Biochem Biophys* 1 (2000) 102.
- [6] H. Tsuchiya, M. Nagayama, T. Tanaka, M.Furisawa, M. Kashimoto, H. Takeuchi, *BioFactors* 16 (2002) 45.
- [7] I. Yu, Y Cheng, L. Xie, R. Zhang, *Nutrition and Cancer* 33 (1999) 100.

Effect of chemotherapeutic agents on free radicals in melanin – comparative analysis

Barbara Pilawa^{*1)}, ***Ewa Buszman***²⁾, ***Magdalena Zdybel***¹⁾, ***Dorota Wrześniok***²⁾

* *Corresponding author: bpilawa@sum.edu.pl*

¹⁾*Department of Biophysics, School of Pharmacy and Division of Laboratory Medicine, Medical University of Silesia in Katowice, Jedności 8, 41-200 Sosnowiec, Poland*

²⁾*Department of Pharmaceutical Chemistry, School of Pharmacy and Division of Laboratory Medicine, Medical University of Silesia in Katowice, Jagiellońska 8, 41-200 Sosnowiec, Poland*

Abstract

Interactions of free radicals of melanin polymers with different drugs were compared. Data published in our earlier works were discussed. The EPR studies of melanin complexes with chloroquine, netilmicin, dihydrostreptomycin, gentamicin, and kanamycin were presented. All the examined chemotherapeutic agents increase free radicals concentration in melanin. Complexing of these drugs with melanin may be responsible for toxic effects in organism during therapy.

Keywords: EPR, free radicals, paramagnetic centers, melanin, drugs

1. Introduction

Melanin is the paramagnetic polymer with the high content of o-semiquinone free radicals [1-6]. Application of EPR spectroscopy to examination of drugs binding to melanin is presented in our earlier works [7-13]. The aim of this work is to compare effect of different drugs on free radicals in melanin. We used the published results for the drugs differ in toxicity [7-13] and comparative analysis was performed.

2. Experimental details

Free radicals in melanin complexes with chloroquine [7-8], netilmicin [9-10, 13], dihydrostreptomycin [11], gentamicin [12, 13], and kanamycin [12, 13] were studied by an X-band (9.3 GHz) electron paramagnetic resonance spectroscopy. Synthetic DOPA-melanin obtained by oxidative polymerization of 3,4-dihydroxyphenylalanine (L-DOPA) in 0.07 M phosphate buffer at pH 8.0 according to the Binns method [14] was studied [7-13]. Eumelanin was studied, because of it mainly exist in human tissues [15]. Chemical structure of the model eumelanin – DOPA-melanin is shown in figure 1 [16]. Chloroquine is the anti-inflammatory drug [17]. Netilmicin, dihydrostreptomycin, gentamicin, and kanamycin are the aminoglycoside antibiotics [17]. Chemical structure of the studied drugs are

presented in figure 2 [17]. The amounts of the drugs bound to melanin [7-13] were determined spectrochemically by the use of UV-VIS spectrophotometer JASCO V-530.

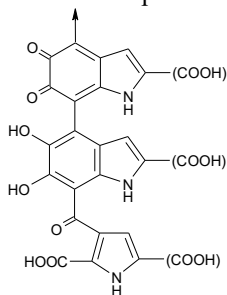
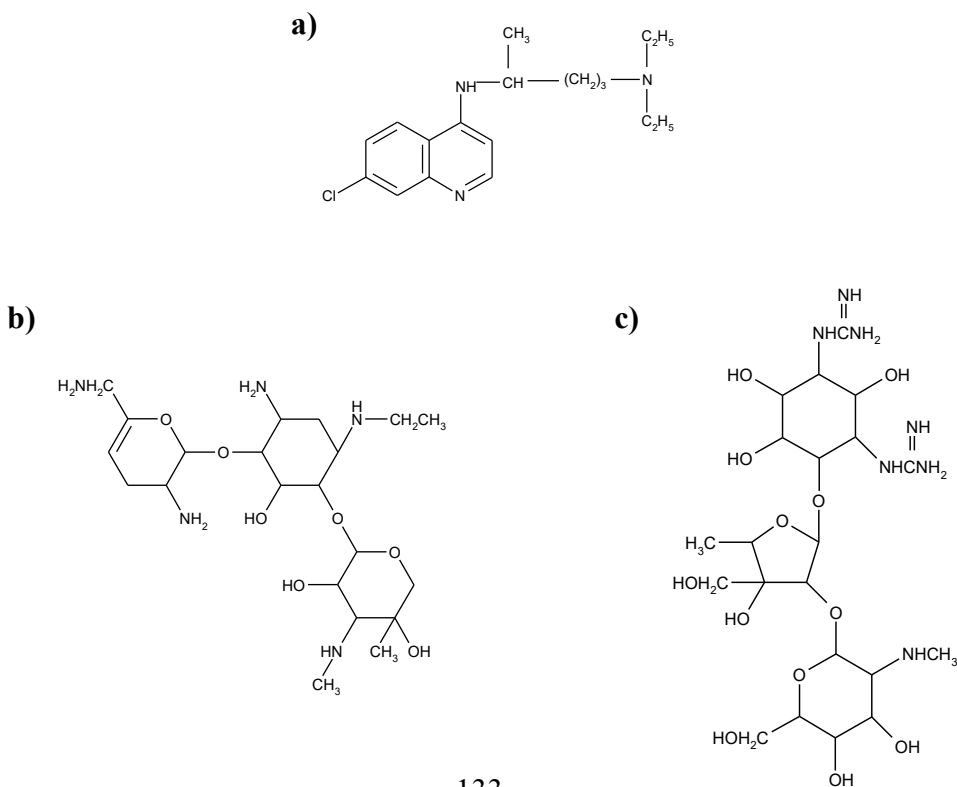


Fig. 1. Chemical structure of eumelanin [16].

EPR spectra were measured for the dry melanin samples at room temperature. For the exemplary samples the effect of temperature on the EPR spectra was analysed. The X-band (9.3 GHz) EPR spectrometers with modulation of magnetic field of 100 kHz produced by RADIOPAN Firm (Poznań, Poland) and BRUKER Firm were used [7-13]. Concentrations of free radicals in the melanin complexes were determined. Ultramarine and the ruby crystal were the references. Influence of microwave power on the EPR spectra was obtained.



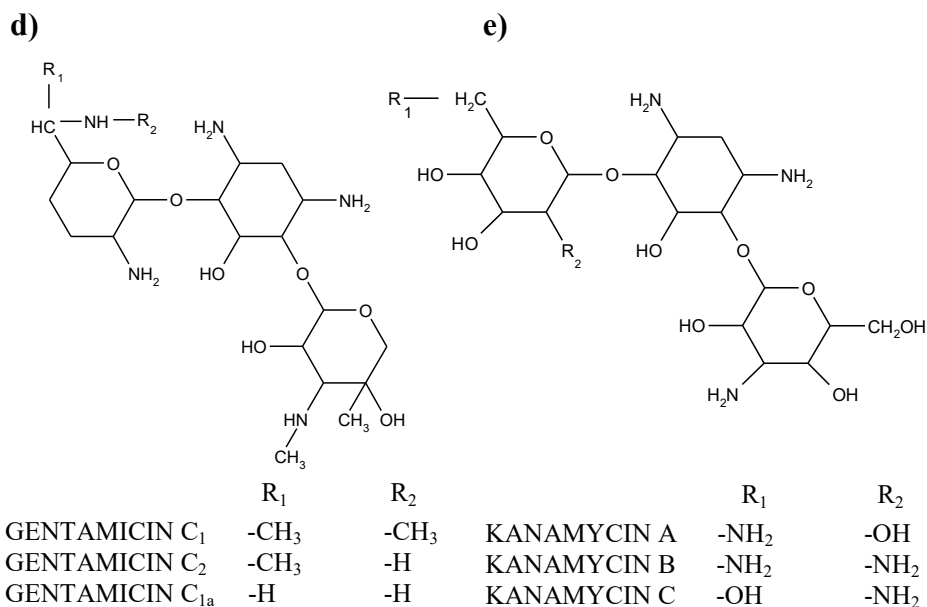


Fig. 2. Chemical structure of chloroquine (a), netilmicin (b), dihydrostreptomycin (c), gentamicin (d), and kanamycin (e) [17].

3. Results and discussion

The tested drugs increase free radical concentrations in DOPA-melanin [7-13]. This effect increases with increasing of drug concentration in the melanin complexes [10-13]. Changes in paramagnetic centers system of DOPA-melanin as the result of binding of kanamycin were also observed by Kozdrowska [18]. Because of the large amount of free radicals in melanin-chloroquine complexes, it is expected that toxicity of the drug incorporated to melanin is the highest for chloroquine than for the aminoglycoside antibiotics [7-13]. The slightly higher formation of free radicals in melanin by drugs was obtained for dihydrostreptomycin, which is one of the most toxic aminoglycoside antibiotics [11].

Chloroquine increases free radicals concentrations in melanin and melanin complexes with metal ions [7-8]. EPR studies of DOPA-melanin, and DOPA-melanin-chloroquine, DOPA-melanin-Zn(II), DOPA-melanin-Co(II), [DOPA-melanin-chloroquine]-Co(II), [DOPA-melanin-Co(II)]-chloroquine, [DOPA-melanin-chloroquine]-Zn(II), [DOPA-melanin-Zn(II)]-chloroquine point out interactions between paramagnetic centers of the melanin polymer and oxygen O₂ [8]. As the result of the quasi-chemical bonds formation between oxygen molecules and the paramagnetic samples free radicals concentration in these complexes decrease. The narrowing of EPR lines for the melanin complexes in

air was observed [8]. Spin-lattice relaxation times T_1 are $\sim 10^{-6}$ - 10^{-5} s, and spin-spin relaxation times T_2 are $\sim 10^{-8}$ s [8]. The fastening of spin-lattice and spin-spin relaxation processes in DOPA-melanin-complexes with chloroquine and Zn(II) and Co(II) ions are obtained after removing of air from the environment of the samples [8].

The formation of free radicals during complexing of DOPA-melanin and DOPA-melanin samples containing metal ions with drugs are discussed [7-10, 13, 18]. Free radicals ($S = 1/2$) and biradicals ($S = 1$) in DOPA-melanin complexes with netilmicin [10] and kanamycin [18] were found. By the first biradicals in melanin complexes with kanamycin and Cu(II) ions were found by Kozdrowska [18]. Microwave saturation of EPR lines of DOPA-melanin complexes with drugs were compared [7-10, 13, 18].

4. Conclusions

EPR studies indicate that free radical formation occur during complexing of melanin with chloroquine [7-8], netilmicin [9-10], dihydrostreptomycin [11], gentamicin [12-13], and kanamycin [12-13, 18]. This effect is stronger for chloroquine [7-8] than for the examined antibiotics [9-13, 18]. Free radical formation in melanin by drugs depend on the presence of paramagnetic and diamagnetic ions in the polymer [7-13, 18].

Acknowledgements

This study was supported by Medical University of Silesia in Katowice.

References

- [1] T. Sarna, J.S. Hyde, H.M. Swartz, *Science* 192 (1976) 1132.
- [2] T. Sarna, *Zagad. Biofiz. Współcz.* 6 (1981) 6.
- [3] W. Froncisz, T. Sarna, J. S. Hyde, *Arch. Biochem. Biophys.* 202 (1980) 289.
- [4] R.C. Sealy, J.S. Hyde, C.C. Felix, I.A. Menon, G. Prota, *Sci.* 217 (1982) 545.
- [5] M. Pasenkiewicz-Gierula, R. C. Sealy, *Biochim. Biophys. Acta* 884 (1986) 510.
- [6] B. Pilawa, E. Chodurek, T. Wilczok, *Appl. Magn. Reson.* 24 (2003) 417.
- [7] B. Pilawa, E. Buszman, M. Latocha, T. Wilczok, *Polish J. Med. Phys. Engin.* 10 (2004) 35.
- [8] B. Pilawa, M. Latocha, E. Buszman, T. Wilczok, *Appl. Magn. Reson.* 25 (2003) 105.
- [9] E. Buszman, B. Pilawa, M. Zdybel, D. Wrześniok, A. Grzegorzczuk., T. Wilczok, *Chem. Phys. Lett.* 403 (2005) 22.
- [10] M. Zdybel, *Doctoral thesis, Medical University of Silesia, Katowice, 2008.*
- [11] E. Buszman, B. Pilawa, M. Zdybel, D. Wrześniok, A. Grzegorzczuk, T. Wilczok, *Acta Phys. Polon.* 108 (2005) 353.
- [12] B. Pilawa, E. Buszman, D. Wrześniok, M. Latocha, T. Wilczok, *Appl. Magn. Reson.* 23 (2002) 181.
- [13] M. Zdybel, B. Pilawa, E. Buszman, D. Wrześniok, *Sci. Rev. Pharm.* 6 (2009) 42.

- [14] F. Binns, R.F. Chapman, N.C. Robson, G.A. Swan, A.J. Waggott, *J. Chem. Soc. C* (1970) 1128.
- [15] E. Buszman, Habilitation thesis, Medical University of Silesia, Katowice, 1994.
- [16] K. Wakamatsu K, S. Ito, *Pigment Cell Res.* 15 (2002) 174.
- [17] A. Zejca, M. Gorczyca, *Chemia leków*, PZWL, Warszawa, 2004.
- [18] L. Kozdrowska, Doctoral thesis, University of Zielona Góra, Zielona Góra, 2006.

Spectroscopic properties of Fe²⁺ (S=2) ions at tetragonal sites in K₂FeF₄ and K₂ZnF₄

Czesław Rudowicz* and Danuta Piwowska

* Corresponding author: crudowicz@zut.edu.pl

Modeling in Spectroscopy Group, Institute of Physics, West Pomeranian University of Technology, Al. Piastów 17, 70–310 Szczecin, Poland.

Abstract

Crystal field (CF) effects and energy levels Fe²⁺(3d⁶) ions in K₂FeF₄ with the ground state multiplet ⁵D split due to a tetragonal crystal field are considered. Microscopic spin Hamiltonian parameters, i.e. the zero field splitting (ZFS) and Zeeman electronic ones, within the orbital singlet ground state ⁵B_{2g} with the spin S=2 are modeled for various ranges of the microscopic parameters, i.e. the spin-orbit coupling constant λ , the spin-spin coupling constant ρ , the CF energy level splittings Δ_i , and the mixing coefficient q , suitable for Fe²⁺ (S=2) ions in K₂FeF₄ and K₂ZnF₄. The results are compared with the available experimental data.

Keywords: Spin Hamiltonian (SH); Zero-field splitting (ZFS); Crystal-field (CF); Electron magnetic resonance (EMR); Fe²⁺ ions in K₂FeF₄ and K₂ZnF₄; Tetragonal site symmetry; Computer modeling packages

1. Introduction

K₂FeF₄ is a planar antiferromagnet with the Neel temperature $T_N \approx 63$ to 67 K and exhibits two-dimensional (2D) easy-plane anisotropy [1]. Magnetic and spectroscopic behaviour of K₂FeF₄ may be described by the isotropic Heisenberg exchange interactions and the zero field splitting (ZFS), which give rise to single-ion magnetic anisotropy [2]. The electronic configuration of Fe²⁺ in K₂FeF₄ is 3d⁶ and the ground state multiplet ⁵D is split due to a tetragonal crystal field (CF) yielding an orbital singlet ground state ⁵B_{2g} with the spin S=2 [3]. Due to the large ZFS, the studies of the S=2 ions require the high frequency and high magnetic field EMR (HMF-EMR) techniques; for references, see [4]. To provide guidance for the novel HMF-EMR studies, we investigate theoretically the spectroscopic properties of Fe²⁺ ions at tetragonal sites. In this presentation preliminary results of the microscopic spin Hamiltonian modeling of the ZFS and Zeeman parameters for Fe²⁺ ions in K₂FeF₄ and Fe²⁺:K₂ZnF₄ are provided. The truncated forms of ZFS Hamiltonians and controversial origin of the rhombic E –term invoked in the previous studies are considered in a separate paper.

2. Microscopic spin Hamiltonian modeling using the computer package MSH/VBA

In view of the experimental difficulties in obtaining reliable values of the ZFS parameters for the S=2 ions, the microscopic spin Hamiltonian (MSH) theory is especially useful since it enables prediction and modeling of the ZFS parameters and the Zeeman electronic ones; for references, see [5]. For MSH analysis of the $3d^4$ and $3d^6$ (S=2) ions at orthorhombic and tetragonal symmetry sites the *Fortran* program MSHORT [6] was developed and later extended into a versatile package MSH/VBA, which includes also graphical capabilities [7, 8]. Comparative analysis of the earlier attempts to derive MSH formulas for the ZFS parameters [3] and our more complete MSH formulas [6] will be carried out in the full paper.

Survey of available experimental data on crystal field effects and ZFS transitions for Fe^{2+} ions at tetragonal sites has provided input data for the package MSH/VBA. Using reasonable ranges of the microscopic parameters: the spin-orbit coupling constant λ , spin-spin coupling constant ρ , the CF energy level splittings Δ_i , and the mixing coefficient q , we obtain the sample results listed in Table 1 and 2 and presented in Fig. 1 and 2.

Table 1. The theoretical ZFS parameters [in cm^{-1}] and the g_i factors [dimensionless] for Fe^{2+} in K_2FeF_4 calculated for the three sets of CF energy levels [in cm^{-1}]: (A) $\Delta_1=\Delta_2=486.6$, $\Delta_3=8341.3$, $\Delta_4=8827.9$; (B) $\Delta_1=\Delta_2=400.0$, $\Delta_3=8433.3$, $\Delta_4=8966.7$; (C) $\Delta_1=\Delta_2=486.6$, $\Delta_3=7729.5$, $\Delta_4=8341.3$.

(λ, ρ)	(-70; 0.2)			(-70; 1.0)		
Δ_1	A	B	C	A	B	C
g_x	2.144	2.137	2.144	2.144	2.137	2.144
g_y	2.144	2.137	2.144	2.144	2.137	2.144
g_z	1.877	1.786	1.882	1.877	1.786	1.882
b_2^0	9.452	12.151	9.299	8.048	11.005	7.895
b_4^0	0.705	1.272	0.704	0.815	1.414	0.817
b_4^4	1.406	2.107	1.469	3.112	4.518	3.185

Table 2. Contributions to the conventional ZFS parameters [in cm^{-1}] for Fe^{2+} in K_2FeF_4 .

(λ, ρ)	(-70; 0.2)			(-70; 1.0)		
Δ_1	A	B	C	A	B	C
$D(\lambda^2)$	7.720	9.926	7.534	7.720	9.926	7.534
$D(\lambda^4)$	-1.196	-2.184	-1.190	-1.196	-2.184	-1.190
$D(\lambda^2 + \lambda^4)$	6.524	7.742	6.344	6.524	7.742	6.344
$D(\lambda^3)$	3.235	4.694	3.262	3.235	4.694	3.262
$D(\rho)$	-0.540	-0.600	-0.540	-3.000	-3.000	-3.000
$D(\rho\lambda)$	0.233	0.315	0.233	1.295	1.575	1.295
D_t	9.452	12.151	9.299	8.048	11.005	7.895
$F(\lambda^4)$	1.438	2.829	1.397	1.438	2.829	1.397
$F(\rho^2)$	0.003	0.004	0.003	0.088	0.109	0.088
$F(\rho\lambda^2)$	-0.171	-0.281	-0.170	-0.950	-1.407	-0.946
F_t	1.270	2.552	1.230	0.576	1.531	0.539
$a(\lambda^4)$	0.414	0.602	0.438	0.414	0.602	0.438
$a(\rho^2)$	0.000	0.000	0.000	0.004	0.004	0.004
$a(\rho\lambda^2)$	0.149	0.240	0.150	0.827	1.201	0.832
a_t	0.563	0.843	0.588	1.245	1.807	1.274

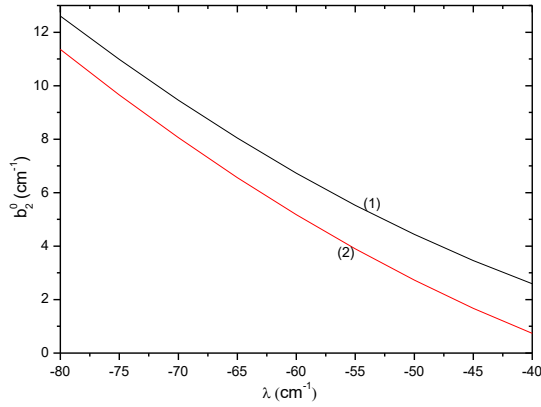


Fig. 1. Variation of the ZFS parameter b_2^0 (total) for set A in Table 1 with the spin-orbit coupling constant λ for two values of the spin-spin coupling constant ρ : (1) $\rho = 0.2$ and (2) $\rho = 1$ [in cm^{-1}].

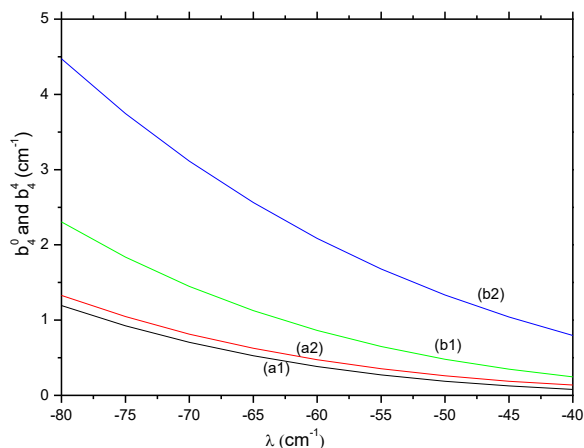


Fig. 2. Variation of the ZFS parameters: (a) b_4^0 (total) and (b) b_4^4 (total) for set A in Table 1 with λ for two values of ρ : (1) $\rho = 0.2$ and (2) $\rho = 1$ [in cm^{-1}].

3. Conclusions

In short, the MSH approach [6-8] has enabled consideration for the first time the fourth-rank ZFS parameters using consistent, i.e. not truncated, forms of spin Hamiltonian. Comprehensive results will be presented together with their analysis and comparison with the available experimental data in the full paper [9]. The results [9] may also be useful for Fe^{2+} ions at axial symmetry sites in related systems, i.e. $\text{Fe}:\text{K}_2\text{MnF}_4$, $\text{Rb}_2\text{Co}_{1-x}\text{Fe}_x\text{F}_4$, $\text{Fe}^{2+}:\text{Rb}_2\text{CrCl}_4$, and $\text{Fe}^{2+}:\text{Rb}_2\text{ZnCl}_4$, for which insufficient input data for modeling of the spin Hamiltonian parameters could be found in literature as yet. The computer packages MSHORT [6] and MSH/VBA [7,8], which facilitate modeling of the microscopic spin Hamiltonian parameters for 3d4 (V^+ , Cr^{2+} , Mn^{3+} , Fe^{4+}) and 3d6 (Mn^+ , Fe^{2+} , Co^{3+} , Ni^{4+}) ions at orthorhombic and tetragonal symmetry sites are available from the authors upon request. These ions exhibit large ZFS and may be best studied using the novel HMF-EMR techniques.

References

- [1] A.F.M. Arts, H.W. de Wijn, *Magnetic Properties of Layered Transition Metal Compounds*, Kluwer Academic Publishers, Netherlands (1990) 191.
- [2] R. Geick: *Magnetic Properties of Non-Metallic Inorganic Compounds Based on Transition Elements*; Landolt-Bornstein Tables: Group III Condensed Matter, ed. H. P. J. Wijn (Springer, Berlin, 2001) Vol. 27, Subvol. J3.
- [3] M.P.H. Thurlings, E. Frikkee, H.W. de Wijn, *Phys. Rev. B*, 25 (1982) 4750.

- [4] C. Rudowicz, H.W.F. Sung, J. Phys. Soc. Japan 72 Supplement B (2003) 61.
- [5] C. Rudowicz, Magn. Reson. Rev. 13 (1987) 1; Erratum, *ibidem* 13 (1988) 335.
- [6] C. Rudowicz, Y. Zhou, Computers & Chemistry 21 (1997) 45.
- [7] C. Rudowicz, H.W.F. Sung, Manual for (2004) - *unpublished*.
- [8] C. Rudowicz, H.W.F. Sung, Physica B 337 (2003) 204.
- [9] C. Rudowicz, D. Piwowarska, *in preparation*.

The EPR measurements of Al₂O₃ powders and mullites used in aircraft industry for cores and shapes

I. Stefaniuk, *P.Potera, J.Cebulski

* Corresponding author: ppotera@univ.rzeszow.pl
Institute of Physics, University of Rzeszow, Rejtana 16a, 35-310 Rzeszow,
Poland

Abstract

In this work the electron paramagnetic resonance (EPR) spectra of Al₂O₃ powders were measured for different size of grains (# 200, # 325) as well as the mullites (0,007 and 0,012). The measurements were executed in room temperature as well as in temperature range since 140K to 380K. The finding of relation between EPR spectra and size of grains of powders as well as identification of EPR spectra were the main purpose of this work.

Keywords: EPR spectra, Al₂O₃, mullit, nanopowder,

1. Introduction

The ceramic nano-powders are widely used in different industry branches. The polymer nanocomposites stiffened by ceramic nano-filling they are characterized by very high hardness and resistance for abrasion with comparison in composites in micrometric scale[1,2].

The annealing of Al₂O₃ powders in temperatures 350, 600, 900°C not influence into size of particles of the investigated powders.

The heating in temperature 1200 ° C leads to the 30% growth of average size of grains (the fritting processes take place) as well as the growth of crystallinity degree of alumina and phase transition $\delta, \gamma, \eta, \epsilon\text{-Al}_2\text{O}_3 \rightarrow \alpha\text{-Al}_2\text{O}_3$ take place [3]. The condition of precursor's synthesis as well as practical his modifier, in essential prepares they influence on morphology formed of Al₂O₃. [4] The also important is the basicity of environment in which the homogenization of both Al₂O₃ and nanometric ZrO₂ powders take place. The environment, in which particles of both powders has the same charge name leads to the forming mechanically resistant agglomerates, that negatively influences on condensation of material during fritting.

In the sinter the cracks with sizes about of hundreds of micrometers as well as inhomogeneity of packing in individual micrometers scale are appeared [5]

The impulse for EPR investigation of this material presented in this work is the problem of cracking of shape.

In this work the investigation by EPR method of basic materials for shapes was discussed.

2. Experimental details

For the experiment the samples of corundum with different size as well as including second phase were used. The detailed data for samples are given in Table 1. The samples of mullite with size of grains in the range 0.007 - 0.012 were also studied.

Table 1. The specification of samples of corundum.

L.p.	Sample	Jakościowa analiza składu fazowego metodą dyfrakcji rentgenowskiej	
1	Al ₂ O ₃ #200	α Al ₂ O ₃ – corund	93,9±0,1 [%]
		NaAl ₁₁ O ₁₇ – β -Al ₂ O ₃	6,1±0,1 [%]
2	Al ₂ O ₃ #325	α Al ₂ O ₃ – corund	95,5±0,1 [%]
		NaAl ₁₁ O ₁₇ – β -Al ₂ O ₃	4,5±0,1 [%]

For the EPR measurements the standard X-band (~ 9 GHz) spectrometer, produced in Wrocław, with digital registration the spectra was used. For the temperature measurements the digital system of control of temperature was used (BRUKER ERAS 4131VT), which permits to get the range of temperatures from 100K to 500K

3. Results and discussion

The obtained EPR spectra are given in Fig1 -4.

In the case of Al₂O₃ powders on the wide line a several considerably narrower lines with width of pick to pick near 3-4 mT for sample # 200 as well as about width a few mT for sample # 325 were observed. The EPR spectra for mullites are very similar for himself and differences appear only for intensity of line for $g = 4.29$. For the EPR spectra of Al₂O₃ powders the differences in the intensity of line and their position were observed. For sample # 200 new line appears in magnetic field equal to 300mT.



Fig.1 The EPR spectra for Al₂O₃ #200 powder in different temperatures

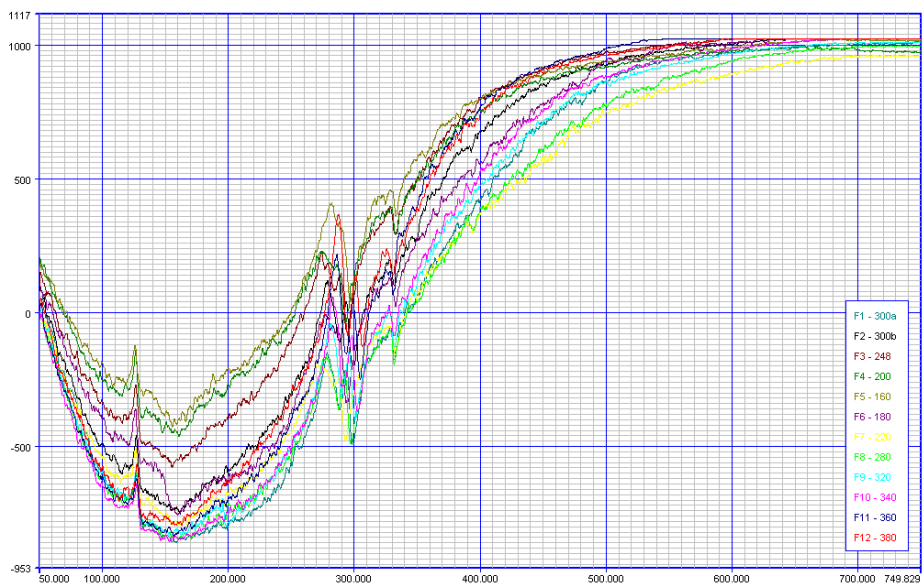


Fig.2 The EPR spectra for Al₂O₃ #3250 powder in different temperatures

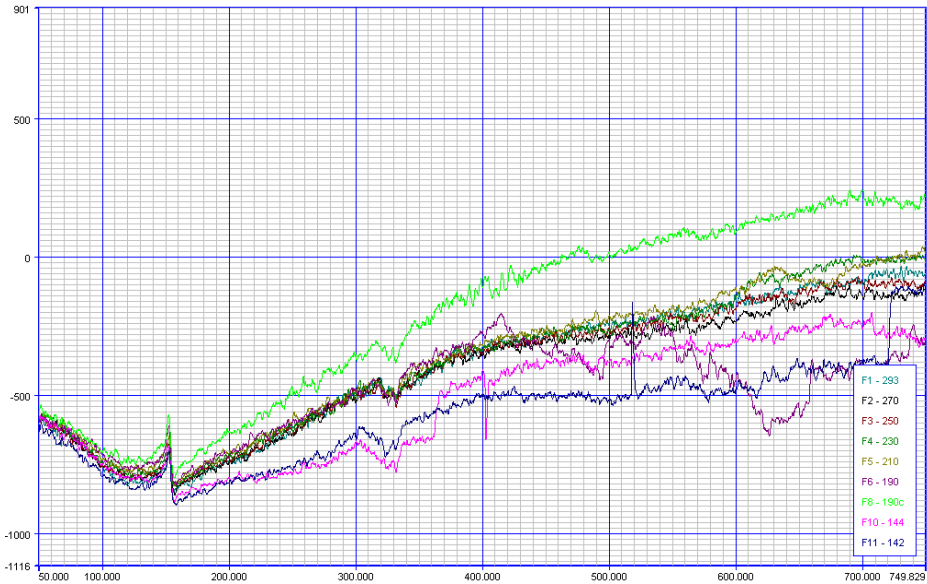


Fig.3 The EPR spectra of mulites 0,007 in different temperatures



Fig.4 The EPR spectra of mulites 0,012 in different temperatures

For the Al₂O₃#200 sample the calculated g_{eff} -factor value for each line as following: $g_{\text{eff}}=4.29$, $g_{\text{eff}}=3.36$, $g_{\text{eff}}=2.57$, $g_{\text{eff}}=1.97$, $g_{\text{eff}}=1.69$. However for the sample #325 are then values: $g_{\text{eff}}=4.28$, $g_{\text{eff}}=2.33$, $g_{\text{eff}}=2.23$, $g_{\text{eff}}=1.97$. All values have been calculated with precisions ± 0.02 . The analysis of lines

positions suggest that lines for $g_{\text{eff}} = 4.28$ $g_{\text{eff}} \approx 2.00$ are connected with Fe^{3+} ($S=5/2$) ions, because they are typical spectrum for „disordered systems” [6] „and in a glassy host” [7]. The intensities of lines were progressively decreased in order to show the evolution of the relative line shapes and intensities at $g = 4.3$ from isolated ions in local tetrahedral (and eventual octahedral) sites [7].

The line with $g_{\text{eff}} = 1.98$ are connected with Cr^{3+} ($S=3/2$) ions in the slight-distorted octahedral site [8,10].

4. Conclusions

In this work the EPR spectra were analyzed as well as those spectra were connected with size of Al_2O_3 powder grain.

EPR lines $g_{\text{eff}} \approx 2.0$ and $g_{\text{eff}} \approx 4.3$ on the spectra of these glasses can be due to the diluted state of Fe^{3+} ions in tetrahedral or orthorhombic coordination.

EPR lines $g_{\text{eff}} \approx 2.0$ on the spectra of these glasses can be due to the diluted state of Cr^{3+} ions in slightly distorted orthorhombic coordination.

Acknowledgements

Financial support of Structural Funds in the Operational Programme - Innovative Economy (IE OP) financed from the European Regional Development Fund - Project "Modern material technologies in aerospace industry", Nr POIG.01.01.02-00-015/08-00 is gratefully acknowledged.

References

- [1] Jurczyk M., Jakubowicz J., Nanomateriały ceramiczne, Wyd. Politechniki Poznańskiej, Poznań 2004.
- [2] Jurczyk M., Nanomateriały, Wybrane zagadnienia, Wyd. Politechniki Poznańskiej, Poznań 2001.
- [3] Aneta Zawada, Anna Boczkowska, Wanda Ziemkowska, Antoni Kunicki Antoni Pietrzykowski, Andrzej Olszyna, KOMPOZYTY (COMPOSITES) 6(2006)1
- [4] AGNIESZKA SOŁGAŁA, ANTONI KUNICKI, ANDRZEJ OLSZYNA MATERIAŁY CERAMICZNE /CERAMIC MATERIALS/, 60, 4, (2008), 262-265 Wpływ modyfi katora prekursora tlenku glinu na morfologię otrzymanego nanoproszku Al_2O_3
- [5] ŁUKASZ ZYCH, KRZYSZTOF HABERKO, MIROSŁAW M. BUĆKO, PAWEŁ RUTKOWSKI, BARBARA TRYBALSKA, JAN PIEKARCZYK, RADOSŁAW LACH, MATERIAŁY CERAMICZNE /CERAMIC MATERIALS/, 60, 4, (2008), 254-257
- [6] D.L. Griscom, J. Non-Cryst. Solids, 40,211,(1980)
- [7] Berger, R.; Kliava, J.; Yahiaoui, E.M.; Bissey, J.C.; Zinsou, P.K.; Béziade, P. J. of Non-Cryst. Solids, v. 180, p. 151, (1995).

- [8] Simion Simon, Andre van der Pol, Edward J. Reijerse, Arno P. M. Kentgens, Geert J. van Moorsel and Engbert de Boer, *J. Chem. Soc., Faraday Trans.*, 1994, 91(10),1519-1522 (1995)
- [9] Signo Tadeu dos Reisa*, Walter M. Pontuschkab, Jinbo B. Yanga, Dalva L A. Fariac, *VMoalt.e r6ia, lNs Ro.e s3e,a 2rc0h0*, 3Vol. 6, No. 3, 389-394, 2003.
- [10] X Karthein, R., Motschi, H., Schweiger, A., Ibric, S., Sulzberger, B., and. Stumm, W., *Inorg. Chem.* 30, 1606 (1991).

EPR examinations of free radical formation in thermally sterilized β -lactam antibiotics

Paweł Ramos^{*}, ***Barbara Pilawa***

Corresponding author: pawelramos@sum.edu.pl
Department of Biophysics, Medical University of Silesia in Katowice, School of Pharmacy and Laboratory Medicine, Jedności 8, 41-200 Sosnowiec, Poland

Abstract

EPR examination of free radicals formed in β -lactam antibiotics sterilized at different temperatures was performed. Asymmetrical EPR lines were measured for the studied heated drugs. Properties and free radical concentration in the heated antibiotics changed during storage after thermal treatment. Effect of microwave power on the spectra was analysed. Optimal conditions of thermal sterilization of ampicilin, crystal penicillin, and piperacyllin were determined.

Keywords: EPR, free radicals, β -lactam antibiotics, thermal sterilization

1. Introduction

Free radicals are formed in heated organic substances and in drugs during thermal sterilization [1-8]. The aim of this work was to determine influence of thermal sterilization on concentration and properties of free radicals in the analysed β -lactam antibiotics. Effect of temperature and time of sterilization on free radicals in these drugs was evaluated. The optimal conditions of thermal sterilization of the studied antibiotics were searched. Effect of the storage time on free radical concentration in the antibiotics sterilized at different temperatures was tested. The results will help to determine of storage conditions for the studied drugs.

2. Experimental details

The three β -lactam antibiotics: ampicilin, crystal penicillin, and piperacyllin, were studied. The chemical structure of these drugs are presented in figure 1 [9]. β -lactam antibiotics are a broad class of antibiotics that include penicillin, cephalosporins, monobactams, and carbapenems [9]. They are the most widely-used group of antibiotics. β -lactam antibiotics are indicated for the prophylaxis and treatment of bacterial infections caused by susceptible organisms [9]. β -lactam antibiotics are bactericidal, and they act by inhibiting the synthesis of the peptidoglycan layer of bacterial cell walls [9].

Sterilization was performed according to the Polish norms [10-12] in hot air oven with air circulation at the following temperatures and times: 160 °C and 120 minutes, 170 °C and 60 minutes, and 180 °C and 30 minutes.

EPR analysis was done for powdered samples at room temperature 20 minutes after thermal sterilization. Changes of EPR spectra of the sterilized drugs with increasing the storage time up to 3 months were tested. An X-band (9.3 GHz) EPR spectrometer with modulation of magnetic field of 100 kHz produced by RADIOPAN Firm (Poznań, Poland) was used. Microwave frequency was measured by MCM101 recorder of EPRAD firm (Poznań, Poland). EPR spectra were recorded in the range of microwave power from 2.2 mW to 70 mW. g -Factor, amplitudes (A), integral intensities (I), and linewidth (ΔB_{pp}) of the spectra were determined. The shapes parameters of the spectra were analysed. Free radical concentration (N) in the samples was determined by the use of ultramarine as the reference.

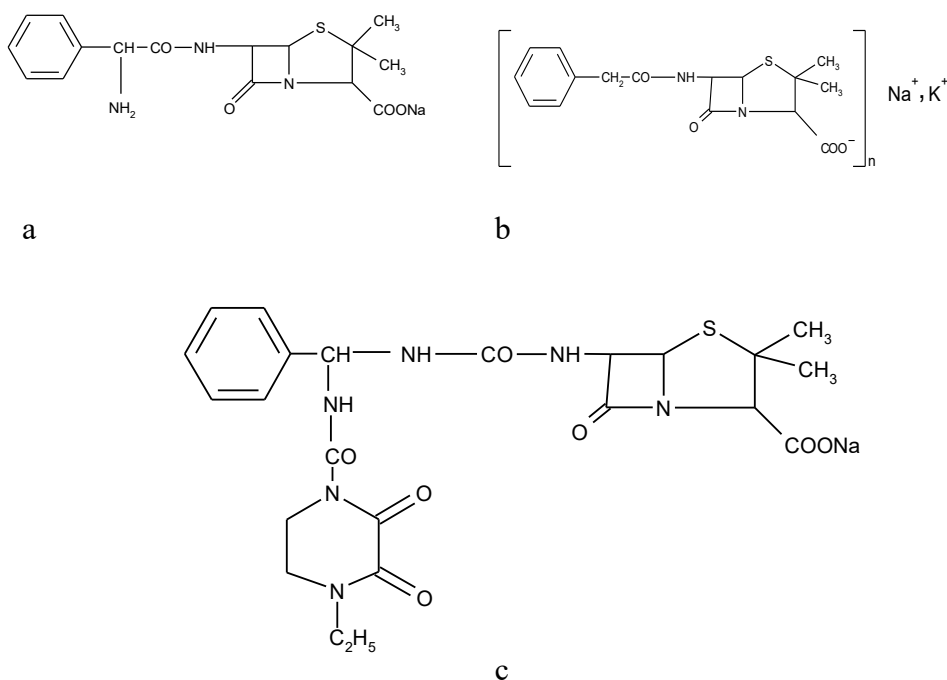


Fig. 1. Chemical structure of: a) ampicillin, b) crystal penicillin, and c) piperacillin [9].

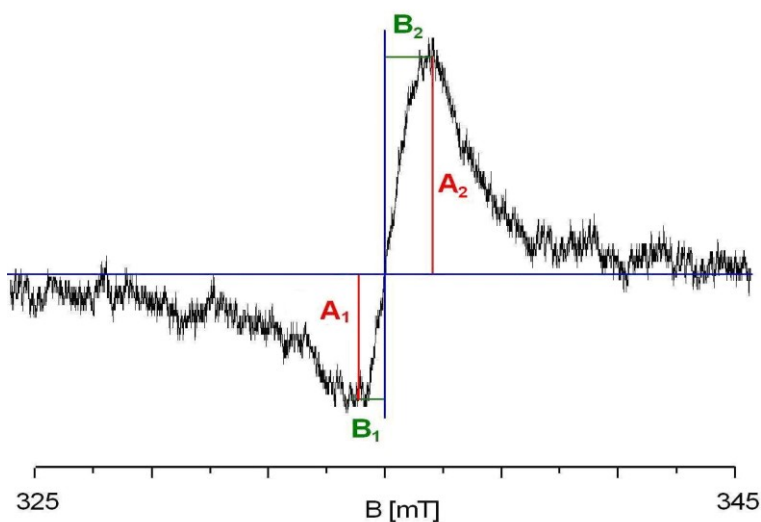


Fig. 2. EPR spectrum of ampicilin sterilized at 160 °C during 120 minutes. The measurement with microwave power of 2.2 mW was done at room temperature 20 minutes after sterilization.

3. Results and discussion

EPR spectra were not obtained for the original non-heated drugs. Thermal sterilization at temperatures 160 °C (120 minutes), 170 °C (60 minutes), and 180 °C (30 minutes) forms free radicals in β -lactam antibiotics. The free radical concentrations in the samples 20 minutes after sterilization were in the range $(0.2-8.0) \times 10^{18}$ spin/g. The highest concentrations of free radicals in ampicilin and crystal penicillin was observed for samples sterilized at 180 °C during 30 minutes. The highest formation of free radicals in piperacyllin appeared at 170 °C during heating by 60 minutes. The amounts of free radicals changes during storage time, but the changes were lower compared to the radiosterilized samples [13]. Interactions with oxygen during storage of the sterilized drugs are responsible for changes in free radicals in the samples.

Shapes of all the spectra of β -lactam antibiotics changes with increasing of microwave power. It probably indicates that more than one group of free radicals exist in the samples. Unpaired electrons in the studied drugs are mainly localized on oxygen atoms. Influence of microwave power on amplitudes of EPR spectra of the examined antibiotics is presented in figures 3-5. The spin-lattice relaxation time in the studied drugs depends on sterilization temperature.

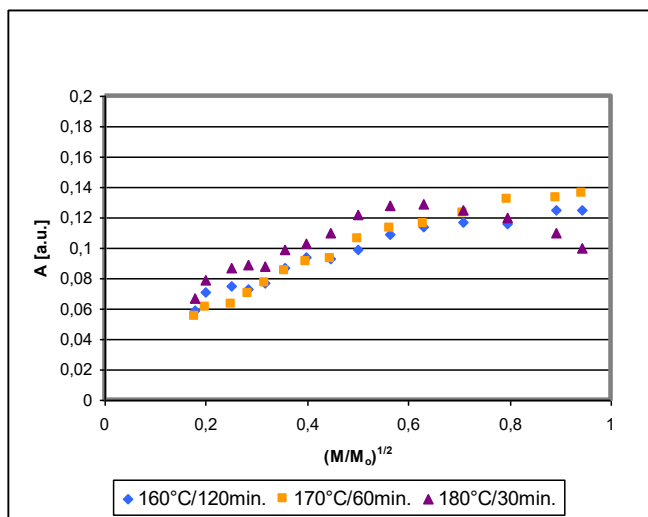


Fig. 3. Influence of microwave power (M) on amplitude (A) of EPR lines of ampicillin sterilized at 160 °C (120 minutes), 170 °C (60 minutes), and 180 °C (30 minutes). M – microwave power used during the measurement, M_0 – the maximal microwave power produced by klystron (70 mW). EPR spectra were recorded in the day of sterilization.

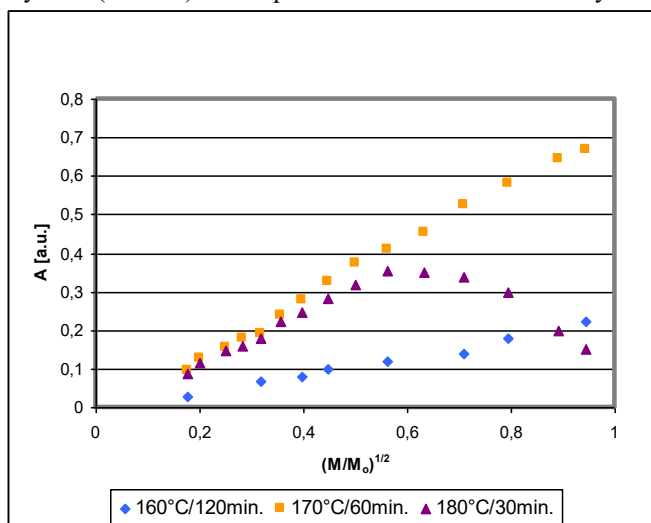


Fig. 4. Influence of microwave power (M) on amplitude (A) of EPR lines of crystal penicillin sterilized at 160 °C (120 minutes), 170 °C (60 minutes), and 180 °C (30 minutes). M – microwave power used during the measurement, M_0 – the maximal microwave power produced by klystron (70 mW). EPR spectra were recorded in the day of sterilization.

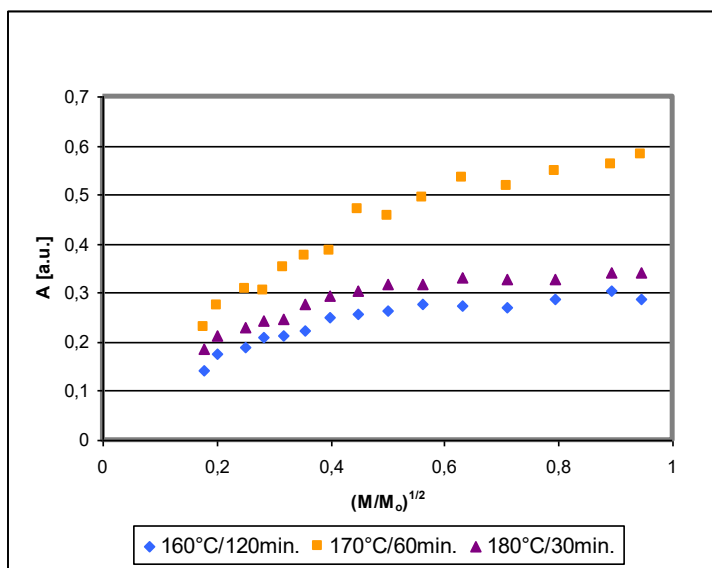


Fig. 5. Influence of microwave power (M) on amplitude (A) of EPR lines of crystal piperacyllin sterilized at 160 °C (120 minutes), 170 °C (60 minutes), and 180 °C (30 minutes). M – microwave power used during the measurement, M_0 – the maximal microwave power produced by klystron (70 mW). EPR spectra were recorded in the day of sterilization.

4. Conclusions

EPR studies indicates that stable paramagnetism ($\sim 10^{17}$ - 10^{18} spin/g) characterizes thermally sterilized β -lactam antibiotics: ampicilin, crystal penicillin, and piperacyllin. Free radicals exist in these drugs 3 months after sterilization. Complex paramagnetic centers system exist in the samples. Dipolar interactions and microwave saturation of EPR lines of the tested drugs depend on temperature of sterilization process. Optimal temperature of sterilization for ampicilin and crystal penicillin is 180 °C. Piperacyllin should be sterilized at 170 °C.

Acknowledgements

This study was supported by Medical University of Silesia in Katowice.

References

- [1] B. Pilawa, R. Pietrzak, H. Wachowska, K. Babel, Acta Phys Polon A 108 (2005) 151.
- [2] B. Pilawa, A.B. Więckowski, M. Lewandowski, Fuel 74 (1995) 1654.
- [3] M. Kościelniak, B. Pilawa, S. Wilczyński, Engin Biomater XI(81-84) (2008) 55.
- [4] M. Kościelniak, S. Wilczyński, B. Pilawa, Engin Biomater XI(81-84) (2008) 61.

- [5] B. Pilawa, S. Wilczyński, P. Ramos, A. Tomasiak, Engin Biomater XI(81-84) (2008) 63.
- [6] P. Ramos, B. Pilawa, M. Kawka, Engin Biomater XII(89-91) (2009), 156.
- [7] B. Pilawa, P. Ramos, S. Wilczyński, K. Czyż, Engin Biomater XI(81-84) (2008) 57.
- [8] P. Ramos, B. Pilawa, S. Wilczyński, K. Czyż, J. Adamczyk, Engin Biomater 87 (2009) 7.
- [9] A. Zejca, Chemia leków, PZWL, Warszawa 2004.
- [10] Farmakopea Polska VIII. PTFarm, Warszawa 2009.
- [11] PN-EN 552. Polish Norm, Warszawa 1999.
- [12] PN-EN 556. Polish Norm, Warszawa 2002.
- [13] S. Wilczyński, Doctoral thesis, Medical University of Silesia in Katowice, Katowice 2008.

The EPR investigation of defects in BGO:Cr single crystal irradiated by high energy uranium ions

I.Stefaniuk, P.Potera, I. Rogalska, D.Wróbel*

* Corresponding author: istef@univ.rzeszow.pl

Institute of Physics, University of Rzeszow, Rejtana 16a, 35-310 Rzeszow, Poland

Abstract

The present work is devoted to investigation of EPR spectra of chromium doped $\text{Bi}_{12}\text{GeO}_{20}$ (BGO) single crystals before and after influence of the ^{235}U ions irradiation with energy 9.35 MeV/u and a fluence $5 \times 10^{11} \text{ cm}^{-2}$. The effect of heating in air on the EPR spectrum of irradiated sample is also studied.

Keywords: EPR spectra, BGO, ^{235}U ions irradiation,

1. Introduction

$\text{Bi}_{12}\text{GeO}_{20}$ (BGO) as well as $\text{Bi}_{12}\text{SiO}_{20}$ (BSO) crystals have been widely used in photorefractive, photoconductive, electro-optical and acousto-optical applications including two-wave mixing, four-wave mixing, phase conjugation, real-time holography, optical data storage, optical computing, electro-optical modulation, thin film optical waveguides [1-4].

The optical and photochromic properties of BGO:Cr crystals were early connected with chromium ions located in the Ge^{4+} tetrahedral positions [5-7]. The chromium ions in BGO:Cr can be in Cr^{4+} and Cr^{5+} state [5,6].

2. Experiment

The BGO:Cr crystal was grown in the Military University of Technology by the Czochralski technique from platinum crucible. The flowing oxygen growth atmosphere was used.

The one sample was irradiated by ^{235}U ions with energy 9.47 MeV/u (the total particle energy was 2 225 MeV) and fluence $5 \times 10^{11} \text{ cm}^{-2}$ at room temperature, without control of temperature and without cooling (denotes as sample no BGO-1). Because the sample of BGO:Cr present strong photochromic effect the sample during irradiation was protected by Al foil (thickness of 5 μm). This foil reduces of particle energy to 2 120 MeV. The specification of samples were given in table 1.

The sample irradiated by high energy uranium ions has cracked perpendicular to the surface into few parts.

The EPR spectra were measured for non-irradiated sample as well as for irradiated sample (before and after annealing in air) in temperature range 140 - 370 K.

After measurements, the heating in air (time of heating was 20 min and temperature – 500 K) were performed by using a LHT 04/16 NABERTHERM furnace with C42 controller. The temperature during each heating was stable with measuring accuracy ± 1 K. The heating samples EPR spectra were measured after it was cooled to the room temperature (sample no BGO-2).

Sample no	Description
BGO-0	The BGO:Cr sample before uranium ions irradiation
BGO-1	The BGO:Cr sample after uranium ions irradiation
BGO-2	The irradiated BGO:Cr sample (BGO-1) after air heating

3. Result and discussion

The EPR of investigated BGO:Cr samples are presented in Fig. 1-3. For non-irradiated sample (BGO-0) the clearly fine structure was presented (Fig 1). This structure is characteristic for Cr doped in high concentration present in four valence state [6]. For BGO-1 sample the angular dependence in room temperature was obtained (Fig 2). This angle dependence show one strong and second weak EPR lines connected with radiation defect appearing during irradiation by uranium ions. The angle dependence for BGO-2 sample is significant different as for BGO-1 sample (fig 3).

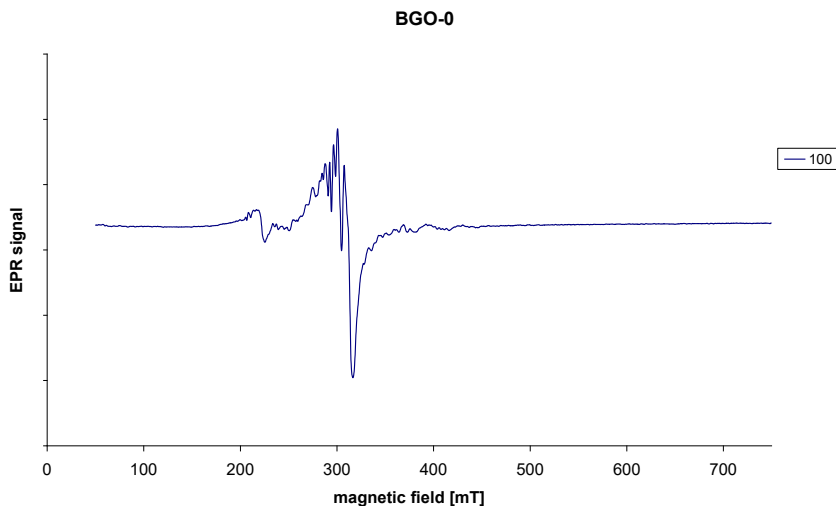


Fig 1. The EPR spectra of BGO-0 sample

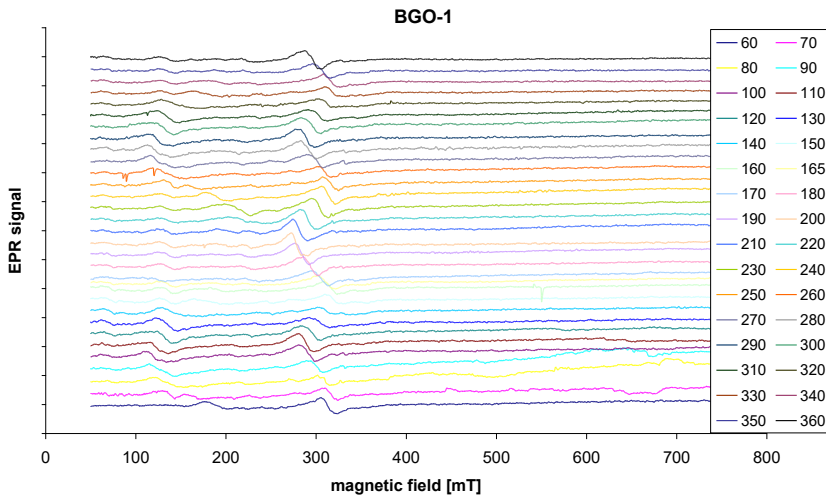


Fig 2 The angular dependence of EPR spectra for BGO-1 sample

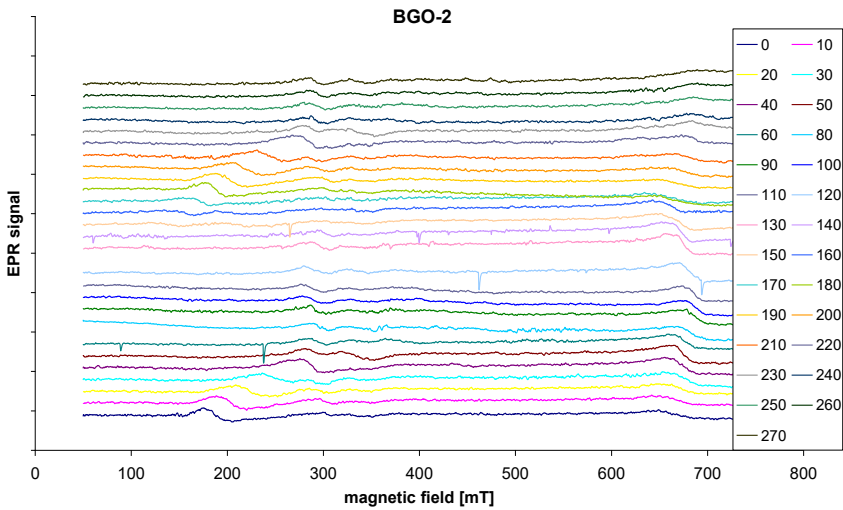


Fig 3 The angular dependence of EPR spectra for BGO-2 sample

For the angular and temperature dependences for samples BGO-1 and BGO-2 the the g_{eff} -value was obtained for each EPR lines (Fig 4a-c). The changes g_{eff} was observed after sample irradiation as well as annealing, but for BGO-2 (sample annealed after irradiation) the temperature dependence is strongly than for BGO-1 (irradiation sample).

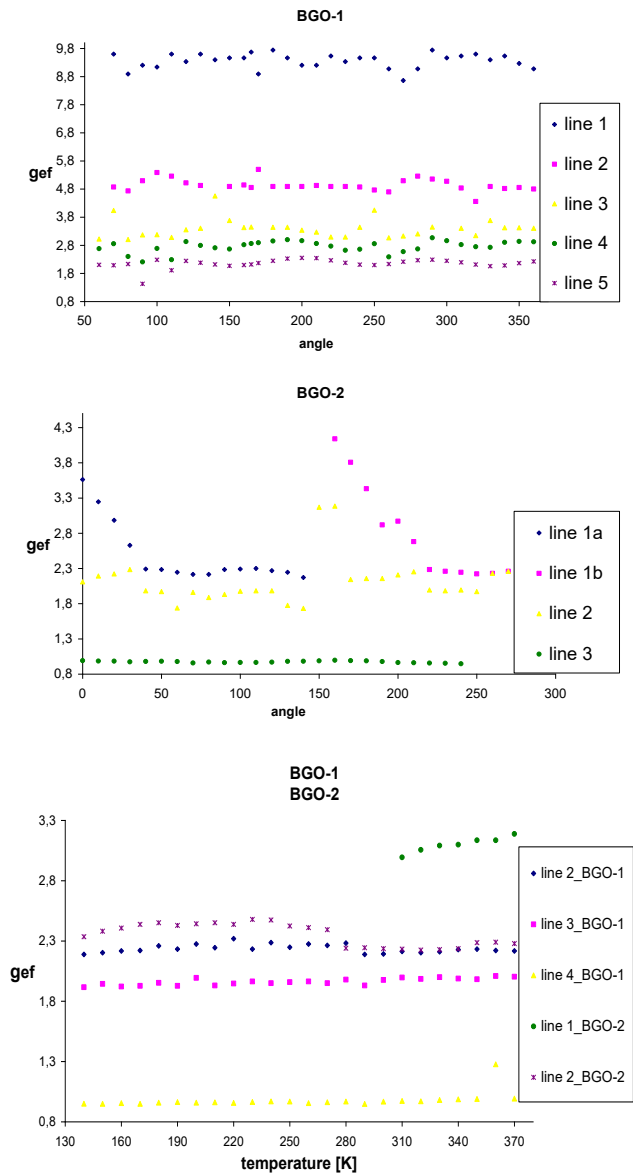


Fig 4. The the g_{eff} -value for BGO-1 and BGO-2 sample

Conclusion

After BGO:Cr irradiation the fine structure of EPR spectra of chromium ions was cleared. Irradiation of BGO:Cr crystals by uranium ions leads to the change of the structure of EPR spectra. The annealing of irradiated sample leads to the changes of lines position and creation of new line in high magnetic field

1. H. Rajbenbach, J. Huignard, "Self-induced coherent oscillations with photorefractive $\text{Bi}_{12}\text{SiO}_{20}$ amplifier," *Opt. Lett.* **10**, 137- (1985)
2. M Miteva, N Dushkina, M.Gospodinov, "Nonstationary amplification of the holographic recording in doped BSO crystals: a base for photorefractive incoherent-to-coherent optical conversion" *Applied Optics* , 34(20), (1995) 4083
3. A. I. Grachev, A. A. Kamshilin, O. V. Kobozev, V. V. Prokofiev, Origin of transient effects in two-wave mixing experiments in BSO crystals, *Optics of Crystals*, V. V. Shepelevich and N. N. Egorov, Editors, Proc. SPIE 4358, (2001),102-108
4. D.Kip, „Photorefractive waveguides in oxide crystals: fabrication, properties, and applications" *Applied Physics B Lasers and Optics*, 67(2), (1998) 131-150.
5. J. S. McCullough, A. L. Harmon Bauer, C. A. Hunt, J. J. Martin"Photochromic response of bismuth germanium oxide doped with chromium" *J.Appl. Phys.*90(12) , (2001) 6017-6021
6. W. Wardzynski, H. Szymczak, K. Pataj T. Łukasiewicz, J. Zmija „Light induced charge transfer processes in Cr doped $\text{Bi}_{12}\text{GeO}_{20}$ and $\text{Bi}_{12}\text{SiO}_{20}$ single crystals" *J. Phys. Chem. Solids* 43(8), (1982), 767-769

Carbon Centred Radicals in Zeolites

Marcin Sterniczuk*, Janusz Turek, Jarosław Sadło, Jacek Michalik
and Grażyna Strzelczak

*Institute of Nuclear Chemistry and Technology, Dorodna 16, 03-195 Warsaw,
Poland, email:m.sterniczuk@ichtj.waw.pl*

Abstract

In this paper we present EPR study on the paramagnetic centers produced after radiolysis of carbon monoxide in H-ZSM-5 and silver hydroxymethyl radical in AgNa-A zeolite. In our studies we used EPR spectroscopy and DFT quantum chemical methods.

Keywords: zeolite, radical, epr, dft, $^{13}\text{CO}^+$ radical cation in H-ZSM-5 zeolite

1. Introduction

Radical intermediates play an important role in many processes of heterogeneous catalysis. They usually are very reactive thus it is extremely difficult to observe them experimentally at process temperature. Therefore reaction mechanisms with active role of radical intermediates have quite often speculative character. However, in some zeolite frameworks radicals are stabilized and then they can be observed by Electron Paramagnetic Resonance (EPR) Spectroscopy.

We present two examples of the EPR studies of carbon centred radicals in zeolites: $\cdot\text{CO}^+$ radical cation in H-ZSM-5 and silver hydroxymethyl radical in AgNa-A.

2. Experimental

Zeolite samples after degassing and dehydration at 130 °C on vacuum line were exposed to ^{13}CO gas or CH_3OH vapour and γ -irradiated in ^{60}Co source at 77 K with dose of 5 kGy. The EPR spectra were recorded using Bruker ESP-300 spectrometer in temperature range 100 – 370 K.

The EPR spectrum of γ -irradiated H-ZSM-5/ ^{13}CO recorded at 300 K is shown in Fig. 1. It consists of two doublets: anisotropic doublet **A** with $g_x = 2.0005$, $g_y = 2.0007$, $g_z = 1.9991$, $A_x = 30.4$ mT, $A_y = 27.5$ mT, $A_z = 25.9$ mT and isotropic doublet **B** with $g_{\text{iso}} = 2.0002$, $A_{\text{iso}} = 21.3$ mT. The doublets are stable at room temperature and start decaying when sample is warmed up. Doublet **A** disappears at 350 K and signal **B** at 370 K. Doublets were not observed when similar experiment was run with ^{12}CO as an adsorbant. That univocally proves that both doublets represent carbon centred radicals excluding assignment to $\cdot\text{CHO}$ radical which was earlier observed in similar system¹.

Anisotropic doublet with similar EPR parameters was observed in γ -irradiated H-Y/ ^{13}CO zeolite by Verdine and Naccache² and assigned to $^{13}\text{CO}^+$ radical cation. As working hypothesis we assumed that anisotropic doublet **A** represents $^{13}\text{CO}^+$ radical interacting with zeolite framework whereas isotropic doublet is a spectrum of freely rotating $^{13}\text{CO}^+$.

To test that hypothesis we applied DFT calculation and were optimizing two structures: the first one with $^{13}\text{CO}^+$ radical cation located close to zeolite lattice and second one with $^{13}\text{CO}^+$ at distant site interacting weaker with lattice nuclei. We expected that those two structures would correspond to the EPR doublets **A** and **B**. Unexpectedly, sites we received very similar values for ^{13}C hyperfine splitting for both. Those values are in very good agreement with experimental value for signal **A**. That allowed us to assign univocally signal **A** to $^{13}\text{CO}^+$ radical cation. However, the isotropic signal **B** remains unidentified.

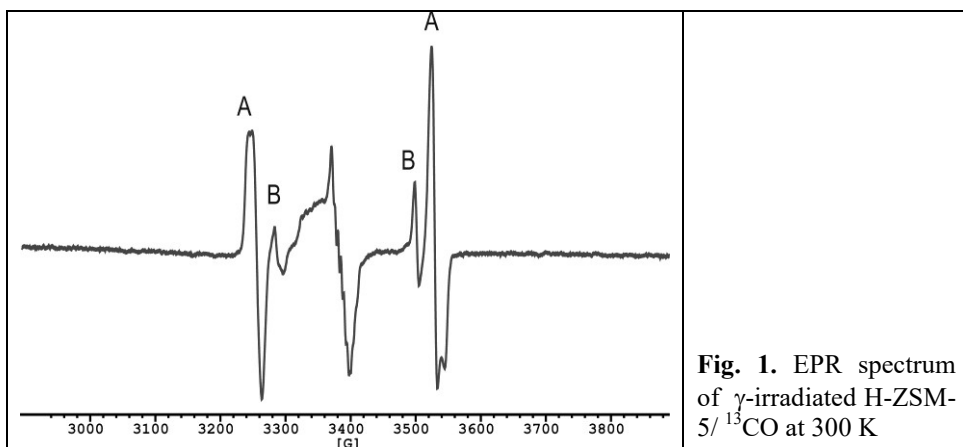


Fig. 1. EPR spectrum of γ -irradiated H-ZSM-5/ ^{13}CO at 300 K

Silver hydroxymethyl radicals in AgNa-A zeolite

In AgNa-A zeolite exposed to methanol vapour and γ -irradiated at 77 K on thermal annealing at 130 K a doublet with $A_{\text{iso}} = 10.12$ mT start appearing. The increase of its intensity is associated with the decay of $\cdot\text{CH}_2\text{OH}$ triplet. Doublet with slightly bigger hyperfine splitting was earlier recorded in γ -irradiated frozen solution of methanol containing silver perchlorate and was assigned to $[\text{Ag}\cdot\text{CH}_2\text{OH}]^+$ radical cation³ formed by attachment $\cdot\text{CH}_2\text{OH}$ radical to Ag^+ cation⁴.

Our DFT calculations proved that one-electron bond between silver and carbon is able to stabilize $[\text{Ag}\cdot\text{CH}_2\text{OH}]^+$ adduct and that EPR doublet cannot originate from $\text{Ag}\cdot\text{O}$ one-electron bond because such configuration gives very low spin density on silver. A comparison of DFT calculations and EPR results

show that $[\text{Ag}\cdot\text{CH}_2\text{OH}]^+$ radical cation interacts only with small fragment of silicalumina framework. Owing to that hyperfine splitting value $A_{\text{iso}}(\text{Ag})$ is structure independent. In zeolites with high cation capacity the electrostatic interaction of silver atom with lattice negative charge centre predominates resulting with decrease of spin density at Ag atom (Fig. 2) because the bonding electron is pushed by repulsive forces to organic fragment of radical. In zeolites with small cation capacity the formation of hydrogen bond between radical hydroxyl group and lattice oxygen plays the major role. O-H bond in interacting hydroxyl group is weaker, thus oxygen atom is stronger electron donor to Ag-C-O bonds system increasing spin density on silver atom.

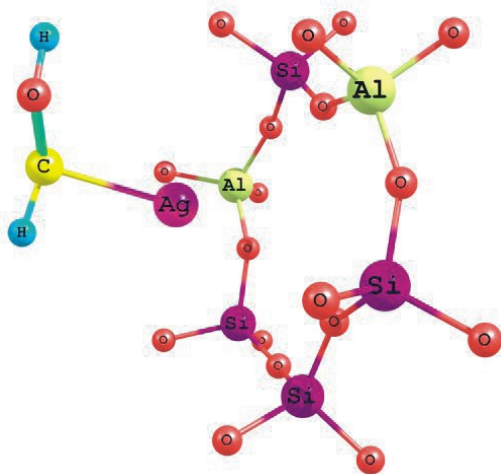


Fig. 2. Electrostatic interaction of $[\text{Ag}\cdot\text{CH}_2\text{OH}]^+$ radical with silicalumina lattice

3. Conclusions

The present results show that radiolysis of adsorbates in zeolites leads to the formation of radical intermediates which can be identified by EPR. The DFT calculations of EPR parameters are very informative to understand the radical interactions with zeolite framework.

References

- [1]. F.J. Adrian, E.L. Cochran, V.A. Bowers, *J. Chem. Phys.*, **36** (1962), 1661
- [2]. J.C. Vedrine, C. Naccache, *Chem. Phys. Lett.* **18** (1972), 190,
- [3]. M.C.R. Symons, R. Janes, A.D. Stevens, *Chem. Phys. Lett.*, **160** (1989), 384
- [4]. J. Michalik, J. Sadło, A van der Pol, E. Reijerse, *A. Chem. Scan.*, **51** (1997), 330

Radicals Generated Radiolytically in Lithium Formate

Janusz Turek^{*1}, ***Jacek Michalik***¹, ***Jarosław Sadło***¹, ***Marcin Sterniczuk***¹, ***Grażyna Strzelczak***¹, ***Henk Vrielinck***², ***Freddy Callens***²

**Corresponding author: j.turek@ichtj.waw.pl*

¹*Institute of Nuclear Chemistry and Technology, Warsaw, Poland*

²*Ghent University, Department of Solid State Sciences, Gent, Belgium*

Lithium formate monohydrate – HCOOLi·H₂O was recently proposed as a new, tissue equivalent, high sensitive material for EPR clinic dosimetry. It is 6 – 7 times more sensitive than an alanine dosimeter using comparable instruments configuration. The linear dose response of the EPR signal in the range 0.2 – 1000 Gy was demonstrated. Irradiated HCOOLi·H₂O shows simple EPR spectrum stable at room temperature and linearly depended with radiation dose. For powder samples a broad singlet with 1.67 mT peak-to-peak width is recorded at X-band. The measurements at Q-band reveal anisotropy of singlet with $g_{\perp} = 2.00117$ and $g_{\parallel} = 1.99657$. It represents predominantly $\cdot\text{CO}_2^-$ radicals. The suggestion that the singlet contains the spectrum of second radical appeared quite early. Recently the stabilisation of reduction product – $\text{HC}^{\cdot}\text{O}(\text{OH}) \text{Li}^+$ was proposed. The subject of our work concerns the EPR and ENDOR study at Q-band of the structure and stability of radical species observed in irradiated HCOOLi·H₂O monocrystal. Lithium formate crystallises in orthorhombic space group Pna2₁. In irradiated monocrystals of lithium formate at room temperature two different radical species are observed at Q-band. In sample measured directly after irradiation $\cdot\text{CO}_2^-$ radicals are dominant species. They are stabilised at orientations similar to orientations of parent HCOO⁻ anions. The EPR spectra in Q-band registered at 70 K at the orientation of [1 0 0] axis along the magnetic field consist of two signals: singlet of $\cdot\text{CO}_2^-$ radicals at $g = 2.00035$ and signal of second radical at $g = 2.00481$. During rotation of monocrystal from [1 0 0] axis to [0 1 0] axis g value for $\cdot\text{CO}_2^-$ radicals increases to 2.00315. Angular variation of Q-band ENDOR spectra shows weak interaction of $\cdot\text{CO}_2^-$ radicals with four magnetically equal groups of hydrogen nucleus and four groups of lithium nucleus in the vicinity. Interactions of second radicals with neighbouring atoms have not been yet fully interpreted. It weakly interacts with one group of lithium nucleus and one or two protons groups. Both radicals are located in two magnetically unequal positions causing splitting of ENDOR signals during rotation of monocrystal. Based on kinetic EPR studies it was shown that the signals in irradiated lithium formate had different stability. The $\cdot\text{CO}_2^-$ signal decreases completely after a few days of storage at room temperature in air. Then the unidentified signal becomes dominant. The decay kinetics of radicals formed radiolytically in HCOOLi will be studied in details in near future.

EPR studies of influence of storage conditions on free radicals in gamma irradiated aminoglycoside antibiotics

Sławomir Wilczyński^{*1)}, Barbara Pilawa¹⁾, Robert Koprowski²⁾, Zygmunt Wróbel²⁾, Marta Ptaszkiewicz³⁾, Janusz Swakoń³⁾, Paweł Olko³⁾

**Corresponding author: swilczynski@sum.edu.pl*

¹⁾Department of Biophysics, Medical University of Silesia in Katowice, School of Pharmacy and Laboratory Medicine, Jedności 8, 41-200 Sosnowiec, Poland

²⁾Institute of Computer Science, University of Silesia, Faculty of Computer Science and Material Science, Będzińska 39, 41-200 Sosnowiec, Poland

³⁾Department of Radiation Physics and Dosimetry, Institute of Nuclear Physics, Radzikowskiego 152, 31-342 Kraków, Poland

Abstract

Free radicals formed in different aminoglycoside antibiotics during sterilization by gamma irradiation were examined. EPR spectra were measured for the irradiated samples in air and in argon atmosphere at room temperature. Evolution of EPR spectra with storage time after radiosterilization was determined. Changes in free radical systems of the analysed drugs during storage were compared.

Keywords: EPR, free radicals, aminoglycoside antibiotics, gamma irradiation, radiosterilization

1. Introduction

Information about free radicals in irradiated drugs is important for choice of method and conditions of their sterilization and storage [1-6]. The aim of this work was to determine concentrations and properties of free radicals in selected aminoglycoside antibiotics after gamma irradiation. Stability of the formed free radicals during storage at different conditions were compared. Interactions of free radicals of antibiotics and oxygen molecules O₂ were analysed.

2. Experimental details

Gamma irradiated aminoglycoside antibiotics: sisomicin, tobramycin, paromomycin, streptomycin, gentamicin and neomycin were examined by EPR spectroscopy. The antibiotics were sterilized according to the norms [7]. Aminoglycoside antibiotics belong to the group of chemotherapeutic agents and are effective against certain types of bacteria. The mechanism of action aminoglycoside antibiotics results from irreversible binding to the bacterial 30S ribosomal subunit. This connection leads to formation of incorrect structure proteins [8].

The analysed antibiotics were gamma irradiated in THERATRON 780E containing izotop ^{60}Co . Dose of gamma irradiation of 25 kGy was used. Concentrations and properties of free radicals in irradiated antibiotics were studied by an X-band (9.3 GHz) electron paramagnetic resonance (EPR) spectrometer of RADIOPAN Firm (Poznań, Poland). EPR spectra were recorded for samples in air and in argon atmosphere. The following parameters of EPR spectra were determined: g factor, integral intensity, amplitude and linewidth. Influence of microwave power (2.2-70 mW) on the EPR lines was analysed. Dependences of free radicals concentrations in irradiated drugs on storage time were determined. These correlations were numerically fitted by theoretical exponential functions by the Gaussa-Newton and Levenberga-Marquardt method.

3. Results and discussion

Free radicals do not exist in the studied non-irradiated antibiotics. EPR lines were recorded for the gamma irradiated drugs. The EPR spectra differ in shape. Complex structure of free radical system in the samples may be responsible for this effect. Gamma irradiation forms free radicals of 10^{17} - 10^{18} spin/g in the studied samples. The highest free radicals concentrations were obtained for irradiated aminoglycoside antibiotics as sisomicin, tobramycin, and paromomycin.

Free radicals concentrations in the studied gamma irradiated antibiotics decreases with increasing of storage time. The faster changes of concentrations were observed in the first time after irradiation. Correlations between free radicals and storage time after irradiation may be fitted by one-exponential function for sisomicin, tobramycin, and paromomycin. Two-exponential functions fit time correlations for the others irradiated drugs. Interactions with oxygen may be responsible for decrease of free radicals concentrations in irradiated drugs during storage. It indicate comparison of EPR parameters for samples in air and in argon environment. Free radicals concentrations in irradiated samples in argon decrease slower than in samples in air.

High g values (2.0036-2.0083) and broad (0.93-2.90 mT) EPR lines were obtained for the studied drugs. Microwave saturation of EPR lines indicates their homogeneous broadening. The analysed EPR lines saturate at low microwave powers, so slow spin-lattice relaxation processes exist in the irradiated antibiotics. The performed spectroscopic studies bring to light information about concentration and properties of free radicals in gamma irradiated antibiotics. The results may be useful for radiosterilization processes of drugs.

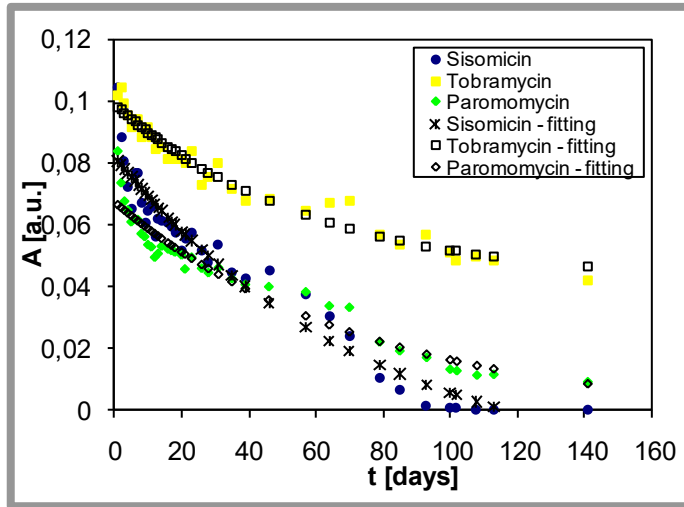


Fig. 1. Influence of storage time (t) on amplitude (A) of EPR lines of gamma irradiated sisomicin, tobramycin and paromomycin for samples in air. The experimental data and results of theoretical fitting to one-exponential functions $A(t) = A_0 + A_1 \exp(-t/\tau_1)$ are presented.

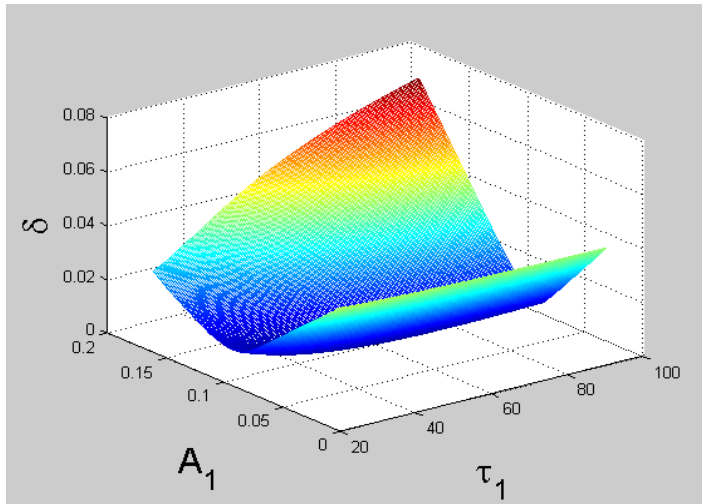


Fig. 2. Correlations between the error δ of theoretical fitting of experimental dependence of amplitude (A) of EPR line on storage time (t) and parameters τ_1 [day] and A_1 [a.u.] for gamma irradiated sisomicin for sample in air.

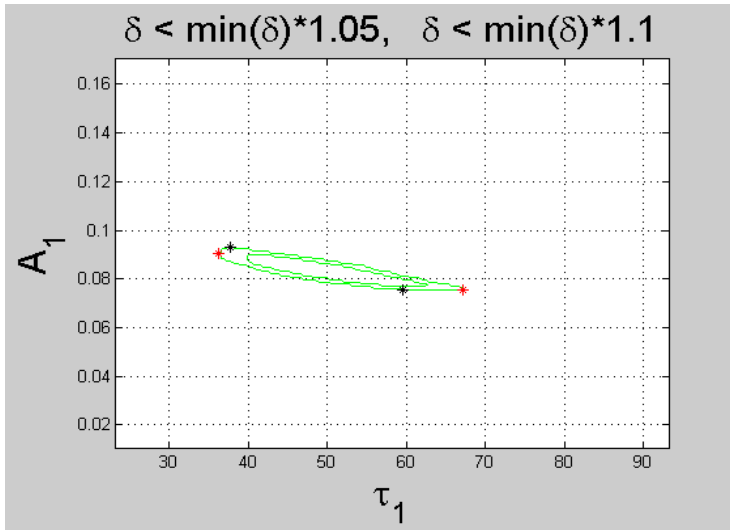


Fig. 3. The range of tolerated variability of parameters τ_1 [days] and A_1 [a.u.] of function model $A(t)$ for $\delta < \min(\delta) \cdot 1.05$ and $\delta < \min(\delta) \cdot 1.10$ for sisomicin.

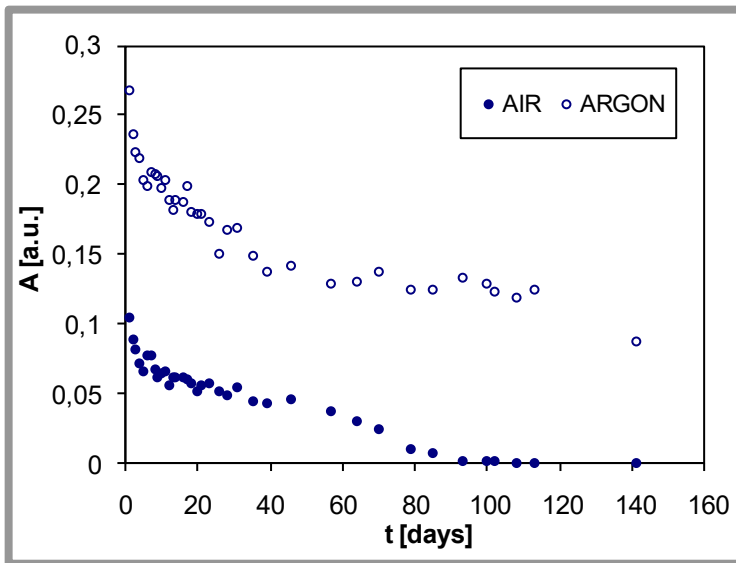


Fig. 4. Comparison of changes of amplitude (A) of EPR lines of gamma irradiated sisomicin with storage time (t) for samples in air and in argon.

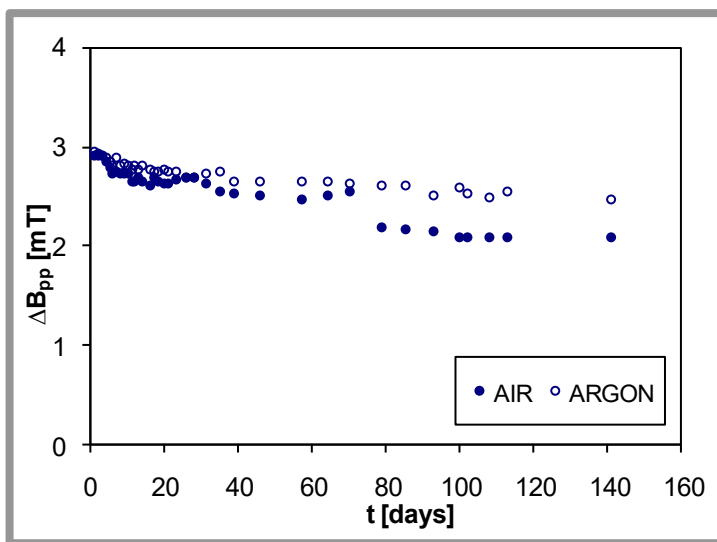


Fig. 5. Comparison of changes of linewidth (ΔB_{pp}) of EPR lines of gamma irradiated sisomicin with storage time (t) for samples in air and in argon.

4. Conclusions

On basis of EPR examination of gamma irradiated aminoglycoside antibiotics with a dose of 25 kGy some conclusions about conditions of radiosterilization and storage of these drugs may be drawn. Because the tested aminoglycoside antibiotics are paramagnetic, it is expected that they cause toxic free radicals effects in living organisms during farmacotherapy. The amount of free radicals strongly decreases during the first several days after gamma sterilization. It was shown that interactions with oxygen O_2 modify free radical properties of irradiated aminoglycoside antibiotics. The samples of radiosterilized drugs should be storage in ambient environment.

Acknowledgements

This study was supported by Medical University of Silesia in Katowice.

References

- [1] M. Gibella, A.S. Crucq, B. Tilquin, P. Stocker, G. Lesgards, J. Raffi, *Radiat. Phys. Chem.* 58 (2000) 69.
- [2] L. Varshney, P.B. Dodke, *Radiat. Phys. Chem.* 71 (2004) 1103.
- [3] S. Onori, M. Pantaloni, P. Fattibene, E. Ciranni-Signoretti, *Appl. Radiat. Isotop.* 47 (1996) 1569.
- [4] B. Katušin-Ražem, K. Hamitouche, N. Maltar-Strmečki, *Radiat. Phys. Chem.* 73 (2005) 116.

- [5] S. Wilczyński, M. Ptaszkiewicz, E. Pierzchała, B. Pilawa, J. Swakoń, P. Olko, *Curr. Top. Biophys.* 31 (2008) 1.
- [6] S. Wilczyński, B. Pilawa, M. Ptaszkiewicz, E. Pierzchała, J. Swakoń, P. Olko, *Sci. Rev. Pharm.* 9 (2009) 8.
- [7] PN-EN 552. Polish Norms, Warszawa, 1999.
- [8] A. Zejc, M. Gorczyca, red. *Chemia leków*. PZWL, 2002.

Antioxidant capacity of serum measured using TEMPO scavenging assay in patients with rheumatoid arthritis

***Katarzyna Zawada*^{*1)}, *Joanna Celińska*¹⁾, *Ewa Matyska-Piekarska*²⁾,
*Iwona Wawer*¹⁾, *Jan K Łącki*²⁾**

** Corresponding author: katarzyna.zawada@wum.edu.pl*

¹⁾ Medical University of Warsaw, Faculty of Pharmacy, Department of Physical Chemistry, Banacha 1, 02-097 Warsaw, Poland

²⁾ Institute of Rheumatology in Warsaw, Clinic of Connective Tissue Diseases, Spartańska 1, 02-637 Warsaw, Poland

Abstract

Serum antioxidant capacity was measured using TEMPO radical scavenging assay. The dependence on disease activity, gender and smoking habits in patients with rheumatoid arthritis (RA) was investigated. The decrease in serum antioxidant capacity was observed for moderate and severe activity of RA as compared with control group. There was no relation observed between serum antioxidant capacity and gender, or between serum antioxidant capacity and smoking habits.

Keywords: TEMPO; Antioxidant capacity; Electron Paramagnetic Resonance; Rheumatoid arthritis; DAS28

1. Introduction

Oxidative stress can be a causative factor in several diseases, including autoimmune ones such as rheumatoid arthritis (RA). It occurs when the balance between prooxidants and antioxidants is disturbed in favour of the former, and can be a consequence of decreased antioxidants level [1]. Therefore, the determination of antioxidant capacity of biological system could potentially give valuable information about the mechanism and probability of autoimmune diseases.

There are different methods of evaluating the antioxidant capacity of human organism, some of them being based on a partial neutralization of a stable radical, like DPPH [2] and nitroxide radicals [3], by body fluids such as blood plasma or serum.

The antioxidant capacity of human serum measured with TEMPO (2,2,6,6-tetramethylpiperidine-1-oxyl) radical is due mainly to vitamin C level [4], which is one of two (the other being uric acid) most abundant water-soluble low molecular weight antioxidants in human blood. Nonetheless, the reaction of TEMPO with other antioxidants, like anthocyanins, is also possible [5].

The aim of this work was to establish the relationship between antioxidant capacity of serum measured with TEMPO radical assay and DAS28 (Disease

Activity Score) factor. DAS28 was chosen as a measure of the activity of rheumatoid arthritis, for patients with moderate and very active disease as compared with healthy subjects. Additionally, the influence of smoking habits and gender on the antioxidant capacity of serum was considered.

2. Experimental details

Patients

Studies were performed on 98 patients diagnosed with RA and 22 healthy subjects (control group). Fasting blood samples were collected in the morning and serum samples were stored at -20°C.

TEMPO scavenging by human serum

The procedure was based on that described by Piehl et al. [4]. 20 µl of TEMPO solution (6.4 mM in PBS buffer, pH = 7.4) was added to 480 µl of human serum. EPR spectra of TEMPO were recorded at room temperature for 30 minutes. Nitroxide signal intensity was measured as the total height of the low field peak.

The antioxidant capacity of serum was calculated as the vitamin C equivalent concentration using the calibration curve of TEMPO concentration change after 30 minutes (Δc) vs vitamin C concentration.

EPR measurements were performed on a X-band Miniscope MS200 spectrometer (Magnettech, Berlin, Germany) using the following instrument settings: modulation amplitude, 0.1 mT; centre field, 334 mT; sweep width, 8 mT; sweep time, 20 s; microwave power, 13 mW.

DAS28

Factor DAS28 was calculated according to the equation:

$$\text{DAS28} = 0.56 \cdot (\text{TEN})^{1/2} + 0.28 \cdot (\text{SW})^{1/2} + 0.7 \cdot \text{LN}(\text{OB}) + 0.014 \cdot \text{VAS}$$

where: TEN - number of joints tender to the touch, SW - number of swollen joints, ESR - erythrocyte sedimentation rate, VAS - patient assessment of disease activity [mm].

Statistical analysis

Data were analyzed with the Mann–Whitney *U* test and the Kruskal–Wallis one-way analysis of variance by ranks. Statistical analysis was performed using data analysis software system Statistica 9 (StatSoft Inc.) .

3. Results and discussion

3.1. Rheumatoid arthritis severity

Antioxidant capacity of serum for patients with severe, moderate and inactive or absent RA was compared. Statistically significant ($p < 0.001$) decrease was observed for both moderate ($n = 25$) and severe ($n = 68$) RA groups as

compared with control group (n = 24) [Fig. 1]. Mean value of Vitamin C equivalent for control group is over two times greater than for the group of patients with severe RA and about 30% than for the moderate RA group. This suggests a relation between oxidative stress and this autoimmune disease severity.

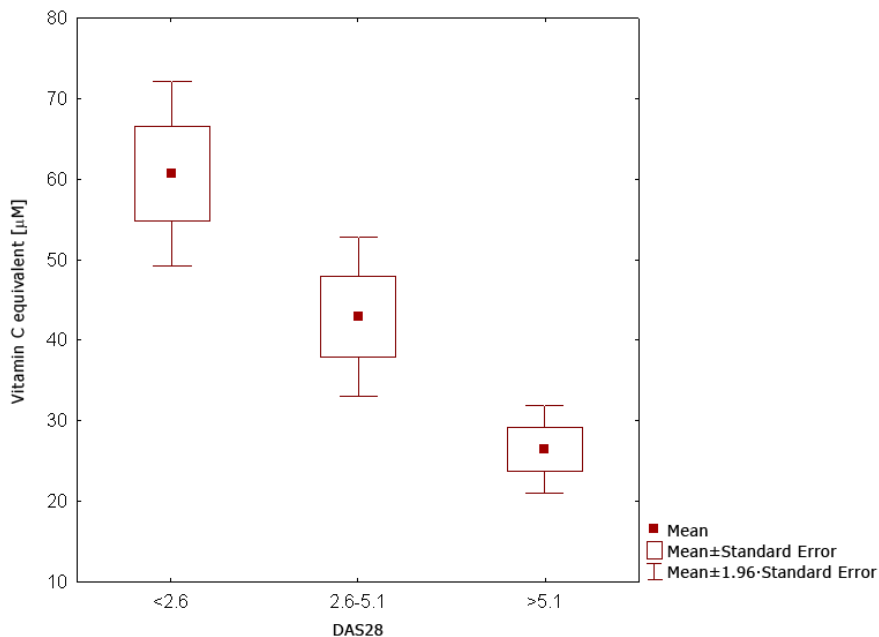


Fig. 1. Antioxidant capacity dependence on severity of RA. DAS28 values < 2.6 correspond to the absence or remission of RA, those between 2.6 and 5.1 to moderate activity of RA, and those > 5.1 to severe activity.

3.2. Gender

The potential influence of gender was investigated. However, the results did not show any relation between gender and antioxidant capacity of serum in RA diagnosed group [Table 1].

Table 1. Antioxidant capacity for women and men

Group	n	Vitamin C equiv. Mean ± SE [µM]
Women	18	32.9 ± 5.8
Men	80	32.9 ± 3.2

3.3. Smoking habits

Among patients, there was no statistically significant difference between smokers and non-smokers groups [Table 2], irrespectively of the RA severity. This is in opposition to the frequently observed decrease of antioxidant capacity in healthy smokers [6]. However, the potential effect of smoking during RA exacerbation may be masked by a strong decrease of serum antioxidant capacity due to RA itself.

Table 2. Antioxidant capacity for smoking and non-smoking patients

Group	n	Vitamin C equiv. Mean \pm SE [μ M]
Smokers	17	31.8 \pm 3.0
Non-smokers	79	39.4 \pm 7.8

4. Conclusions

The antioxidant capacity of human serum measured with TEMPO assay is decreased in patients with rheumatoid arthritis as compared with a control group of healthy volunteers. This effect is more pronounced for severe AR activity group than for moderate AR activity one.

There was no significant influence of gender or smoking habits on antioxidant capacity in patients diagnosed with RA.

Acknowledgements

EPR measurements were accomplished at the Structural Research Lab., Medical University of Warsaw, Faculty of Pharmacy, Poland. SRL was established with financial support from European Regional Development Fund in the Sectoral Operational Programme "Improvement of the Competitiveness of Enterprises, years 2004-2006" project no: WKP_1/1.4.3./1/2004/72/72/165/2005/U.

References

- [1] B. Halliwell, J. C. Gutteridge, *Free Radicals in Biology and Medicine*, Fourth Ed., Oxford University Press, 2007.
 - [2] S. Martinez, L. Valek, J. Rešetić, D. Ferenc Ružić, *J. Electroanal. Chem.* 588 (2006) 68.
 - [3] J. Fuchs, N. Groth, T. Herrling, G. Zimmer, *Free Rad. Biol. Med.* 22 (6) (1997) 967.
 - [4] L. L. Piehl, G. B. Facorro, M. G. Huarte, M. F. Desimone, G. J. Copello, L. E. Díaz, E. Rubín de Celis, *Clin. Chim. Acta* 359 (2005) 78.
 - [5] V. Butković, *Croat. Chem. Acta* 82 (3) (2009) 707.
- I. Rahman, E. Swarska, M. Henry, J. Stolk, W. MacNee, *Thorax* 55 (2000) 189

EPR studies of *Cladosporium cladosporioides* mycelium with flucytosine

***Magdalena Zdybel*^{*1)}, *Barbara Pilawa*¹⁾, *Ewa Buszman*²⁾, *Teresa Witoszyńska*²⁾, *Honorata Cieśla*¹⁾**

*Corresponding author: mzdybel@sum.edu.pl

¹⁾Department of Biophysics, School of Pharmacy and Division of Laboratory Medicine, Medical University of Silesia in Katowice, Jedności 8, 41-200 Sosnowiec, Poland

²⁾Department of Pharmaceutical Chemistry, School of Pharmacy and Division of Laboratory Medicine, Medical University of Silesia in Katowice, Jagiellońska 8, 41-200 Sosnowiec, Poland

Abstract

Free radicals in *Cladosporium cladosporioides* cultured with flucytosine were studied by an X-band EPR spectroscopy. Different drug concentrations were used. The results were compared to data for the model eumelanin - DOPA-melanin. It was shown that similar paramagnetic properties characterizes complexes of *Cladosporium cladosporioides* mycelium with flucytosine and DOPA-melanin-flucytosine complexes.

Keywords: EPR, free radicals, flucytosine, Cladosporium cladosporioides mycelium

1. Introduction

Mainly o-semiquinone free radicals exist in melanin biopolymers [1-9]. EPR line of eumelanin dominates in *Cladosporium cladosporioides* spectra [7-9]. The aim of this work is to determine effect of flucytosine on free radicals in *Cladosporium cladosporioides* mycelium. Free radical properties of the natural samples with those of synthetic DOPA-melanin were compared.

2. Experimental details

Free radicals in mycelium of *Cladosporium cladosporioides* cultured with the synthetic antifungal drug as flucytosine were studied by an X-band (9.3 GHz) electron paramagnetic resonance spectroscopy. *Cladosporium cladosporioides* culture is shown in figure 1. The chemical structure of flucytosine - the derivative of pyrimidine is presented in figure 2 [9]. The following two concentrations of flucytosine: 25 µg/ml culture medium and 50 µg/mg culture medium, were used. DOPA-melanin and DOPA-melanin-flucytosine complexes were also tested.

Free radical concentration was determined as compared to the concentration in ultramarine as the reference. g-Factor, amplitude (A), integral intensities (I),

and linewidth (ΔB_{pp}) were analysed. Influence of microwave power (M) in the range of 2.2-70 mW on the spectra was evaluated.



Fig. 1. Culture of *Cladosporium cladosporioides*.

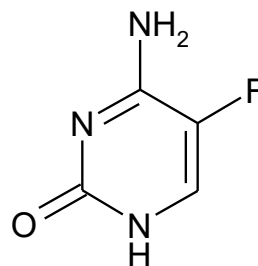


Fig. 2. Chemical structure of flucytosine [10].

3. Results and discussion

Single EPR lines and complex EPR spectra (fig. 3) were measured for the studied DOPA-melanin, and *Cladosporium cladosporioides* samples, respectively. EPR spectra of *Cladosporium cladosporioides* mycelium with flucytosine (50 μg flucytosine/ml culture medium) recorded at two different microwave powers are presented in figure 3. EPR spectra of *Cladosporium cladosporioides* mycelium and the mycelium with flucytosine revealed complex character. They are superposition of the component line of eumelanin, the line of pheomelanin, and the line of the other part of organic matter of the mycelium.

Mainly EPR component of the eumelanin exist in the resonance absorption curve (fig. 3). The line of pheomelanin is visible in the spectra of *Cladosporium cladosporioides* mycelium and the mycelium with flucytosine measured with the relatively higher microwave powers (fig. 3). Concentrations of free radicals and the parameters of the spectra of the examined samples are compared in table 1. Influence of microwave power on amplitudes (A) and linewidth (ΔB_{pp}) of EPR lines of the studied samples is shown in figures 4 and 5, respectively.

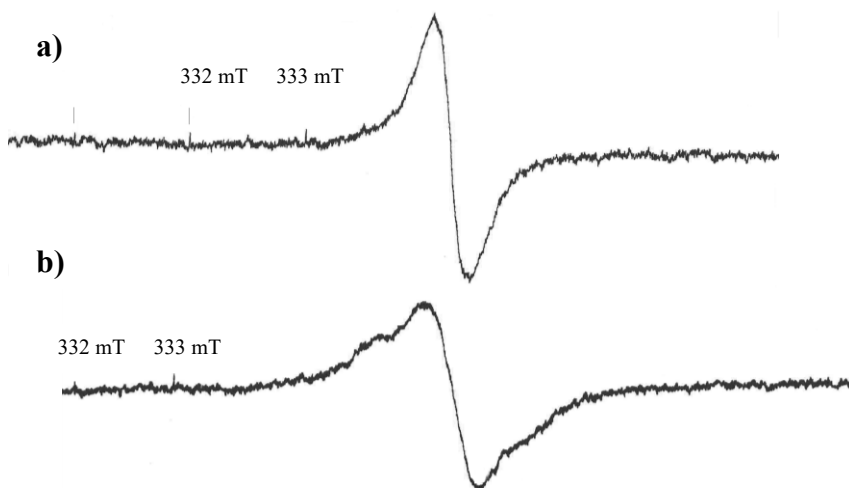


Fig. 3. EPR spectra of *Cladosporium cladosporioides* mycelium with flucytosine recorded at 2.2 mW (a) and 70 mW (b), respectively.

Table 1. Free radical concentration (N), g-factor, and linewidth (ΔB_{pp}) of EPR spectra of *Cladosporium cladosporioides* mycelium and the mycelium with flucytosine.

Sample	$N \times 10^{18}$ (spin/g)	g (± 0.0002)	ΔB_{pp} (± 0.02 mT)
<i>Cladosporium cladosporioides</i> mycelium	0.3	2.0034	0.39
<i>Cladosporium cladosporioides</i> mycelium with flucytosine (25 μ g flucytosine/ml culture medium)	0.4	2.0035	0.37
<i>Cladosporium cladosporioides</i> mycelium with flucytosine (50 μ g flucytosine/ml culture medium)	0.3	2.0037	0.41
DOPA-melanin	8.5	2.0037	0.45
DOPA-melanin-flucytosine complex (50 μ g flucytosine/mg DOPA-melanin)	8.4	2.0038	0.46

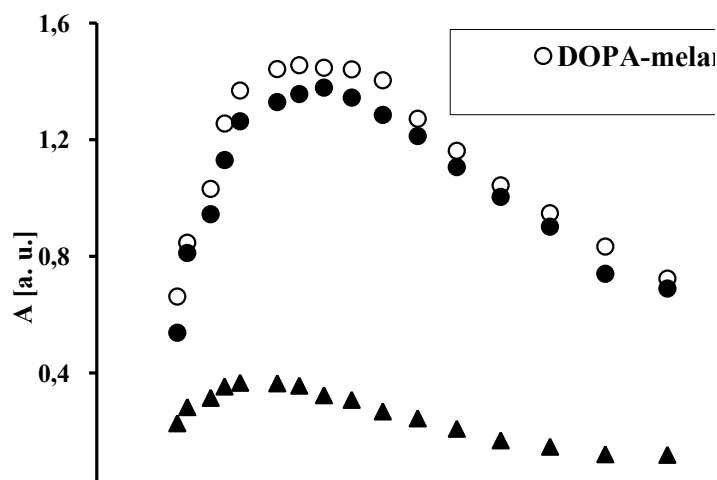


Fig. 4. Influence of microwave power (M/M_0) on amplitude (A) of EPR spectra of DOPA-melanin, *Cladosporium cladosporioides* mycelium, and their complexes with flucytosine. M – microwave power used during the measurement, M_0 – total microwave power produced by klystron (70 mW). Samples with 50 μg flucytosine/ml culture medium and 50 μg flucytosine/mg DOPA-melanin were tested.

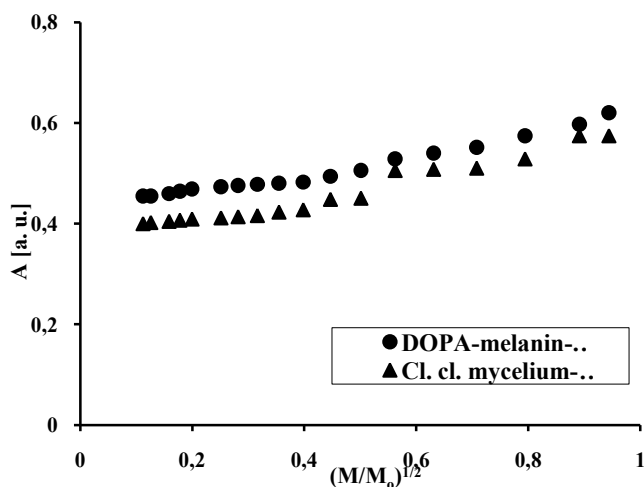


Fig. 5. Influence of microwave power (M/M_0) on linewidth (ΔB_{pp}) of EPR spectra of DOPA-melanin and *Cladosporium cladosporioides* mycelium with flucytosine. M – microwave power used during the measurement, M_0 – total microwave power produced by klystron (70 mW). Samples with 50 μg flucytosine/ml culture medium and 50 μg flucytosine/mg DOPA-melanin were tested.

g -Values (2.0034-2.0038) characteristic for o-semiquinone free radicals were obtained for *Cladosporium cladosporioides* mycelium and DOPA-melanin samples (table 1). Broad EPR lines were measured for both mycelium (ΔB_{pp} :

0.37-0.41 mT) and DOPA-melanin (ΔB_{pp} : 0.46 mT) samples (table 1). Dipolar interaction may be responsible for line broadening. Homogeneous broadening of EPR line was observed (fig. 4-5). Slow spin-lattice relaxation processes exist in all the examined samples (fig. 4). Addition of flucytosine to *Cladosporium cladosporioides* mycelium and to DOPA-melanin did not change microwave saturation of their EPR spectra (fig. 4). EPR lines of *Cladosporium cladosporioides* samples saturated at relatively lower microwave power than EPR lines of synthetic eumelanin (fig. 4). Probably flucytosine does not change spin-lattice relaxation processes in mycelium and DOPA-melanin samples. The pulse spectroscopic studies in this matter are necessary.

Flucytosine does not change free radicals concentration in *Cladosporium cladosporioides* mycelium and in DOPA-melanin (table 1). Such effect was not observed earlier for dry *Cladosporium cladosporioides* mycelium complexed with flucytosine [9]. It can be then concluded that different free radical reactions exist in the liquid fungal culture with flucytosine and in the sample of flucytosine added to dry mycelium. It is expected that in *Cladosporium cladosporioides* mycelium the interactions between free radicals of its melanin biopolymer and flucytosine appeared. Because of the main content of eumelanin in *Cladosporium cladosporioides* mycelium, the changes of free radical concentrations in DOPA-melanin after complexing with flucytosine were not observed similar to the natural sample (table 1). The role of melanin's free radicals in binding of drugs to this polymer was described in the works [9, 10-11]. The performed EPR studies pointed out that properties of the whole paramagnetic centers system remain unchanged after formation of melanin – flucytosine complexes in *Cladosporium cladosporioides* mycelium. These result differ from the data obtained for melanin complexes with the others drugs [11-12].

4. Conclusions

The performed EPR studies pointed out that interactions of flucytosine with *Cladosporium cladosporioides* mycelium containing melanin biopolymers differ from interactions of model eumelanin with the others drugs. Flucytosine does not changed free radical concentrations in the natural sample. The influence of fungal organic structures on these interactions may be responsible for this effect.

Acknowledgements

This study was supported by Medical University of Silesia in Katowice.

References

- [1] T. Sarna, J.S. Hyde, H.M. Swartz, Science 192 (1976) 1132.
- [2] T. Sarna, Zagad. Biofiz. Wspólcz. 6 (1981) 6.

- [3] R.C. Sealy, J.S. Hyde, C.C. Felix, I.A. Menon, G. Prota, *Sci.* 217 (1982) 545.
- [4] M. Pasenkiewicz-Gierula, Habilitation thesis, Jagiellonian University in Krakow, Kraków, 1990.
- [5] A. Krzywda, E. Petelenz, D. Michalczyk, P.M. Płonka, *Cell Mol. Biol. Lett.* 13 (2008) 130.
- [6] M. Okazaki, K. Kuwata, Y. Miki, S. Shiga, T. Shiga, *Archiv. Biochem. Biophys.* 242 (1985) 197.
- [7] E. Buszman, B. Pilawa, M. Zdybel, S. Wilczyński, A. Gondzik, T. Witoszyńska, T. Wilczok, *Sci. Total Environ.* 363 (2006) 195.
- [8] M. Matuszczyk, E. Buszman, B. Pilawa, T. Witoszyńska, T. Wilczok, *Chem. Phys. Lett.* 394 (2004) 366.
- [9] B. Pilawa, M. Zdybel, E. Buszman, T. Witoszyńska, H. Cieśla, *Engin. Biomater.* 89-91(XII) (2009)167.
- [10] A. Zejca, M. Gorczyca, *Chemia leków, PZWL, Warszawa, 2004.*
- [11] E. Buszman, Habilitation thesis, Medical University of Silesia, Katowice, 1994.
- [12] D. Wrześniok, Doctoral thesis, Medical University of Silesia, Katowice, 2004.

Magnetic frustration in M-Fe-V-O system

G. Żolnierkiewicz^{*1)}, N. Guskos^{1,2)} i J. Typek¹⁾

* Corresponding author: gzolnierkiewicz@zut.edu.pl

¹⁾ Institute of Physics, West Pomeranian University of Technology, Szczecin, Al. Piastow 17, 70-310 Szczecin, Poland;

²⁾ Solid State Section, Department of Physics, University of Athens, Panepistimiopolis, 15 784 Zografou, Athens, Greece

Abstract

Vanadium compounds M-Fe-V-O (M (II) = Zn (II), Mg (II), Cu (II), Mn (II) and Co (II)) with magnetic and non-magnetic ions in cationic sublattices exhibit structural randomness (iron ions can occupy positions of ions M(II)). Deficiency of oxygen in these compounds may be responsible for the emergence of competing magnetic interactions which prevent the formation of the long-range magnetic ordering at high temperatures. Study of the temperature dependence of magnetic susceptibility and electron paramagnetic resonance (EPR) spectra of compounds from the M-Fe-V-O system has revealed the presence of significant spin frustration. It may be due to the Fe^{3+} ions located in cationic sublattices. Magnetic measurements of these systems show the existence of strong antiferromagnetic interaction at high temperatures with a relatively high value of the Curie-Weiss temperature. Competing magnetic interaction allow to form a long range magnetic ordering only at low temperatures. In particular, the static magnetic susceptibility for compounds $\text{M}_2\text{FeV}_3\text{O}_{11}$ (M(II)= Zn(II) and Mg(II)) revealed the existence of antiferromagnetic interaction between the Fe^{3+} spins with the Curie-Weiss temperature of about $\theta = -55$ K and the phase transition to a spin glass state at $T_f = 2.5$ - 2.8 K. Strong changes of EPR parameters was observed at about 50 K. Similarly, in $\text{M}_3\text{Fe}_4\text{V}_6\text{O}_{24}$ compound the high-temperature long-range magnetic ordering was not registered. For these compounds the Curie-Weiss temperature is high. Competition and frustration of magnetic processes may be responsible for the lack of the long-range order at high temperatures despite the presence of a strong coupled correlated spin system.

Keywords: EPR, spin frustration, vanadate oxide, magnetic interactions

1. Introduction

After the discovery of Kagome system ($\text{M}_3\text{V}_2\text{O}_8$ (M(II) = Cu(II), Ni(II) and Co(II)) with polyphase magnetic states the magnetic frustration phenomena have been intensively studied [1]. The real microscopic quantum effect manifests itself by plateau and a step change in the temperature dependence of magnetization [2]. These systems hold promise of new opportunities in practical applications [3]. These systems are in glass spin [4] or in frozen spin states [5]. Measurements of the temperature dependence of the specific heat have showed the existence of phase transitions at temperatures of 6 and 11 K [6].

Vanadium compounds in the M-Fe-V-O (M (II) = Zn (II), Mg (II), Cu (II), Mn (II) and Co (II)) system in the cation sublattice exhibit random structural and oxygen deficiency is play important role in ordered magnetic processes at high temperatures [7]. Trivalent iron ions in different sublattices (competing magnetic effects) may be mainly responsible for the frustration of the spin system [8]. Dc magnetic susceptibility for compounds $M_2FeV_3O_{11}$ (M(II) = Zn(II) and Mg(II)) showed the presence of the strong antiferromagnetic coupling with Curie-Weiss temperature, $\theta = -55$ K, and the phase transition to spin glass state at $T_f = 2.5-2.8$ K [9]. These compounds are interesting in many applications [10]. The introduction of additional competing magnetic ions (eg $Ni_2FeV_3O_{11}$) may lead to more complicated structural analysis [11]. TGA measurements $Zn_3Fe_4V_6O_{24}$ compound indicated the existence of processes related to oxygen deficiency [12]. Analysis of the spectra ERP $M_2InV_3O_{11}$ non-magnetic compounds (M (II) = Zn (II) and Mg (II)) showed that the spectra are derived from complexes with vanadium ions at a lower level of oxidation [13]. Antiferromagnets have a geometrically frustrated spin-glass states and the random distribution of magnetic fields [14].

The aim of this report is to present our work on magnetic properties of compounds from the M-Fe-V-O system studied by dc magnetization and magnetic resonance technique.

2. Results and discussion

Figures 1a and 1b present the crystallographic structure of the compounds $Mn_3Fe_4V_6O_{24}$. It consists of two sublattices of iron ions and two sublattice of a cation (magnetic or not magnetic). Disordering processes causing distribution of iron ions in a cationic sublattice are not so evident in these compounds as in $M_2FeV_3O_{11}$ [7,15].

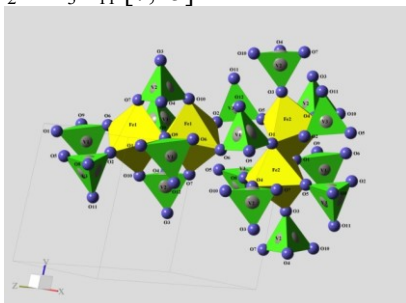


Fig. 1a Alignment of the iron Fe (1) and Fe (2) dimers, together with the surrounding vanadium tetrahedra.

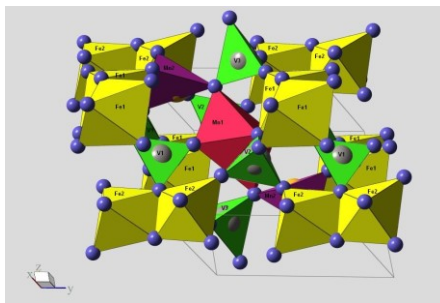


Fig. 1b Spatial arrangement of iron and manganese units in $Mn_3Fe_4V_6O_{24}$.

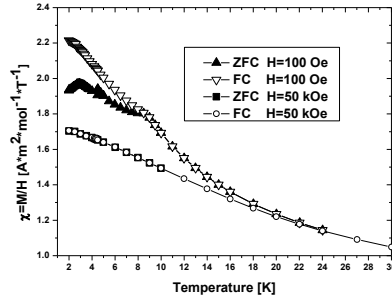
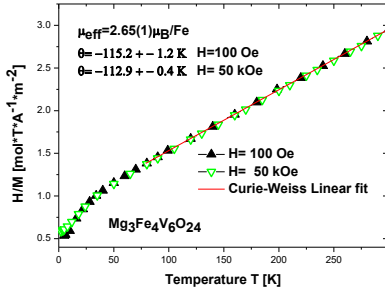


Fig. 2a Temperature dependence of inverse magnetic susceptibility, $\chi^{-1} = (\text{MZFC} / H)^{-1}$, for $\text{Mg}_3\text{Fe}_4\text{V}_6\text{O}_{24}$ at $H = 100$ Oe and 50 kOe. The solid lines are Curie-Weiss fits for high temperatures ($T > 60$ K) [8]

Fig. 2b Temperature dependence of ZFC and FC magnetization for two different values of magnetic fields for the $\text{Mg}_3\text{Fe}_4\text{V}_6\text{O}_{24}$ compound at low temperatures.

Figures 2a and 2b present the temperature dependence of magnetic susceptibility for the $\text{Mg}_3\text{Fe}_4\text{V}_6\text{O}_{24}$ compounds [8]. The nature of the change is similar in that a strong antiferromagnetic interaction with the Curie-Weiss temperature $\Theta = -111$ (1) K and $\Theta = -50$ (1) K for $\text{Mg}_2\text{FeV}_3\text{O}_{11}$ are registered [8]. The long-range antiferromagnetic order is only observed at low temperatures (Fig. 2b). Temperature dependence of $\chi^{-1}(T)$ is qualitatively similar for all compounds after the application of high magnetic fields, which is particularly evident at low temperatures. This dependence is often observed in the frustrated antiferromagnets, especially if diluted magnetic ions in the lattice are present. This implies the presence of antiferromagnetically correlated spin clusters and the relatively loose spins [16].

Figure 3a shows the observed EPR spectra for the $\text{M}_3\text{Fe}_4\text{V}_6\text{O}_{24}$ compounds at room temperature. The linewidth of the resonance line depends on the type of used ions. ERP line broadens with decreasing temperature, while decreases rapidly at lower temperatures (> 30 K). At lower temperatures, after disappearance of the main resonance line many weak and narrow resonance lines appear, which are likely to come from other paramagnetic centres such as complexes of V(IV) ions [12] or iron (III) at low-symmetry sites of the crystal field. Analysis of lineshapes showed that lines can be properly fitted by Lorentzian function. Resonance absorption signal includes also contribution from the negative fields due to linearly polarized microwave field. This contribution has a significant effect when the linewidth is comparable with the resonant field. Distortion of the shape of the resonance line and its broadening suggests searching for the long-range magnetic ordering at high temperatures.

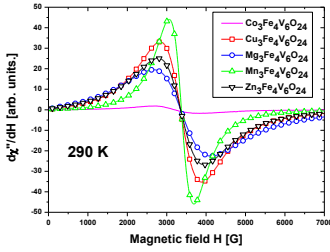


Fig.3a ERP spectra of $M_3Fe_4V_6O_{24}$ ($M(II)=Co(II)$, $Cu(II)$, $Mg(II)$, $Mn(II)$ I $Zn(II)$) compound at low temperatures.

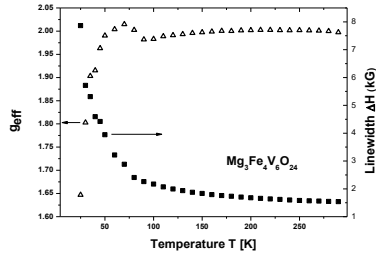


Fig. 3b Temperature dependence of g_{eff} (left axis) and linewidth ΔH_{pp} (right axis) for $Mg_3Fe_4V_6O_{24}$.

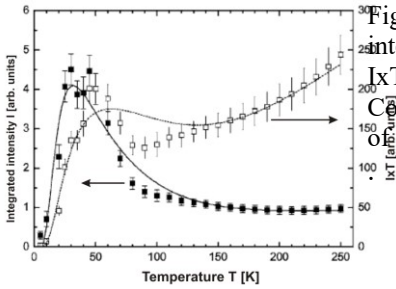


Fig. 3c Temperature dependence of integrated intensity $I(T)$ and product $I \times T$ (right axis) for $Mg_3Fe_4V_6O_{24}$. Continuous line presents the fitting of $Fe(III)-F(III)$ dimer model [8]

Figures 3b and 3c show the temperature dependence of $g_{eff}(T)$ and the resonance linewidth $\Delta H_{pp}(T)$ obtained by fitting of the experimental spectrum by Lorentzian function. Significant change is observed for both parameters at temperatures below 80 K, and above $T_1 \sim 8.5$ K and $T_2 \sim 3$ K. Broadening of the resonance linewidth in the temperature range ($3 < T/T_N < 10$) observed often for AFM dielectrics is usually associated with the change of static magnetic susceptibility [16]. Temperature dependence of the resonance linewidth $\Delta H_{pp}(T)$ can be represented by the following relationship: $\Delta H_{pp}(T) = [\chi_o(T)/\chi(T)]\Delta H_o$ where $\chi_o(T) = C/T$ is a free single-ion magnetic susceptibility, C is a Curie constant of the coupled paramagnetic system, while $\chi(T)$ is the static magnetic susceptibility and ΔH_o is temperature independent linewidth (at high temperatures) combined with a contribution from the anisotropic spin-spin interaction [8]. In this case, for $[\Delta H_{pp}(T)\chi_o(T)/\Delta H_o\chi(T)]$ a minimum at 90 K is observed, and there is correlation with a shift towards lower fields of $g_{eff}(T)$ factor. Measurements of dc magnetization and ERP in the $M_3Fe_4V_6O_{24}$ compounds revealed the existence of significant magnetic frustration due to loss of oxygen and no-equivalence of two magnetic sublattices. Dc magnetic susceptibility showed that the spin freezing at low temperatures can be produced in two magnetic sublattices with $T_f = 3$ K and 6 K, and there is a strong

correlation between the AFM at high temperatures. ERP studies showed the presence of AFM interactions and revealed the contribution of the magnetic ordering processes at around 230 K, that the static magnetization measurements have not confirmed. High frequency EPR (HF-EPR) measurements allowed to observe changes in the temperature dependence of g-factor and to compare it with the measurements at low frequency (X-band) ERP. Moreover, the use of HF-EPR can isolate the dominant type of magnetic interactions due to the use of very large magnetic fields [17].

3. Conclusions

Vanadium compounds M-Fe-V-O have been investigated their structure and magnetic properties. The competition magnetic processes is responsible for no formation long range magnetic ordering processes at higher temperature range. It was observed at low temperatures spin frustration state. The disorder of magnetic ions in their sublattice and oxygen deficiency processes could be mainly influence on the magnetic competition phenomena.

References

- [1]. N. Rogado, M. K. Haas, G. Lawes, D. A. Huse, A. P. Ramirez, and R. J. Cava, *J. Phys.: Condens. Matter* **15**, 907 (2003); G. Balakrishnan, O. A. Petrenko, M. R. Lees, and D. M. K. Paul, *J. Phys.: Condens. Matter* **16**, L347 (2004); G. Laves, M. Kenzelmann, N. Rogado, K. H. Kim, G. A. Jorge, R. J. Cava, A. Aharony, O. Entin-Wohlman, A. B. Harris, T. Yildirim, Q. Z. Huang, S. Park, C. Broholm, and A. P. Ramirez, *Phys. Rev. Lett.* **93**, 247201 (2004); G. Laves, A. B. Harris, T. Kimura, N. Rogado, R. J. Cava, A. Aharony, O. Entin-Wohlman, T. Yildirim, M. Kenzelmann, C. Broholm, and A. P. Ramirez, *Phys. Rev. Lett.* **95**, 087205 (2005); R. Szymczak, M. Baran, J. Fink-Finowski, M. Gutowska, A. Szewczyk, and H. Szymczak, *Phys. Rev. B* **73**, 094425 (2006).
- [2]. H. Kageyama, K. Yoshimura, R. Stern, N. V. Mushnikov, K. Onizuka, M. Kato, K. Kosuge, C. P. Slichter, T. Goto, and Y. Ueda, *Phys. Rev. Lett.* **82**, 3168 (1999); K. Mitsura, *J. Phys.: Condens. Matter* **14**, L559 (2002); R. Moessner and S. L. Sondhi, *Phys. Rev. B* **68**, 064411 (2003); D. C. Cabra, M. D. Grynberg, P. C. W. Holdsworth, and P. Pujol, *Phys. Rev. B* **65**, 094418 (2002); Y. Narumi, K. Katsumata, Z. Honda, J.-C. Domenge, P. Sindzingre, C. Lhuillier, Y. Shimaoka, T. C. Kobayashi, and K. Kindo, *Europhys. Lett.* **65**, 705 (2004); T. Ono, H. Tanaka, O. Kolomiets, H. Mitamura, T. Goto, K. Nakajima, A. Oosawa, Y. Koike, K. Kakurai, J. Klenke, P. Smeibidle, and M. Meissner, *J. Phys.: Condens. Matter* **16**, S773 (2004); K. Hida, *J. Phys. Soc. Jpn.* **70**, 3673 (2001); M. E. Zhitomirsky, *Phys. Rev. Lett.* **88**, 057204 (2002); A. Honecker, J. Schulenburg, and J. Richter, *J. Phys.: Condens. Matter* **16**, S749 (2004); J. Schnack, H.-J. Schmidt, J. Richter, and J. Schulenburg, *Eur. Phys. J. B* **24**, 475 (2001); J. Schulenburg, A. Honecker, J. Schnack, J. Richter, and H.-J. Schmidt, *Phys. Rev. Lett.* **88**, 167207 (2002); A. P. Ramirez, B. S. Shastry, A. Hayashi, J. J. Krajewski, D. A. Huse, and R. J. Cava,

- Phys. Rev. Lett. **89**, 067202 (2002); J. Richter, J. Schulenburg, A. Honecker, J. Schnack, and H.-J. Schmidt, J. Phys.: Condens. Matter **16**, S779 (2004).
- [3]. M. E. Zhitomirsky, Phys. Rev. B **67**, 104421 (2003).
- [4]. B. Canals and C. Lacroix, Phys. Rev. Lett. **80**, 2933 (1998).
- [5]. A. P. Ramirez, A. Hayashi, R. J. Cava, R. Siddhant, and B. S. Shastry, Nature (London) **399**, 333 (1999); S. T. Bramwell and M. J. P. Gingras, Science **294**, 1495 (2001).
- [6]. G. Balakrishnan, O. A. Petrenko, M. R. Lees, and D. M. K. Paul, J. Phys.: Condens. Matter **16**, L347 (2004).
- [7]. N. Guskos, M. Wabia, M. Kurzawa, A. Bezkrvnyj, J. Typek, I. Rychlowska-Himmel, and A. Blonska-Tabero, Radiation Effects and Defects in Solids **158**, 369 (2003); N. Guskos, J. Typek, A. Bezkrvnyj, V. Likodimos, M. Wabia, M. Kurzawa, E.A. Anagnostakis and G. Gasiorek, J. All. Com. **377**, 47 (2004).
- [8]. V. Likodimos, N. Guskos, S. Glenis, R. Szymczak, A. Bezkrvnyy, M. Wabia, J. Typek, G. Gasiorek, M. Kurzawa, I. Rychlowska-Himmel, and A. Blonska-Tabero, Eur. Phys. J. B **38**, 13 (2004); N. Guskos, V. Likodimos, J. Typek, G. Zolnierkiewicz and A. Blonska-Tabero, J. Non-Cryst. Solids **352**, 4250 (2006); N. Guskos, V. Likodimos, S. Glenis, G. Zolnierkiewicz, J. Typek, R. Szymczak, and A. Blonska-Tabero, J. Appl. Phys. **101**, 103922 (2007).
- [9]. M.A. Lafontaine, J.M. Greneche, Y. Laligant, G. Ferrey, J. Solid State Chem. **108** (1994) 1; X. Wang, D.A. Vander Griend, Ch.L. Stern, K.R. Poepfelmeier, J. Alloys Compd. **298** (2000) 119.
- [10]. G. Zolnierkiewicz, N. Guskos, J. Typek, and A. Blonska-Tabero, J. Non-Cryst. Solids **352**, 4362 (2006); K. Binder and A. P. Young, Rev. Mod. Phys. **58**, 801 (1986).
- [11]. N. Guskos, J. Typek, G. Zolnierkiewicz, A. Blonska-Tabero, M. Kurzawa, S. Los, and W. Kempinski, Materials Science-Poland **24**, 985 (2006); N. Guskos, V. Likodimos, S. Glenis, J. Typek, J. Majszczyk, G. Zolnierkiewicz, A. Blonska-Tabero, and C.L. Lin, Rev. Adv. Mat. Sci. **14**, 85 (2007).
- [12]. G. Zolnierkiewicz, J. Typek, N. Guskos, and M. Bosacka, Appl. Mag. Res. **34**, 101 (2008); J. Non-Cryst. Solids. **354**, 4506 (2008).
- [13]. V. Jaccarino and A. R. King, Physica A **163**, 291 (1990).
- [14]. D. P. Belanger and A. P. Young, J. Magn. Magn. Mater. **100**, 272 (1991); A. P. Ramirez, Annu. Rev. Mater. Sci. **24**, 453 (1994).
- [15]. N. Guskos, A. Bezkrvnyj, J. Typek, N. Yu. Ryabova, A. Blonska-Tabero, M. Kurzawa, and M. Maryniak, J. All. Comp. **391**, 20 (2005); A. Bezkrvnyi, N. Guskos, J. Typek, N. Yu. Ryabova, M. Bosacka, A. Blonska-Tabero, M. Kurzawa, I. Rychlowska-Himmel, and G. Zolnierkiewicz, Materials Science-Poland **23**, 883 (2005).
- [16]. A. Tobo, A. Ito, and K. Motoya, J. Phys. Soc. Japan **65**, 2249 (1996) S. M. Gorun and S. J. Lippard, Inorg. Chem. **30**, 1625 (1991).
- [17]. N. Guskos, H. Ohta, G. Zolnierkiewicz, S. Okubo, Wei-min Zhang, J. Typek, C. Rudowicz, R. Szymczak, M. Bosacka, T. Nakamura, J. Non-Cryst. Solids **355**, 1419 (2009).

INDEX OF AUTHORS

A

Açıkgöz M., 115

B

Bester M., 100
Bidzińska E., 23, 120
Burke J., 84
Buszman E., 132, 175

C

Callens F., 162
Camenisch T., 84
Cebulski J., 142
Celińska J., 170
Cieniek B., 102
Cieśla H., 175
Cytlak U., 56
Czapla Z., 41

Ć

Ćwieląg-Piasecka I., 104

D

Drzewiecki A., 109
Dubowik J., 19
Duclaux L., 66
Dyrek K., 23
Dziliński K., 29

F

Fedaruk R., 110
Filek M., 120

G

Gałecka K., 56
Gawron A., 127
Głogowska E., 56
Głowiński H., 19

Gnutek P., 77, 115
Godlewski M., 35
Gralka E., 58
Gruszecki W.I., 127
Guskos N., 36, 181

H

Havlicek M., 98
Hrabański R., 41

J

Jackowska M., 41
Jackowski T., 29
Jantsch W., 98
Jerzykiewicz M., 104
Jerzykiewicz, M., 47

K

Kaczmarzyk T., 29
Kempiński M., 52, 54
Kempiński W., 52, 54, 66
Kittell A., 84
Komorowska M., 56
Koprowski R., 164
Kozłowski H., 58
Kruk D., 60
Kubica A., 60
Kuźma M., 64, 100

Ł

Łabanowska M., 120
Łabuz M., 100
Łastawska K., 121
Łącki J. K., 170
Łoś S., 66

M

Makarova K., 121
Markevich S.A., 110
Markowski D., 54
Matyska-Piekarska E., 170

Michalik J., 159, 162
Misiak L.E., 127

N

Najder-Kozdrowska L., 67

O

Obal K., 120
Olko P., 164

P

Padlyak B.V., 109
Pawlikowska-Palęga B., 127
Pietrzyk P., 72, 86
Pilawa B., 132, 148, 164, 175
Piwowarska D., 137
Połomska M., 66
Potera P., 142, 154
Ptaszkiewicz M., 164

R

Ramos P., 148
Rogalska I., 154
Rudowicz Cz., 12, 77, 115, 137

S

Sadło J., 159, 162
Saiko A.P., 110
Sarna T., 84
Smyrnov O.O., 109
Sojka Z., 72, 86
Stefaniuk I., 64, 91, 100, 102, 154
Sterniczuk M., 159, 162
Strzelczak G., 159, 162
Swakoń J., 164
Szewczyk G., 84
Szyrwiel Ł., 58

Ś

Śliwińska-Bartkowiak M., 52

T

Trybuła M., 14
Trybuła Z., 14
Turek J., 159, 162
Typek J., 181
Typek J., 36

U

Ungier W., 98

V

Valensin D., 58
Valensin G., 58
Virt I., 102
Vrielinck H., 162

W

Wapłak S., 17, 97
Wawer I., 121, 170
Wenda E., 23
Więckowski A. B., 67
Wilamowski Z., 98
Wilczyński S., 164
Witoszyńska T., 175
Witwicki M., 104
Wróbel D., 154
Wróbel Z., 164
Wrześniok D., 132

Z

Zaręba M., 84
Zawada K., 121, 170
Zdybel M., 132, 175

Ż

Żądło A., 84
Żołnierkiewicz G., 36, 181